UNIVERSITY

of

GLASGOW

The Structure and Function of the Mitochondrial Peroxiredoxin SP-22

Louise Jane Gourlay BSc.(Hons)

This thesis is presented for the degree
Doctor of Philosophy
January 2003

Institute of Biomedical and Life Sciences
University of Glasgow

Declaration

I declare that this thesis, submitted for the degree of Doctor of Philosophy (Ph.D.) contains results from work carried out entirely by myself, and does not include work forming part of a thesis presented for another degree in this or another University.

For Dad and Mum

" *Anyone who has never made a mistake has never tried anything new"*
- Albert Einstein

Acknowledgements

Abstract

Substrate protein-22 (SP-22) is a 22kDa bovine protein that functions as a thioredoxin-dependent peroxidase in the mitochondrial matrix. The exact physiological targets of SP-22 remain to be elucidated; however its antioxidant activity has been well documented in the protection of several free radical-sensitive enzymes. SP-22 has been assigned to a novel peroxidase family called the peroxiredoxins (Prxs). Prxs use electrons provided by free thiol groups to reduce hydrogen peroxide, a potent oxidising agent that can contribute to oxidative stress either directly or via the hydroxyl radical generated by the Fenton reaction. Prxs can be divided into two sub-groups (1-Cys and 2-Cys) depending on the number of conserved cysteine residues they possess. SP-22 is a 2-Cys Prx with three cysteines, not an uncommon feature, at positions 47, 66 and 168. Following sequence analysis C47 is proposed to be the catalytic residue, containing a sulphenic acid group, functioning as a 2-electron redox centre.

The cloning and overexpression of recombinant SP-22 and three cysteine mutants (C47S, C66S and C168S) in bacterial cells as N-terminal His-tag proteins is reported. The overexpression conditions for optimal protein solubility and the subsequent purification by metal chelate chromatography were also determined. A comparison of reducing and non-reducing SDS-PAGE of wild type and mutant SP-22s established that SP-22 contains a dimeric unit linked by two intermolecular disulphide bonds, in its oxidised state. These involve C47 of one monomer and C168 of the opposing subunit. This result is consistent with findings for other 2-Cys Prx members.

It is known that 2-Cys Prxs can further adopt a larger decameric toroid conformation, comprising five dimeric units. It was elucidated using size exclusion chromatography and Analytical Ultracentrifugation (AU) that SP-22 forms an additional oligomeric form with an apparent molecular weight of between 500-600,000 M_r, equivalent to 20-24 monomers. Following negative staining of purified SP-22 and Transmission Electron Microscopy (TEM) it was established that the oligomer was toroidal in conformation with an average

diameter of 15nm. It also can form stacks in a lateral arrangement of two or three rings accounting for the observed increased molecular weight. Unusual structural features of radial spikes and material within the central cavity were also observed. The number of subunits per ring is proposed to be ten in accord with findings for other members of the 2-Cys group; however due to the tight arrangement of the subunits in the SP-22 toroid it was not possible to confirm this accurately.

Size exclusion chromatography of the mutants also established that the disulphide bonds were not structural, and did not direct oligomer assembly. The molecular weights were comparable with wild type SP-22, however the C47S mutant had a tendency to aggregate. TEM highlighted the lateral stacking of C47S, which was largely present in long tubular structures of up to 15 rings. The stacking of both wild type and C47S is particularly ordered, however the factors mediating stacking and the physiological relevance remains to be fully elucidated.

Using the technique of Circular Dichroism (CD) the SP-22 oligomer was found to be extremely stable, remaining partially folded even at the highest urea concentration. The cysteine mutants although slightly destabilised, remained intact and resistant to complete unfolding, confirming that the cysteines are not required for oligomer integrity.

Recombinant SP-22 was active, determined *in vitro* by assessing its protective effect towards enolase in the presence of a metal-catalysed free-radical generating system. C47 was confirmed to be the catalytic residue as C47S exhibited no protection towards enolase. C168S interestingly did protect enolase suggesting that *in vitro* this mutant can function in the same manner as a 1-Cys Prx, bypassing the necessity for disulphide bond formation with thioredoxin, that presumably occurs *in vivo* during catalysis. By comparing hydrogen peroxide removal by catalase and SP-22, the differing mechanisms of hydrogen peroxide removal were observed.

Previous work in this laboratory involving the purification of the mitochondrial 2-oxoacid dehydrogenase member, pyruvate dehydrogenase (PDC) from bovine heart, and its subsequent separation into its three enzyme components by size exclusion chromatography, established that the dihydrolipoamide dehydrogenase component (E3) co-eluted with another contaminating protein. Following N-terminal sequencing this protein was identified to be SP-22. Preliminary results using the techniques of Isothermal Titration Calorimetry (ITC) and Surface Plasmon Resonance (SPR) have confirmed a physical association between SP-22 and E3, binding with an affinity in the micromolar range. The functional significance of this interaction is discussed with respect to the possible protection of PDC and the oxoglutarate dehydrogenase complex (OGDC) against oxidative modification of the catalytically-active thiol groups possessed by the individual components.

Contents

Declaration

Quotation

Acknowledgements

Abstract

Table of contents

List of figures

List of tables

Abbreviations

Chapter 2-Materials and Methods

Chapter 3.1. The Cloning, Overexpression and Purification of Bovine SP-22

Chapter 3. 2. The Mutagenesis of Mature SP-22 and the Overexpression and Purification of the Cysteine Mutants

Chapter 4.1. The Determination of the Molecular Weight of SP-22 by Analytical Ultracentrifugation

Chapter 4.2. Secondary Structure Determination of SP-22 and Assessment of Oligomer Stability

Chapter 4.3. Fluorimetry Analysis of SP-22

Chapter 5.1. Gel Filtration Studies of Wild Type SP-22 and the Cysteine Mutants

Chapter 5.2. Negative Staining and Transmission Electron Microscopy Studies

Chapter 6.1. Inactivation of Enolase with a Free Radical-generating System, and Protection by SP-22

Chapter 6.2. Inactivation of Bovine, E3, PDC and OGDC By Hydrogen Peroxide

Chapter 7.1. Binding Studies Between SP-22 and Bovine E3

Chapter 7.2. Probing the Functional Relationship Between SP-22 and the 2-Oxoacid Deydrogenase Complexes

List of Figures

Chapter 4

Chapter 5

Chapter 6

Chapter 7

List of Tables

Abbreviations

Å	angstrom
AD	Alzheimer's disease
Amp	ampicillin
Ahp	alkylhydroperoxide reductase
AUC	analytical ultracentrifugation
BCOADC	branched-chain 2-oxoacid dehydrogenase complex
CD	circular dichroism
Cys	cysteine
Da	daltons
dH_2O	distilled water
DNA	deoxyribonucleic acid
DTNB	5-5'-dithionitrobenzoic acid
DTT	dithiothroeitol
E1	pyruvate decarboyxlase
E2	dihydrolipoamide transacetylase
E3	lipoamide dehydrogenase
E3BP	E3-binding protein
ECL	enhanced chemiluminescence
EDTA	ethylenediaminetetra-acetic acid
En	enolase
EtBr	ethidium bromide
FPLC	fast protein liquid chromatography
GdmCl	guanidine hydrochloride
GPx	glutathione peroxidase
GS	glutamine synthetase
GSH	glutathione
GSSG	glutathione disulphide
FA	Freidrich's ataxia
FAD	flavin adenine dinucleotide
Fig.	figure

FRS	free-radical generating system
h	hour
HBP23	haem-binding protein 23
HEPES	N-(2-hydroxyethyl)piperazine-N'-(4-butanesulphonic acid)
His	histidine
H_2O_2	hydrogen peroxide
HSP-60	heat-shock protein 60
IPTG	isopropyl β–D-thio-galactopyranoside
ITC	isothermal titration calorimetry
kb	kilobase
kDa	kilodalton
KPi	potassium phosphate
l	litre
LB	Luria broth
M	moles per litre
MA	mAmps
MeSOX	methionine sulphoxide
min	minutes
ml	millilitres
MOPS	3-(N-Morpholino)propanesulphonic acid
M_r	relative molecular mass
MSUD	maple syrup urine disease
μl	microlitres
μM	micromolar
mt	mitochondrial
MW	molecular weight
M_w,app	apparent molecular weight
NAD^+	nicotinamide adenine dinucleotide (oxidised)
NADH	nicotinamide adenine dinucleotide (reduced)
$NADP^+$	nicotinamide adenine dinucleotide phosphate (oxidised)
NADPH	nicotinamide adenine dinucleotide phosphate (reduced)

nm	nanometer
NMR	nuclear magnetic resonance
NO	nitic oxide
NO_2	nitrogen dioxide
NP-40	nonidct
NTB	nitrothiobenzoate anion
$O2^{\bullet-}$	superoxide anion
$^{\bullet}OH$	hydroxyl radical
OGDC	2-oxoglutarate dehydrogenase complex
$ONOO^-$	peroxynitrite
ORF6	open-reading frame protein 6
8-oxo-dG	8-oxo-deoxyguanosine
PAGE	polyacrylamide gel electrophoresis
PBS	primary biliary cirrhosis
PCR	polymerase chain reaction
PD	Parkinson's disease
PDC	pyruvate dehydrogenase complex
PEG	poly ethylene glycol
PEP	Phosphoenol pyruvate
2-PGA	2-phosphoglyceric acid
PMSF	phenylmethylsulphonyl fluoride
Prx	peroxiredoxin
Q	ubiquinone
RNS	reactive nitrogen species
ROS	reactive oxygen species
rpm	revolutions per minute
RSS	reactive sulphur species
s	second
SDS	sodium dodecyl sulphate
SE	sedimentation equilibrium
SEU	sedimentation equilibrium ultracentrifugation

-SH	sulphydryl group
-SOH	sulphenic acid
-SO$_2$H	sulphinic acid
-SO$_3$H	sulphonic acid
SOD	superoxide dismutase
SP-22	substrate protein 22
SPR	surface plasmon resonance
TCA	trichloroacetic acid
TEM	transmission electron microscopy
TEMED	N,N,N'N' –tetramethylethyeneldiamine
ThDP	thiamine diphosphate
TPx-B	thioredoxin peroxidase-B
Tris	2-amino-2-(hydroxymethyl)-1,3-propanediol
Trp	tryptophan
Trx	thioredoxin
TrxR	thioredoxin reductase
UV	ultra violet
V	volts
V$_e$	elution volume
V$_o$	void volume
Vol	volume
v/v	volume to volume
w/v	weight to volume

Chapter 1

Introduction

1.0. Oxidative Stress

Oxidative stress is a term used to describe severe oxidative damage to cells, arising from an imbalance in the metabolism of redox-active species. This imbalance occurs when the generation of reactive oxidising species exceeds their removal, giving rise to impaired cell function, and ultimately cell death. The principal targets of oxidative damage are the key biomolecules of the cell, namely proteins, lipids and nucleic acids. Accumulation of these damaged biomolecules is contributory to, or characteristic of, the ageing process and several major pathologies, particularly neurodegenerative diseases which are discussed further in later sections.

The principal types of oxidising species are reactive oxygen species (ROS) and reactive nitrogen species (RNS). Recent studies have implicated an additional group of oxidising agents as contributors of oxidative stress – reactive sulphur species (RSS).

All aerobic organisms generate the most prevalent oxidising species ROS, as a consequence of normal cellular metabolism. Despite the destructive properties of ROS, physiological concentrations are required for normal cellular function; indeed some such as hydrogen peroxide serve as second messenger molecules in cell signalling pathways (Finkel, 2000; Kamata and Hirata, 1999). It is well established that the mitochondrion is the major cellular generator of ROS, principally via the process of oxidative phosphorylation. It is estimated that 1-2% of electrons passing down the electron transport chain leak out to molecular oxygen, forming ROS. Recent studies have elucidated the flavin mononucleotide group of complex I (NADH-ubiquinone oxidoreductase) and complex III (ubiquinol-cytochrome c oxidoreductase), as the primary sites of ROS generation (Finkel and Holbrook, 2000; Liu et al, 2002) (Fig.1.1). It is necessary to establish the site of electron leakage in order to design drugs to delay the onset of ageing and ROS-related diseases.
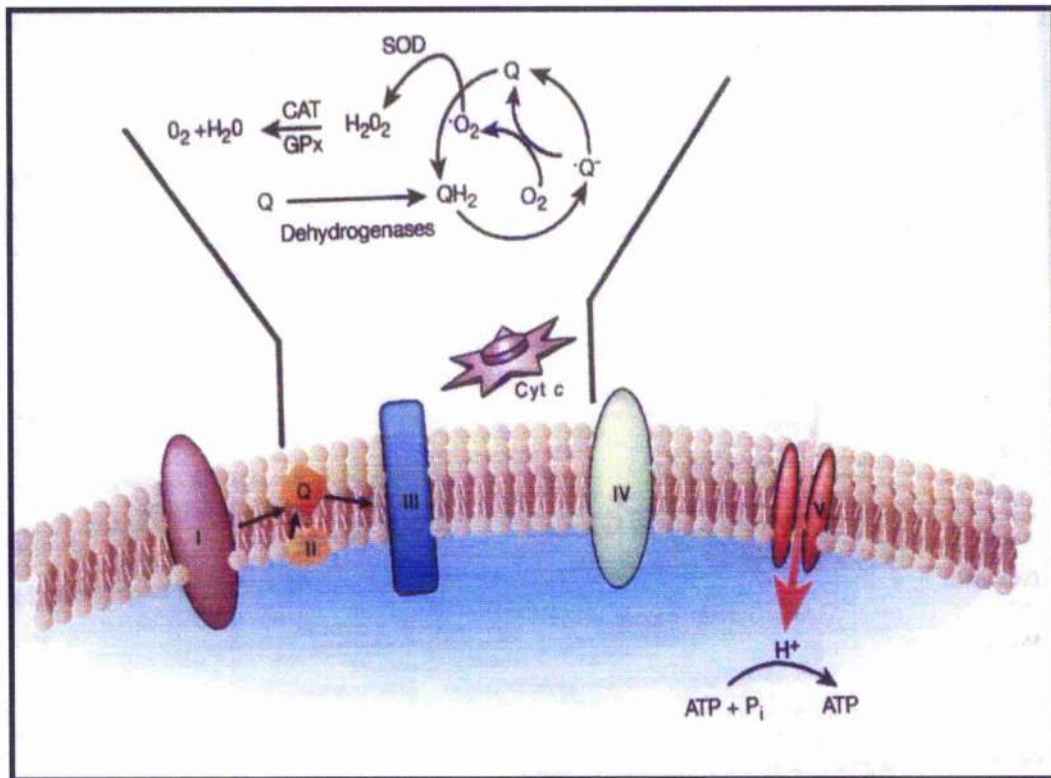
Figure 1.1. Generation of Superoxide via Electron Leakage from Complex III of the Electron Transport Chain

This diagram shows the principal sources of the superoxide anion ($^{\bullet}O_2^-$) via leakage from complex III of the electron transport chain. Electrons generated by complex I (NADH dehydrogenase) and complex II (ubiquinone-cytochrome c reductase) are transferred to ubiquinone (Q), which is subsequently reduced by cytochrome b and c (Cyt.c). Ubiquinone is reduced by two one-electron reductions during which the semiquinone ($^{\bullet}Q^-$) is generated after the first reduction. This anion can interact directly with molecular oxygen to form superoxide. Superoxide can then spontaneously dismutate to form hydrogen peroxide (H_2O_2), accelerated by the enzyme superoxide dismutase (SOD). Hydrogen peroxide is subsequently scavenged by the various antioxidant systems present within the mitochondria. Adapted from Finkel and Holbrook (2000).

1.1. Reactive Oxygen Species (ROS)

There are three major ROS generated via the escape of electrons from the mitochondrial respiratory chain: the superoxide radical ($O_2^{\bullet-}$), hydrogen peroxide (H_2O_2) and the hydroxyl radical ($^{\bullet}OH$) (Eq.1-5, Fig.1.2). The superoxide radical can alternatively be generated by flavoenzymes such as xanthine oxidase and lipoxygenase, or via exogenous sources such as ultraviolet light and ionising radiation. Superoxide is the least destructive ROS as it is unable to permeate lipid bilayers, restricting it to the inner mitochondrial compartment. Superoxide however can overcome this restriction via a reaction involving two molecules of superoxide spontaneously interacting to generate hydrogen peroxide and molecular oxygen (Eq.3, Fig.1.2). This reaction can be accelerated by the actions of the enzyme superoxide dismutase (SOD). Unlike superoxide, hydrogen peroxide easily traverses lipid membranes, accounting for its highly destructive properties. Hydrogen peroxide is a powerful oxidant, but not a free radical. Its most toxic effects are ascribed to its key role as a reaction intermediate in the formation of the most potent ROS, the hydroxyl radical. The reduction of hydrogen peroxide to hydroxyl radicals is catalysed by the transition metal ions (Fe^{2+} or Cu^+) and is called the Fenton Reaction (Eq.4, Fig.1.2). The superoxide radical is involved in re-oxidising the metal ions for subsequent cycles (Eq.5, Fig.1.2). The sum of the Fenton reaction and this re-oxidising reaction is called the Haber-Weiss reaction.

1.2. Reactive Nitrogen Species (RNS)

RNS are mainly generated via the intracellular messenger nitric oxide (NO). NO is generated endogenously from the oxidation of L-arginine to L-citrulline by a family of NADPH-dependent enzymes called the NO synthases. The mitochondrion and cytosol are the primary sites of NO production with the most recently identified NO synthase being located in the mitochondrion (Ghafourifar and Richter, 1997). The functions of NO include roles in coagulation, relaxation of smooth muscle, neurotransmission and regulation of apoptosis (Gewaltig and Kojda, 2002).

Equation 1: Summary of ROS Formation

$$O_2 \xrightarrow{e^-} O_2^{\bullet-} \xrightarrow[2H^+]{e^-} H_2O_2 \xrightarrow{e^-} {}^{\bullet}OH + {}^-OH \xrightarrow[2H^+]{e^-} 2H_2O$$
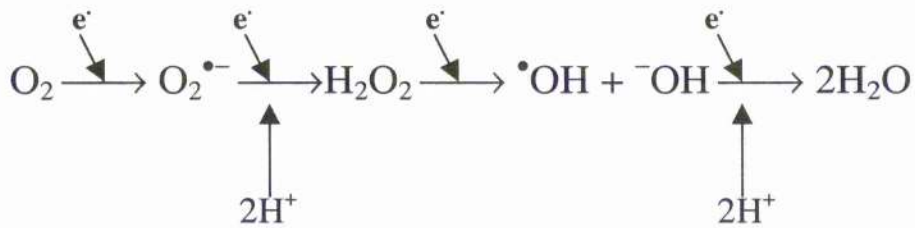
Equation 2: Superoxide Formation

$$O_2 + e^- \longrightarrow O_2^{\bullet-}$$

Equation 3: Hydrogen Peroxide Formation

$$O_2^{\bullet-} + O_2^{\bullet-} \xrightarrow[\text{SOD}]{2H^+} H_2O_2 + O_2$$
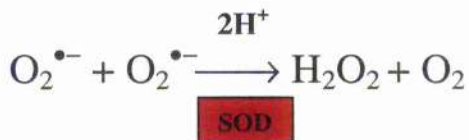
Equation 4: Hydroxyl Radical Formation

(The Fenton Reaction)

$$H_2O_2 + Cu^+/Fe^{2+} \longrightarrow {}^{\bullet}OH + {}^-OH + Cu^{2+}/Fe^{3+}$$

Equation 5: Recycling of Transition Metal Ions

$$Cu^{2+}/Fe^{3+} + O_2^{\bullet-} \longrightarrow Cu^+/Fe^{2+} + O_2$$

Figure 1.2. An Overview of Reactive Oxygen Species Formation

NO is involved in both the prevention and induction of apoptosis via a complex signalling network (Curtin *et al*, 2002). There are three chemical forms of NO (NO⁻, NO* and NO⁺) accounting for its vast range of biochemical functions and reactivities. NO itself, like superoxide is not particularly destructive, despite its unpaired electron. It does however readily react with other free radicals, particularly lipid peroxyl and alkyl radicals. In effect NO can be regarded as a free radical scavenger, as such reactions give rise to a less reactive product. Glutathione, the thiol buffer of the cell, quenches excess NO giving rise to an S-nitroso-glutathione adduct which is subsequently degraded into glutathione and NO by the antioxidant enzyme thioredoxin reductase or the entire thioredoxin system (Nikitovic and Holmgren, 1996). The thioredoxin system will be discussed further in section 1.7.0. The major destructive effect of NO arises from its interaction with superoxide, forming the extremely cytotoxic peroxynitrite (ONOO⁻) that has the ability to diffuse intra-and inter-cellularly. Peroxynitrite destruction occurs mainly through its modification of free thiol groups (Equation 2, Fig. 1.3) and the nitration of the aromatic side-chains of tyrosine and tryptophan. Peroxynitrite formation occurs rapidly in areas of simultaneous NO and superoxide production and can oxidise thiols 10^3 times faster than hydrogen peroxide (Radi *et al*, 1991a). Peroxynitrous acid can also be generated by protonation of peroxynitrite, but then decomposes rapidly due to its poor stability, to a hydroxyl-like species and nitrogen dioxide (Equation 1, Fig. 1.3). Consequently peroxynitrite formation can be regarded as an important mechanism of oxygen radical-mediated toxicity.

1.3. Reactive Sulphur Species (RSS)

In general, molecules containing sulphur are considered to possess antioxidant activity due to their ability to quench free radical sites generated via hydrogen atom abstraction by reactive species. Glutathione (GSH) is the principal low molecular weight thiol antioxidant, responsible for maintaining the redox- buffer status of the cell by scavenging ROS (Dickinson and Forman, 2002). The enzyme glutathione peroxidase (GPx) catalyses the reduction of hydrogen peroxide via the oxidation of GSH to glutathione disulphide (GSSG). GSSG is subsequently

$$O_2^{\bullet-} + {}^{\bullet}NO \rightarrow ONOO^- \Leftrightarrow ONOOH \rightarrow {}^{\bullet\bullet}OH' + NO_2$$
$$H^+$$
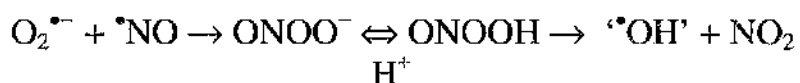
Equation 1: Peroxynitrite production

$$2RSH + ONOO^- \rightarrow NX + RSSR$$
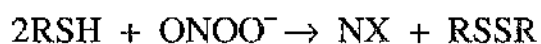
Equation 2: Peroxynitrite interaction with thiols

Figure 1.3. Formation of Peroxynitrite and its Interaction With Thiols

Equation 1 shows the generation of peroxynitrite ($ONOO^-$) via the interaction of the superoxide anion ($O_2^{\bullet-}$) with nitric oxide (${}^{\bullet}NO$) and the subsequent degradation of its protonated form, peroxynitrous acid (ONOOH), into a hydroxyl-like species (${}^{\bullet}OH'$), and nitrogen dioxide (NO_2). Equation 2 shows the reaction between peroxynitrite and a thiol-containing compound (RSH) to form the cognate disulphide (RSSR), and an unidentified nitrogen-containing species (NX).

reduced back to GSH by NADPH-dependent glutathione reductase (GS). Additional higher oxidation states of sulphur are sulphenic (-SOH), sulphinic (-SO$_2$H) and sulphonic (-SO$_3$H) acids. These latter two states are irreversible and relatively inactive; until recently it has been assumed that they do not readily participate in further redox reactions. The assumption that RSS do not contribute to oxidative damage under oxidising conditions has been re-addressed. Recent studies have highlighted the role of RSS in oxidative damage (Giles and Jacob, 2002a). The quenching of free radical sites by thiols and the oxidation of thiols by peroxynitrite can generate a thiyl radical (RS$^{\bullet}$) by-product. Thiyl radicals cause further destruction by hydrogen atom abstraction, exerting deleterious effects on intracellular biomolecules.

With the increasing resolution of enzyme structures by X-ray crystallography, higher oxidation states of sulphur have been identified in several biological systems. It has become apparent that several redox-active proteins contain a cysteine-sulphenic acid group essential for catalysis, including the peroxiredoxin family of peroxidases discussed further in section 1.8.0. The oxidation of sulphydryl groups to sulphenic acid is a key regulatory mechanism in some enzyme activities (Claiborne *et al*, 1999).

In addition to sulphenic acid and the thiyl radical, additional types of RSS exist including, disulphides (R$_1$-S-S-R$_1$), disulphide-S-monoxides (R$_1$-SO-S- R$_1$) and disulphide-S-dioxides (R$_1$-SO$_2$S- R$_1$). Disulphide-S-monoxides and dioxides can be generated *in vitro* by mixing equal amounts of hydrogen peroxide and glutathione at pH 6.0, and have been shown to damage alcohol dehydrogenase and glyceraldehyde-3-phosphate dehydrogenase via oxidative modification of their thiol groups (Giles *et al*, 2002). Various antioxidant compounds including ascorbate and melatonin were assessed for their protective effects towards damage caused by disulphide-S-oxides; however only elevated levels of glutathione were preventative. This implies that even in conditions of high antioxidant concentration, RSS production can still occur. Following the oxidation of thiols by disulphide-S-monoxides and dioxides, mixed disulphides are formed,

generating sulphenic or sulphinic acid in the process. Mixed disulphides can further oxidise thiols, generating the fully reduced protein and the disulphide of the reducing species e.g. GSSH from GSH. (For an overview of RSS generation see Figure 1.4).

1.4. Lipid Damage

Lipid peroxidation is the main consequence of lipid oxidation by ROS due to the high susceptibility of the double bonds within polyunsaturated fatty acids to oxidative damage. Arachidonic acid and docosahexaenoic acids, which are abundant in the brain, are particularly susceptible to lipid peroxidation. Consequences of lipid peroxidation include an increase in aldehyde formation, mainly 4-hydroxyalkenals which exhibit potent cytotoxic effects. In neuronal cells, 4-hydroxyalkenals have been demonstrated to inhibit DNA, RNA and protein synthesis, in addition to glycolysis, supporting a probable role of oxidative stress in neurodegenerative disorders. Lipid hydroperoxide formation is also characteristic in the pathogenesis of several other diseases, particularly cardiovascular disease where it is involved in atherosclerotic plaque formation (Gorog *et al*, 2002).

Lipid hydroperoxides can become degraded to free radicals in the presence of bivalent metal ions, such as the peroxyl radical, which enhances the production of numerous reactive compounds. Interestingly lipid hydroperoxides have been demonstrated to induce directly the expression of the cryoprotective proteins including the heat-shock proteins crucial in the stress response (Calabrese *et al*, 2002).

1.4.1. DNA Oxidative Damage

DNA bases and the deoxyribose backbone are targets of oxidative damage. ROS exert their destructive effects on nucleic acids by inducing mutations via
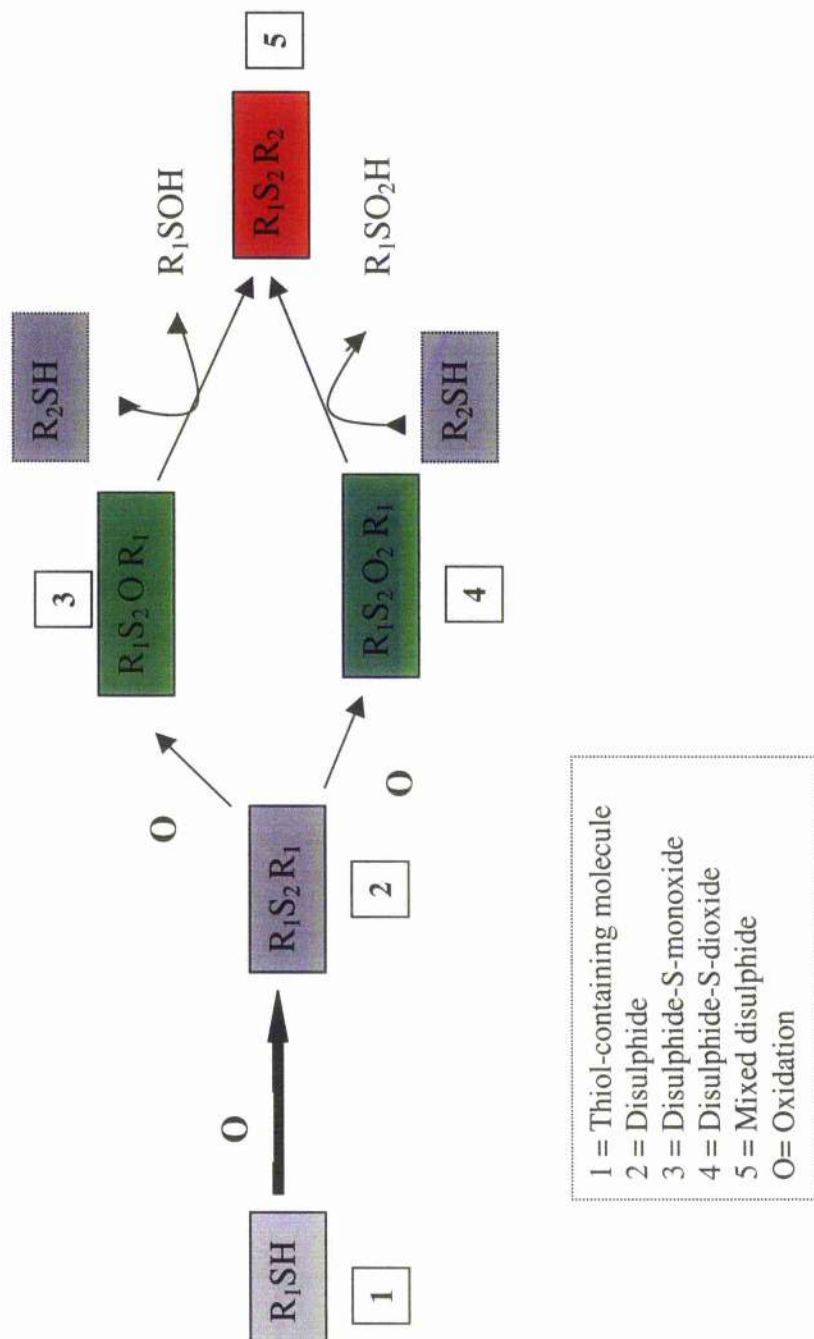
Figure 1.4. Overview of RSS Formation From the Oxidation of a Thiol-Containing Molecule (R₁SH)

1 = Thiol-containing molecule
2 = Disulphide
3 = Disulphide-S-monoxide
4 = Disulphide-S-dioxide
5 = Mixed disulphide
O= Oxidation

processes such as DNA-protein cross-links, purine oxidation and DNA strand breaks. It is proposed that the principal ROS threat to DNA is the hydroxyl radical (Aust and Eveleigh, 1999; Henle and Linn, 1997), and the protonated form of peroxynitrite (peroxynitrous acid). As the hydroxyl radical is extremely reactive, it is unlikely that it diffuses into the nucleus. It is more probable that hydrogen peroxide diffuses into the nucleus where it is degraded into the hydroxyl radical. Peroxynitrous acid on the other hand can diffuse freely across membranes and into the nucleus. The DNA lesion involving the formation of 8-oxo-deoxyguanosine (8-oxo-dG) has been the most intensively studied as it is methodologically easy to detect. 8-oxo-dG is extremely mutagenic and has been reported to introduce spontaneous mutations in several genes. Other mutagenic lesions resulting from DNA oxidation include 5-hydroxyuracil and 5-hydroxy-deoxycytidine (Marnett, 2000). DNA can also be damaged by products of lipid peroxidation, for example malondialdehyde, which forms a DNA adduct with a mutagenic potential comparable to that of 8-oxo-dG (Marnett, 1999).

If DNA modifications are left un-repaired, incorrect base pairing occurs and somatic mutations accumulate, a feature of several human pathologies including many types of cancer. Mitochondrial DNA is particularly susceptible to oxidative damage due to its close proximity to ROS production and the fact that it is unprotected by histones unlike chromosomal DNA. The level of oxidatively damaged bases in mtDNA is 10-20-fold higher in comparison to nuclear DNA. Studies have underlined a connection between damage to mtDNA and apoptosis (Esteve et al, 1999). Mitochondrial genome lesions, together with damaged mitochondrial enzymes are proposed to be the major players in ageing which has become a rapidly expanding, and profitable area of research in recent years (Wei and Lee, 2002).

1.4.2. Protein Oxidative Damage

The oxidative modification of proteins is less well characterised than DNA and lipid damage. Destruction is attributed mainly to the hydroxyl radical, generated by the Fenton reaction, giving rise to various modifications including the oxidation of amino acid side-chains, formation of protein-protein cross-links and

polypeptide backbone oxidation resulting in chain fragmentation (Berlett and Stadtman, 1997; Stadtman and Berlett, 1991). In general, the oxidative modification of a protein results in an overall conformational change in structure, misfolding and thus impaired function. A prime example is the distortion of metal binding sites and the modification of amino acid residues that are essential for enzyme regulation, for example, serine residues that are the sites of phosphorylation. All amino acid side-chains are susceptible to oxidation; however favoured targets are the sulphur-containing amino acid residues, cysteine and methionine, and the aromatic amino acids tryptophan and tyrosine. Cysteine and methionine residues are especially vulnerable targets for all ROS, even at reduced levels. Cysteine-sulphydryl groups become oxidised to disulphides, and methionine residues are oxidised to methionine sulphoxide residues (MeSOX). These modifications are the only examples of reversible oxidative reactions. The enzymes responsible for the reduction of cysteine and methionine residues, back to their original states are disulphide reductases and MeSOX reductases, respectively.

Other common oxidative modifications include the conversion of histidine to asparagine, and proline residues to glutamic semialdehyde residues. All amino acids, especially lysine, can generate carbonyl derivatives as a consequence of oxidative damage. Carbonyl derivatives provide a means by which the oxidative damage to a protein can be assessed. Studies were carried out in *Saccharomyces cerevisiae* and *Escherichia coli* to elucidate which proteins were susceptible to oxidative damage when exposed to hydrogen peroxide and the superoxide anion, by measuring the carbonyl content of each enzyme. The major targets were found to be mitochondrial proteins, including the dihydrolipoyl acetyltransferase (E2) component of the pyruvate dehydrogenase- and 2-oxoglutarate dehydrogenase complexes, aconitase, and the molecular chaperone HSP-60 (Cabiscol *et al*, 2000; Tamarit *et al*, 1998). This is not surprising given the extremely high ROS concentrations in mitochondria, and further supports the role of impaired mitochondrial function in ageing and oxidative-stress related disorders (Cadenas and Davies, 2000).

1.5. The Role of Oxidative Stress in Disease

Cells and tissues compromised by oxidative stress are characteristic features of several human diseases, particularly autoimmune diseases including diabetes mellitus and inflammatory diseases such as rheumatoid arthritis. Furthermore, several neurodegenerative pathologies including Alzheimer's disease (AD), Parkinson's disease (PD), Freidrich's ataxia, and Creutzfeld-Jakob Syndrome, are associated with high levels of oxidatively modified proteins (Floyd, 1999; Gilgun-Sherki *et al*, 2001). In AD, the major protein targets of oxidation have been found to be glutamine synthetase, creatine kinase and α-enolase (Castegna *et al*, 2002). Accumulation of these damaged proteins is likely to account for the late onset of the mentioned neurodegenerative disorders. The brain is particularly vulnerable to oxidative damage due to its abundant oxygen supply. Furthermore the insignificant levels of the hydrogen peroxide scavengers, catalase and glutathione, together with the high lipid content of the brain also enhances susceptibility to oxidative destruction.

Redox-active transition metals mainly copper, manganese and iron, are proposed to be the main contributors to the onset of oxidative stress in the tissues of patients with neurodegenerative disorders (Sayre *et al*, 2000). These metals are crucial for maintaining normal biochemical function within cells, functioning as co-factors for several enzymes, predominantly those involved in respiration. As a consequence, any reduction in the level of metal ions can give rise to compromised organ function, and damage to the central nervous system. In contrast, an elevation in the level of metals has a cytotoxic effect, mainly due to a cognate elevation in free radical concentrations, primarily via the Fenton reaction. In PD iron and lipid peroxide levels are elevated and glutathione levels are decreased, supporting the oxidative stress hypothesis. In AD aluminium, mercury, and iron are all contributory although iron is the most destructive existing in two valence states, the stable ferrous (Fe^{2+}) form, and the reactive ferric (Fe^{3+}) form. Metal ions can also directly interfere with the folding of protein and peptides by altering their conformations and ultimately their activities. This also is a common parameter in neurodegenerative diseases.

1.6. Antioxidant Systems: Non-Enzymatic and Enzymatic

To combat oxidative stress, a network of interacting antioxidant defence systems has evolved encompassing both enzymatic and non-enzymatic systems. Non-enzymatic systems of ROS removal involve a number of macromolecules with free radical-scavenging activity such as vitamins A, C, E and lipoic acid (Fang *et al*, 2002). Other compounds can indirectly scavenge ROS following conversion to a more reactive metabolite with antioxidant activity such as uric acid and bilirubin. These compounds are the breakdown products of urea and haemoglobin respectively.

The principal detoxifying enzymes are superoxide dismutase (SOD), catalase, glutathione peroxidase and the thioredoxin system (Nordberg and Arner, 2001). SODs were one of the first ROS-scavenging enzymes to be discovered and serve as a first line of defence against free radicals in eukaryotes. SOD enzymes accelerate the formation of hydrogen peroxide and molecular oxygen from two spontaneously interacting molecules of superoxide (Eq.3, Fig.1.2). There are three metal-containing SOD isoforms; one cytosolic copper/zinc (Cu/Zn) isoform, one Cu/Zn-requiring extracellular isoform (EC-SOD) and one mitochondrial manganese (Mn) isoform (Zelko *et al*, 2002). In addition to their distinct compartmental localisations, the SOD isoenzymes differ in their sizes and structures. The EC-SOD is the least well characterised, as it is the most recently discovered.

In order to assess the contributions of SOD enzymes in ageing and various pathologies related to oxidative stress, several transgenic mice models have been produced containing deletions in their SOD genes (Noor *et al*, 2002). Mice lacking the mitochondrial Mn-SOD are either not viable or die soon after birth due to severe neurodegenerative damage. These findings are not unexpected reflecting the importance of Mn-SOD in superoxide removal from its main site of production, the mitochondrion. Transgenic mice lacking cytosolic SOD display a normal phenotype implying that this isoform is less critical for viability than the mitochondrial isoform. In order to study Mn-SOD mutations in more detail it was

necessary to generate mice with longer viability; therefore liver-specific Mn-SOD knockouts were generated which have normal life spans and display no obvious morphological abnormality, suggesting this enzyme is not so critical in the liver (Ikegami *et al*, 2002). Recognition of the mitochondrial enzyme as the more important isoform is supported by the finding that oxidative stress and thioredoxin can both induce expression of the mitochondrial SOD form, but not the cytosolic enzyme. This was established in a study using cultured human endothelial cells in which increased mitochondrial SOD mRNA levels were detected in addition to a cognate increase in activity when incubated with low levels of thioredoxin (Das *et al*, 1997). Despite this, mutations in the cytosolic SOD have been identified as responsible for the neurodegenerative disease amyotrophic lateral sclerosis (ALS). This disorder is a consequence of increased peroxidase activity in point mutants of SOD, resulting in eventual death. For a review of the superoxide anion and the SOD enzymes, see Fridovich, (1997).

Catalases are also efficient ROS-metabolising enzymes, with such a high turnover number that they cannot be saturated by their substrate hydrogen peroxide at any physiological concentration. Their primary intracellular location is the peroxisome where the levels of hydrogen peroxide generation are extremely high; however they are also detected at low levels in the cytosol. Catalases are typically tetrameric, haem-containing enzymes, which promote the dismutation of hydrogen peroxide to water and molecular oxygen (Eq.1a, Fig.1.5). Removal of hydrogen peroxide results in lower levels of hydroxyl radicals produced by the Fenton reaction. Catalases offer further protection by detoxifying alternative compounds such as phenols and alcohols. This detoxification reaction is coupled to the reduction of hydrogen peroxide to water and the substrate's respective metabolite (Eq.1b, Fig.1.5). The only mitochondrial catalase activity identified to date is in rat heart. It was detected by biochemical means and by immunoblotting with an anti-catalase antibody (Radi *et al*, 1991b). Despite the presence of catalase in mitochondria, studies using rat heart suggest its role in hydrogen peroxide removal is redundant with GPx being the predominant peroxidase. This was observed even in extreme oxidising conditions (Antunes *et al*, 2002).

The glutathione peroxidase (GPx) antioxidant system is regarded as the most important hydrogen peroxide scavenger in mammals as it exhibits a higher affinity for its substrate than catalase and it is present in the cytosol, endoplasmic reticulum, nuclei and mitochondria. The GPx system is not well understood, although its role in protection against oxidative stress is well reported. There are four GPx isoforms all requiring a selenocysteine group for function but distinct in their tissue distributions (Arthur, 2000). The reaction catalysed by these enzymes is the reduction of hydrogen peroxide to water coupled to the oxidation of GSH to GSSG (Eq.2, Fig.1.5). Lipid peroxides are alternatively metabolised by GPx to their corresponding alcohols and water. The selenoate group of GPx is proposed as the target of oxidation being converted to a selenenic acid during catalysis. Selenoate group regeneration is coupled to GSH oxidation. GSSH is subsequently converted back to GSH by the NADPH-dependent flavoenzyme glutathione reductase. As mentioned previously, GSH is the major sulphydryl buffer of the cell. It does however participate in various detoxification reactions involving other cellular enzymes such as glutathione-S-transferases, glutaredoxins and thioredoxins.

1.7. The Thioredoxin System

The protein thioredoxin (Trx) and the enzyme thioredoxin reductase (TrxR) constitute the thioredoxin system, serving as a supporting line of defence against free radical damage (Arner and Holmgren, 2000). This system is ubiquitously found in prokaryotes and eukaryotes.

Trxs are a rapidly expanding family of low molecular weight proteins (~12 kDa) with divergent functions (Powis and Montfort, 2001). The interest in Trx was initiated following its identification as a hydrogen donor for the enzyme ribonucleotide reductase, responsible for a key regulatory step in the synthesis of deoxynucleotides and DNA. Trxs are now recognised as the major cellular protein disulphide reductases. Additional functions have been assigned to Trx, including the regulation of key enzymes involved in protection against oxidative stress with Trx expression itself being induced by this oxidative state. Control of

transcription factors such as NF-κB, regulation of cell proliferation and protein folding are additional functions of Trx. Mitochondrial Trx has been reported to activate the 2-oxoacid dehydrogenase multi-enzyme complexes (see section 1.10.6 for further discussion).

The thiol-disulphide oxidoreductase activity of thioredoxin is mediated by a conserved active site motif: Cys-Gly-Pro-Cys, which is reversibly oxidised during catalysis. Trx is returned to its reduced state in a NADPH-dependent reaction, catalysed by the cognate flavoenzyme TrxR (Eq.3, Fig.1.5). There are numerous TrxR isoenzymes present in the cytoplasmic compartment and mitochondria. They are all homodimeric flavoenzymes, containing a redox active disulphide and one molecule of FAD per monomer. TrxRs can be divided into two classes, the low M_r type characterised by the *E. coli* enzyme, and the high M_r type present in higher eukaryotes. The latter class of enzymes has similarities with glutathione reductase, lipoamide dehydrogenase from the mitochondrial 2-oxoacid dehydrogenase complexes, and other members of the pyridine nucleotide-disulphide oxidoreductase family both in structure and catalytic mechanism. All mammalian TrxR enzymes possess a C-terminal region containing a cysteine-seleocysteine sequence critical for activity. TrxR has an important role in the function of selenium in cellular systems, metabolising several selenium compounds.

Trx is not the exclusive substrate of TrxR. Several other protein disulphides and oxidised low molecular weight compounds can be utilised instead. The initial stages of catalysis are common to the other pyridine nucleotide-disulphide oxidoreductases, involving the transfer of electrons from NADPH via the FAD group, to the active site disulphide. The subsequent stages involve the transfer of electrons to a selenylsulphide formed by the Cys-selenocysteine pair at the C-terminus of the adjacent subunit in the homodimer. The reduced selenolthiol group can then reduce Trx, which can subsequently reduce protein disulphides non-enzymatically.

$$2H_2O_2 \longrightarrow O_2 + 2H_2O$$
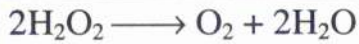
Equation 1a: Catalase reaction

$$H_2O_2 + R'H_2 \longrightarrow R' + 2H_2O$$

Equation 1b: Catalase detoxification of phenols and alcohols

$$ROOH + 2GSH \longrightarrow ROH + GSSG + H_2O$$

$NADP^+$ ◄─── GR ─── $NADPH + H$
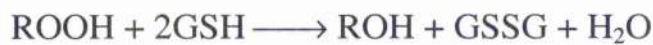
Equation 2: Reaction catalysed by Glutathione Peroxidase

Glutathione (GSH), glutathione disulphide (GSSG), glutathione reductase (GR), hydroperoxide (ROOH) and alcohol (ROH).

Substrate$_{ox}$ $NADPH + H^+$ $Trx\text{-}S_2$ Protein-(SH_2)/Product$_{red}$

TrxR

Product$_{red}$ $NADP^+$ Trx-(SH_2) Protein-S_2/Substrate$_{ox}$
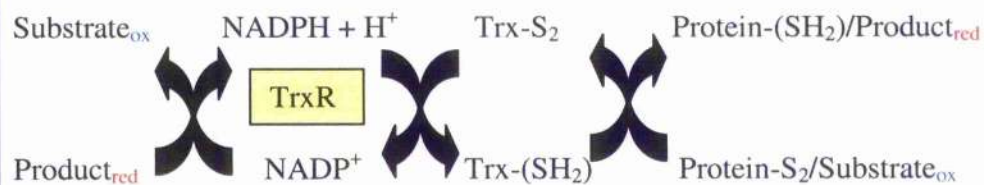
Equation 3: The reaction scheme of the Thioredoxin system

Thioredoxin (Trx), thioredoxin reductase (TrxR), disulphide (S-S), sulphydryl groups (-SH). Oxidised and reduced states are highlighted in blue and red font respectively.

Figure 1.5. Reactions Catalysed by the Key Antioxidant Systems

TrxR can independently exhibit antioxidant activity via the direct reduction of peroxides; however this typically only occurs at elevated levels of peroxides. Regulation by negative feedback also occurs as TrxR activity is inhibited by hydrogen peroxide. Inhibition of the Trx system in general will result in pro-oxidant effects. Recent interest in the Trx system is with respect to removal of hydrogen peroxide by the thioredoxin system, in conjunction with a novel family of antioxidant enzymes called the peroxiredoxin (Prx) family (Chae *et al*, 1994a)

1.8. The Peroxiredoxins

The bacterial enzyme alkylhydroperoxide reductase (AhpC), later called the thiol-specific antioxidant (TSA) protein, gave the Prx family their original name-the AhpC/TSA family. AhpC and a second component called AhpF, a member of the FAD-dependent protein-disulphide reductase family, participate in a system that catalyses the NADH-dependent reduction of organic hydroperoxides (or hydrogen peroxide) to the corresponding alcohol and water (Fig.1.6a) (Poole *et al*, 1996; Poole *et al*, 2000). Recently AhpC has also been shown to catalyse the detoxification of peroxynitrite to nitrite at an extremely rapid rate, implying that the peroxidase function of the Prxs may extend to reactive nitrogen species too (Bryk *et al*, 2000). In the case of mammalian Prxs, the reducing equivalents are provided by the thioredoxin system (Fig.1.6b). Prxs are distinct from other peroxidase families by lacking a cofactor (Rhee *et al*, 1999). The diverse functions of the Prxs include roles in complex cell-signalling cascades, transcriptional regulation, apoptosis, immunity and infection; however the recent major focus of research concerns their antioxidant properties (Kang *et al*, 1998b).

This emerging family of enzymes has been shown to reduce peroxides both *in vitro* and *in vivo* using thiol groups as a source of electrons. The Prxs can be divided into two groups (1-Cys and 2-Cys), depending on the number of conserved cysteine residues they possess within their primary sequence. There
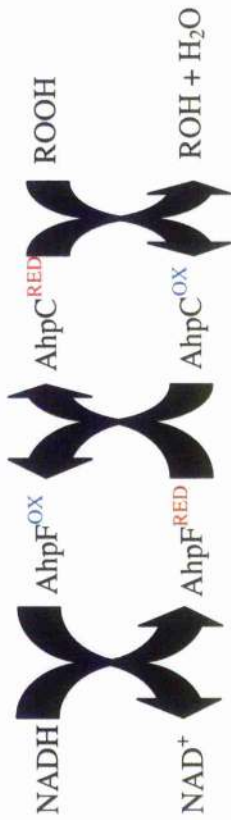
Figure 1.6a. The Alkylhydroperoxide Reductase System

Alkylhydroperoxide (ROOH), alcohol (ROH), oxidised form (OX), and reduced form (RED).
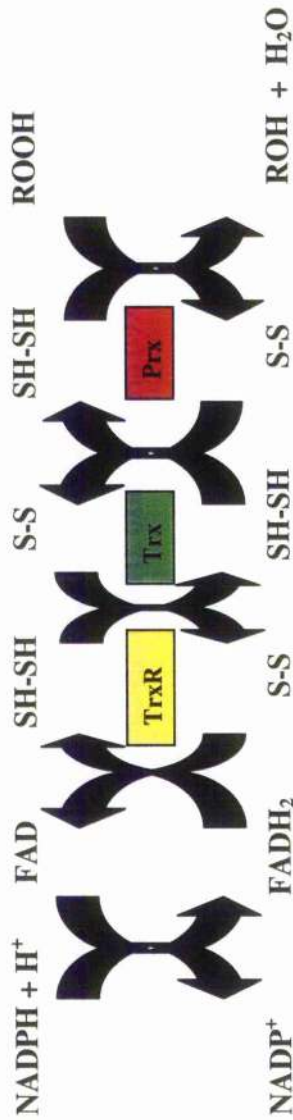
Figure 1.6b. The Sequence of Electron Transfer During Catalysis by the 2-Cys Peroxiredoxins

Peroxiredoxin enzyme (Prx), thioredoxin (Trx), thioredoxin reductase (TrxR). The oxidised form of the enzyme (S-S), the reduced form (SH), alkylhydroperoxide (ROOH) and corresponding alcohol (ROH).

are to date approximately thirteen mammalian Prx members that are further classified into at least five distinct groups numbered Prx I to VI, according to their amino acid sequence, tissue distribution and cellular localisation. The Prx I-V groups are all 2-Cys enzymes whereas Prx VI represents the 1-Cys subgroup.

1.8.1. The 1-Cys Peroxiredoxins

1-Cys members are homodimers containing a single cysteine residue located at the N-terminus which is the catalytic residue (Kang et al, 1998a). In vitro small thiol reducing agents such as dithiothreitol (DTT) and ascorbic acid (vitamin C) are suitable donors. For the majority of cases it been determined that Trx or GSH cannot replace these reducing agents. To date there is only one example of a 1-Cys Prx that uses the thioredoxin system. It was isolated from Saccharomyces cerevisiae and was demonstrated to have an integral role in protection against oxidative stress (Pedrajas et al, 2000). The in vivo physiological electron donor for the remaining 1-Cys sub-group remains to be identified; however recent research has identified cyclophilin A (CyP-A) as an electron donor for the 1-Cys Prxs and possibly the 2-Cys Prx isoforms (Lee et al, 2001). Cyclophilins are a prokaryotic and eukaryotic protein family that have the ability to bind the immunosuppressive drug, cyclosporin A (CsA). They also have peptidyl-prolyl cis-trans isomerase catalytic activity, and participate in protein folding and protein interactions. CyP18 is a cyclophilin located in human T-cells that has been reported to bind to the 2-Cys Prx Aop1 stimulating its activity (Jaschke and Tropschug, 1998).

1.8.2. The 2-Cys peroxiredoxins

The 2-Cys enzymes, as their name suggests, contain two redox-active cysteine residues positioned at the N- and C-terminal regions of the protein. It is not uncommon for a third cysteine residue to be present although this feature varies between members. Comparable with the 1-Cys subgroup, the N-terminal cysteine is the site of catalysis. 2-Cys Prxs are also homodimeric but can form intermolecular disulphide bonds between the N-terminal residue of one monomer and the C-terminal cysteine of the opposing subunit. The 2-Cys Prxs differ from

the 1-Cys Prxs not only in the number of conserved cysteines but also in their source of reducing equivalents. The 2-Cys Prxs are generally referred to as Trx-dependent peroxidases as *in vivo* these enzymes were initially proposed to exclusively utilise Trx as their electron donor (Chae *et al*, 1999). As mentioned earlier a new report suggests that they may also be reduced by cyclophilins.

1.8.3. The Catalytic Mechanism of the Peroxiredoxins

Mutation analysis has established that the active site of the both Prx subgroups is the conserved N-terminal cysteine (Chae *et al*, 1994b). X-ray crystallography of the human 1-Cys Prx open reading frame protein 6 (hORF6), elucidated that the active site sulphydryl group is oxidised to a sulphenic acid, an early stage intermediate of catalysis (Choi *et al*, 1998; Peshenko and Shichi, 2001). Sulphenic acid groups serve as reversible two-electron oxidation states that can either be reduced to the initial thiol or oxidised further to sulphinic acid. In 1-Cys Prxs, the active site cysteine is located at the bottom of a narrow active-site pocket making it inaccessible to the bulk solvent. This implies the occurrence of a conformational change in the active-site region during catalysis. The sulphenic acid group is stabilised via interactions with two positively charged amino acids- a histidine and an arginine. An interaction between the sulphenic acid and a magnesium ion has also been suggested. It is proposed that these stabilising associations function to lower the pK_a of the active-site cysteine, therefore enhancing its reactivity. *In vivo* the sulphenic acid residue of the 1-Cys Prxs is reduced back to its thiol group by cyclophilin A, but not Trx or GSH as mentioned previously.

Studies on the 2-Cys Prx haem-binding protein 23kDa (HBP23), the rat homologue of the human proliferation-associated gene product (PAG), have provided an insight into the catalytic mechanism of the 2-Cys Prxs. PAG was previously called natural-killer enhancing factor A due to its initial role in enhancing the action of natural killer cells which provide a first line of defence against tumours by targeting and destroying several types of tumour cells. The tissue expression of both HBP23 and PAG, and in fact numerous Prx members, is

induced by oxidative stress (Mitsumoto *et al*, 2001). Additional functions of HBP23 include the control of cell differentiation and proliferation. In fact PAG can directly interact with the cell signalling protein tyrosine kinase c-Abl. This protein exerts a cytostatic effect on cell growth; therefore it is proposed that PAG may counteract this effect (Wen and Van Etten, 1997).

Structural studies on HBP23 illustrate clearly that the 2-Cys Prx active-site residue forms an intermolecular disulphide bond with the C-terminal cysteine of the opposing subunit. Several hydrophobic residues encase this disulphide interaction. As with hORF6, the active-site cysteine is completely buried in the active site channel, therefore rendering it inaccessible to the solvent interface. It is postulated that the active site residue is only buried in its oxidised state (Cys-SOH) and is completely accessible to hydrogen peroxide in its reduced form (Cys-SH).

The initial stage of catalysis involves the oxidation of the N-terminal cysteines on both subunits to a Cys-SOH by hydrogen peroxide or alkyl hydroperoxides (Fig.1.7- step 1). This moiety spontaneously reacts with the C-terminal cysteine of the opposing subunit to form an intermolecular disulphide bond, coupled with the elimination of water (Fig.1.7-step 2) (Seo *et al*, 2000). In order for the 2-Cys Prx to be regenerated back to its active state, the disulphide bonds are reduced by Trx or DTT in the artificial system (Fig.1.7-step 3). The reduction of the resulting intramolecular disulphide bond formed within Trx is carried out by the cognate flavoenzyme TrxR.

There are two alternative fates of the Prx enzyme following the initial oxidation step; the sulphenic acid groups may be further oxidised to sulphinic ($-SO_2H$) or sulphonic ($-SO_3H$) acid groups. As these higher oxidation states are irreversible, the enzyme becomes trapped in its inactive conformation.
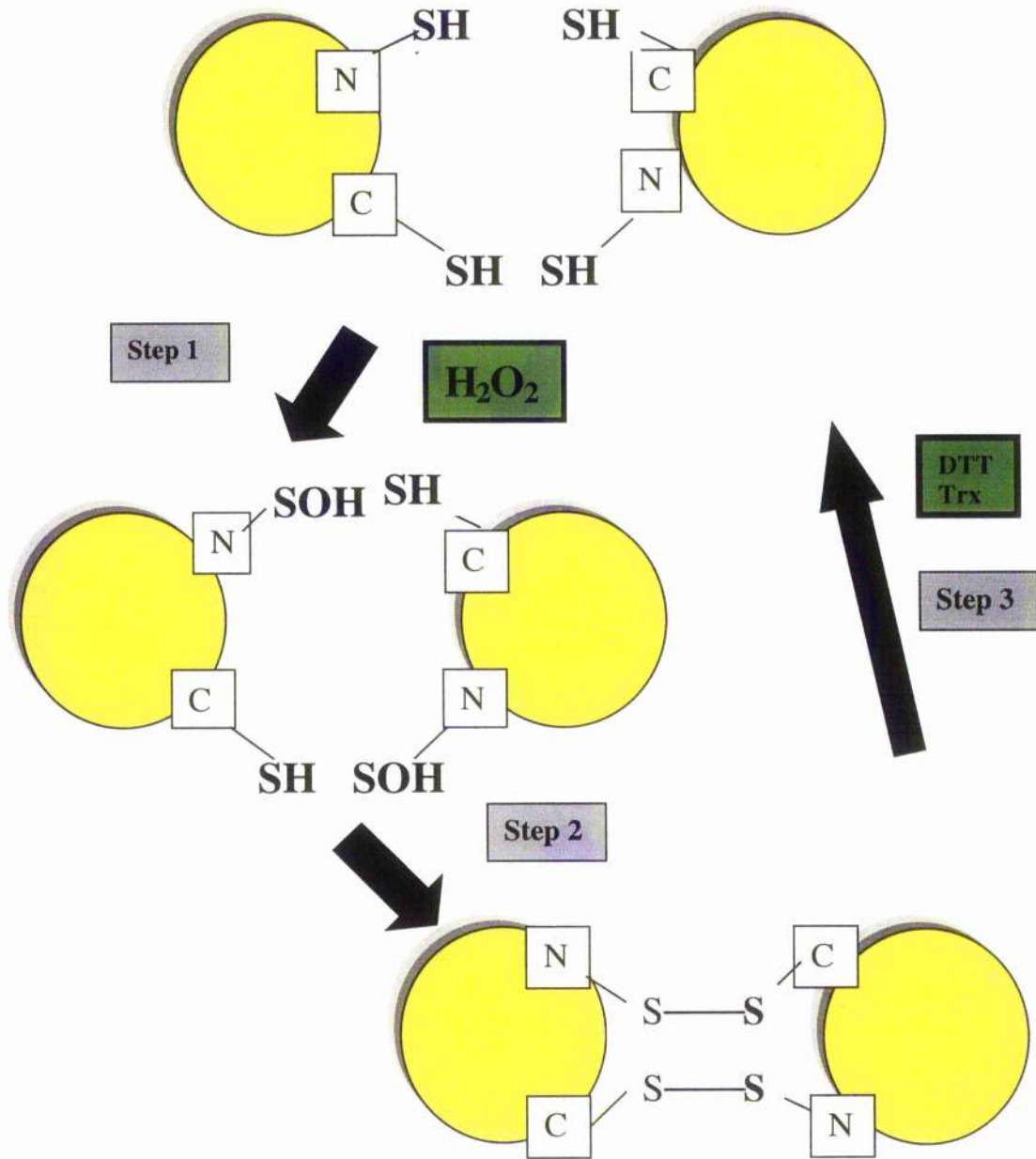
Figure 1.7. Proposed Catalytic Mechanism of The 2-Cys Peroxiredoxins

Sulphydryl group (-SH), sulphenic acid (-SOH), disulphide bond (S-S), dithiothreitol (DTT), thioredoxin (Trx), hydrogen peroxide (H_2O_2) and C- and N-terminal cysteines.

1.8.4. Peroxiredoxin Oligomers

To date, the oligomeric conformations of several Prxs of both the 1-Cys and 2-Cys sub-groups have been successfully determined by various techniques, including electron microscopy and X-ray crystallography. Typically both 1-Cys and 2-Cys Prxs exist as homodimers (α_2), linked mainly via hydrophobic interactions. A second, toroidal decameric form comprising five dimeric units ($\alpha_2)_5$ is an increasingly recurring theme, particularly for the 2-Cys members. One of the first structures to be solved was that of HBP23, which has been identified to form a dimer, comprising two tightly associated monomers, flattened and ellipsoidal in shape (Hirotsu et al, 1999). The principal interactions involved in dimerization are hydrogen bonds, hydrophobic interactions, salt bridges and Van der Waals forces. A feature, ubiquitously observed throughout the 2-Cys Prx members is disulphide bond formation between the conserved cysteine residues of the C- and N-terminal regions of opposing subunits, in a head-to-tail interaction. This oxidised form of the protein is a likely peroxidation reaction intermediate.

The human erythrocyte 2-Cys Prx called thioredoxin-peroxidase-B (TPx-B), previously named natural-killer enhancing factor B, has been shown to adopt a ring-like decameric form comprising five disulphide-linked dimeric units (Fig.1.8) (Schroder et al, 1999; Schroder et al, 2000). TPx-B is the third most abundant protein in erythrocytes functioning to increase natural killer cytotoxicity against tumour cells, hence its original name. Sequence analysis assigned TPx-B to the Prx family and its antioxidant role was confirmed (Shau and Kim, 1994; Shau et al, 1997). In atherosclerosis, monocyte recruitment and adhesion to the arterial wall triggered by the presence of oxidised low density lipoproteins (LDL) and lipopolysaccharides (LPS) is a characteristic feature. An in vitro binding assay demonstrated that TPx-B blocks monocyte attachment to endothelial cells reinforcing its role in increasing cellular resistance to oxidative stress (Kim et al, 1997).
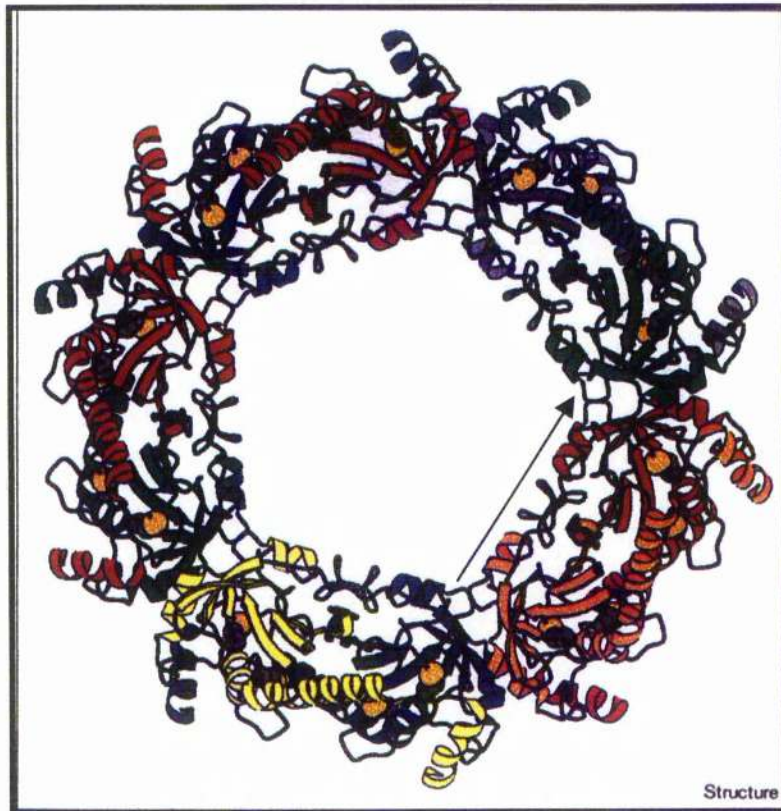
Figure 1.8. Decameric Toroidal Structure of TPxB

This diagram shows the decameric structure of the human erythrocyte 2-Cys peroxiredoxin, Thioredoxin Peroxidase-B (TPx-B). The pentagonal symmetry of the central cavity is clearly observed. The arrow indicates one dimeric unit. (Adapted from Schroder *et al*, 2000).

The decameric structure of TPx-B was determined by molecular replacement using the co-ordinates of the dimeric 1-Cys Prx, hORF6 as a search model. The interactions between the dimers are weaker than monomer-monomer interactions. It has become apparent that decameric toroids are a common feature of Prxs, supported by recent reports demonstrating that hORF6 may also adopt this conformation.

The structure of one mitochondrial 2-Cys Prx, PRDX5 has been elucidated (Declercq et al, 2001). It is not exclusively mitochondrial, however, and is also found in peroxisomes and cytosol implying a broader range of functions. The peroxisomal location implies a critical role as an antioxidant given the elevated levels of ROS generated in this compartment. As previously mentioned, Prxs have a role in modulating hydrogen peroxide-mediated cellular responses. It has become apparent that PRDX5 expression is upregulated in degenerative human tendon and cartilage tissue, characteristic in ageing and osteoarthritis (Wang et al, 2001; Wang et al, 2002). Inflammatory cytokines including tumour necrosis factor α are involved in inducing increased expression of PRDX5 in these tissues by increasing intracellular ROS generation. The exact mechanism of PRDX5 upregulation is not understood, however hydrogen peroxide concentration is certainly contributory given that the presence of catalase in cultured chondrocytes prevented elevated mRNA levels of PRDX5.

PRDX5 represents a novel type of mammalian Prx possessing a distinctive structure in comparison with other members. Despite the high amino acid conservation including the three conserved cysteine residues, it does not form a dimer or a decamer and for reasons that are unclear remains exclusively as monomers. A further distinguishing feature is the presence of an intramolecular disulphide in comparison to the intermolecular disulphides present in the 2-Cys Prxs.

By comparing the oxidised and reduced states of a select few 2-Cys Prxs, it is proposed that these enzymes inter-convert between these two oligomeric forms regularly during catalysis (Wood et al, 2002). The factors that determine the transition remain to be elucidated; however in vitro decamer stability may be affected by changes in pH, with dissociation into dimers favoured above pH 7.0. Furthermore,

high ionic strength and oxidative conditions have been shown to promote decamer stability. It has been suggested that the decameric structure is prevalent following oxidation of the N-terminal cysteine, to sulphenic acid, implying that this form may be adopted in response to oxidative stress. Electron microscopy has raised the possibility of toroid stacking, via the interaction of adjacent decamers (Harris *et al*, 2001). This feature is not uncommon and has been observed with the molecular chaperone GroEL.

1.9. SP-22

SP-22 is a small (22kDa) bovine mitochondrial protein, so-called due to its initial identification as a substrate of a mitochondrial ATP-dependent protease (Watabe *et al*, 1993; Watabe *et al*, 1994). It is exclusively located in the mitochondrial matrix constituting approximately 5% of total matrix protein. Previous work investigating SP-22 is limited; therefore its exact physiological function and biochemical mechanism remains to be elucidated. However in the available literature its role as a free-radical scavenger has been well documented, functioning with thioredoxin-dependent peroxidase activity accounting for its recent assignation to the Prx family (Watabe *et al*, 1995; Watabe *et al*, 1997). NADPH as in all 2-Cys Prx reactions is the ultimate source of reducing equivalents for the SP-22/Trx system.

SP-22 has been demonstrated to protect several free-radical sensitive enzymes from oxidative damage *in vitro* including glutamine synthetase and enolase. The antioxidant activity of SP-22 has been further supported in studies illustrating that the expression of SP-22 is enhanced in bovine aortic endothelial cells and mouse placenta when subjected to various oxidative stresses (Araki *et al*, 1999; Ejima *et al*, 2000). This implies a possible protective role for SP-22 in the cardiovascular system and placental mitochondria, respectively.

1.9.1. The Primary Structure of SP-22

The complete amino acid sequence of SP-22 has been determined in both its precursor and mature forms (Hiroi *et al*, 1996). Figure 1.9. shows the coding sequence of SP-22 and its homology with the 2-Cys Prx members, HBP23 and TPx-B. It can be seen that the degree of homology is ≥90%. SP-22 contains a 62 amino acid long

mitochondrial targeting presequence that is subsequently cleaved upon entry in the mitochondrion, allowing the protein to fold correctly. In accordance with other 2-Cys Prxs, SP-22 contains a catalytic N-terminal cysteine (C47), a C-terminal cysteine (C168) and a third conserved cysteine (C66). By sequence analysis of mature SP-22 C47 was proposed to be the site of catalysis as it contained a sulphinic acid group. In its native state it was postulated that the C47 side-group is a sulphenic acid group, enabling it to function as a two-electron redox centre-a common feature of both 2-Cys Prxs and redox proteins in general.

1.9.2. The Function of SP-22

Although SP-22's role as an antioxidant protein has been well documented, the exact physiological function of SP-22 remains to be elucidated. Within the cellular compartment peroxides are mainly scavenged by the catalase and GPx systems. As mentioned previously the enzymatic systems responsible for removal of oxidising species within the mitochondrial compartment include the SOD system, the GPx system, the Trx system and in one report catalase (rat heart). It is possible that SP-22 in conjunction with the Trx system could offer an additional line of defence against oxidative stress. As mitochondria are the site of aerobic respiration, any oxidative damage to participating enzymes would severely compromise cellular function and the organism's viability as a whole. Therefore a requirement for several scavenging systems acting in concert may be essential in this case.

1.9.3. Why Investigate SP-22?

The interest in SP-22 arose following the purification of the dihydrolipoamide dehydrogenase (E3) component from the bovine heart pyruvate dehydrogenase complex (PDC). The purification of PDC or OGDC was carried out under associative conditions and the enzyme components were separated by gel exclusion chromatography using a FPLC system. An additional protein initially believed to be a contaminant in PDC/OGDC preparations was identified to co-elute with the E3 component. Subsequent N-terminal amino acid sequencing elucidated the first 24 residues of the protein, and established that the unidentified protein had high amino acid identity with bovine SP-22.

```
                   10        20        30        40        50        60
                    |         |         |         |         |         |
Contig# 1   *||  ||
HBP23       MSSGNAK---------------------------------------------------|---IGH
TPx-B       MSSGNAR---------------------------------------------------▼--IGK
SP-22       MAATAGRLFRASLIRHVSAIPWGISASAALRPAASRRMCLTNALWSGSDQAKFAFSTSSSYHAPAVTQ

                   70        80        90       100       110       120       130
                    |         |         |         |         |         |         |
Contig# 1   ** **|***|  *  **||  *  *|****|*|*****************|     |  *|*||  **
HBP23       PAPSFKATAVMPDGQFKDISLSDYKGKYVVFFFYPLDFTFVCPTEIIAFSDRAEEFKKLNCQVIGASV
TPx-B       PAPDFKATAVV-DGAFKEVKLSDYKGKYVVLFFYPLDFTFVCPTEIIAFTTVKRTSAKLGCEVLGVSV
SP-22       HAPYFKGTAVVS-GEFKEISLDDFKGKYLVLFFYPLDFTFVCPTEIIAFSDKASEFHDVNCEVVAVSV

                   140       150       160       170       180       190       200
                    |         |         |         |         |         |         |
Contig# 1   **|* *********|*|**** |**|*||*  |  || *****   | *||!******* |*|||!||!|**
HBP23       DSHFCHLAWINTPKKQGGLGPMNIPLVSDPKRTIAQDYGVLKADEGISFRGLFIIDDKGILRQITIND
TPx-B       DSQFTHLAWINTPRKEGGLGPLNIPLLADVTRRLSEDYGVLKNDEGIAYRGLFIIDGKGVLRQITVND
SP-22       DSHFSHLAWINTPRKNGGLGHMNIALLSDLTKQISRDYGVLLEGPGLALRGLFIIDPNGVIKHLSVND

                   210       220       230       240       250
                    |         |         |         |         |
Contig# 1   *******|* ****|***|  |  ******* *  *   ****|   *|*** *  ||
HBP23       LPVGRSVDEILRLVQAFQFTDKHGEVCPAGWKPGSDTIKPDVNKSKEYFSK-QK
TPx-B       LPVGRSVDEALRLVQAFQYTDEHGEVCPAAWKPGRDTIKPNVDDSKEYFSK-HN
SP-22       LPVGRSVFETLRLVKAFQFVEAHGEVCPANWTPESPTIKPHPTASREYFEKVNQ
```

Figure 1.9. Protein Sequence Alignment of SP-22, HBP23 and TPx-B

The start of the mature sequence of SP-22 is indicated by the arrow. The conserved cysteine residues are shown in blue. Residue identity between sequences is indicated by dots. Alignment is between SP-22, the rat 23kDa haembinding protein (HBP23) and human thioredoxin peroxidase-B (TPx-B) 2-Cys peroxiredoxins.

This co-purification suggests a possible interaction between SP-22 and E3, which may help determine the exact physiological function of SP-22 within the mitochondrion.

Such an interaction is not an unlikely suggestion as E3 has high sequence homology with the C-terminal portion of AhpF, and SP-22 has high homology with AhpC. Furthermore in *Mycobacterium tuberculosis* (Mtb) which exhibits an extremely powerful antioxidant defence system, the AhpC component of the alkyl hydroperoxide reductase system has recently been demonstrated to interact with E3 and the dihydrolipoamide succinyltransferase (E2) component found in the 2-oxoglutarate dehydrogenase complex (OGDC) (Bryk *et al*, 2002). AhpC is shown to interact with E3 and E2 via an adaptor protein called AhpD, together constituting a NADH-dependent peroxidase system facilitating the removal of peroxides and peroxynitrite.

1.10. The Mitochondrial 2-Oxoacid Dehydrogenase Complexes

The 2-oxoacid dehydrogenase complexes are a family of mitochondrial matrix enzymes that participate in carbohydrate and amino acid metabolism. PDC, OGDC and the branched-chain 2-oxoacid dehydrogenase complex (BCOADC) are all members of this family, and are individually responsible for the irreversible oxidative decarboxylation of their cognate 2-oxoacid substrates (McCartney *et al*, 1998). The general reaction catalysed by the 2-oxoacid dehydrogenase complexes is illustrated in Fig.1.10). The products of oxidative decarboxylation are an acyl CoA derivative, NADH and CO_2. The reactions follow a precise, consecutive, multi-step mechanism, each catalysed by one of three distinct enzyme components designated as E1, E2 and E3 that together constitute the overall multi-enzyme complex (Patel and Roche, 1990). An additional enzyme component called the E3-binding protein (E3BP), previously named protein X is also a component of eukaryotic PDC (McCartney *et al*, 1997). The importance of the 2-oxoacid dehydrogenase complexes has been underlined with the identification of specific mutations giving rise to various metabolic disorders such

as congenital lactic acidosis and maple syrup urine disease (Patel and Harris, 1995).

1.10.1. The Individual Enzyme Components of PDC

PDC plays a pivotal role in the oxidation of pyruvate to acetyl coenzyme A (acetyl CoA) and is one of the largest multi-enzyme complexes identified to date with an immense M_r value of 9-10 x 10^6. The individual enzymes of PDC are pyruvate decarboxylase (E1), dihydrolipoyl acetyltransferase (E2) and dihydrolipoyl dehydrogenase (E3). PDC of mammalian origin is composed of a 60-meric E2 core with icosahedral symmetry. There are $30\alpha_2\beta_2$ E1 tetramers and 6-12 E3 homodimers, tightly but non-covalently bound along the edges and faces of the E2 core, respectively. In addition 12 copies of E3BP are found, tightly associated with the E2 core. The copy numbers of the enzyme components and symmetry of the E2 core varies between PDC species. Mammalian, yeast and gram-positive bacterial PDC all have 60-meric E2 cores with icosahedral symmetry. In contrast E2 cores from gram-negative organisms e.g. *E. coli* PDC and all sources of OGDC and BCOADC are organised as 24-meric octahedrons. The conditions for the complete subunit dissociation and subsequent reconstitution of PDC and OGDC activity have been established *in vitro* (Sanderson *et al*, 1996).

1.10.2. Pyruvate Decarboxylase (E1)

The E1 component of PDC is complex-specific existing as a homodimer in OGDC and a heterotetramer in PDC and BCOADC. The PDC E1 component catalyses the rate-limiting step of the overall reaction. E1 catalyses two partial reactions - the initial thiamine diphosphate (ThDP) –dependent decarboxylation of pyruvate and subsequent reductive acetylation step resulting in the covalent binding of an acetyl group to the prosthetic group of the E2 lipoyl domain (Hawkins *et al*, 1990). Studies in *Bacillus stearothermophilus* have elucidated that the E1α subunit houses the ThDP binding motif; however recognition of the lipoyl domain of the E2 subunit occurs across the interface spanning E1α and E1β (Howard *et al*, 2000; Perham, 1991).

1.10.3. Dihydrolipoyl Acetyltransferase (E2)

E2 is a 59.6kDa, complex-specific subunit that provides the scaffold for the overall multi-subunit structure of the 2-oxoacid dehydrogenase complexes. The E2 component is responsible for the transfer of the acetyl group from the lipoic acid moiety to CoA, producing acetyl CoA and a reduced lipoate group. During core assembly, the E2 subunits tend to form trimeric intermediates. The E2 component has a prominent multi-domain structure with each domain having a distinct role in complex function or assembly. In *Bacillus stearothermophilus* the C-terminal inner domain contains the active site and also mediates core oligomerisation. A 35 amino acid long region called the peripheral subunit-binding domain, responsible for E1 and E3 binding follows this domain. The final region of E2 can be composed of one to three, 80 amino acid long lipoyl domains, depending on the source of PDC. Mammalian E2 PDC contains two lipoyl domains, each with a prosthetic lipoic acid group attached via a key lysine residue (Patel and Roche, 1990). It has been established that E2 must be correctly folded with this key lysine residue exposed at the tip of a β-turn, for the lipoic acid moiety to be attached successfully by the lipoyl ligase enzyme (Liu *et al*, 1995). Extending between each lipoyl domain are linker regions 20 to 30 amino acids long, rich in alanine, proline and charged amino acids. The PDC reaction is easily executed due to the flexible nature of these inter-domain or hinge regions within the E2 structure, enabling easy access to all three active sites in a process termed substrate channelling or active site coupling (Wallis *et al*, 1996).

1.10.4. Dihydrolipoamide Dehydrogenase (E3)

E3 is the only enzyme component that is common to all the 2-oxoacid dehydrogenase complexes. E3 is a member of the pyridine nucleotide-disulphide oxidoreductase family of flavoproteins, together with TrxR, glutathione reductase and alkyl hydroperoxide reductase F (Carothers *et al*, 1989). There are four principal functional domains of E3; the FAD binding domain which contains the disulphide active site; the NAD^+ binding domain; the central domain and the interface domain. E3 exists as a homodimer, with one FAD molecule non-covalently bound per subunit, and functions to re-oxidise the reduced lipoic acid
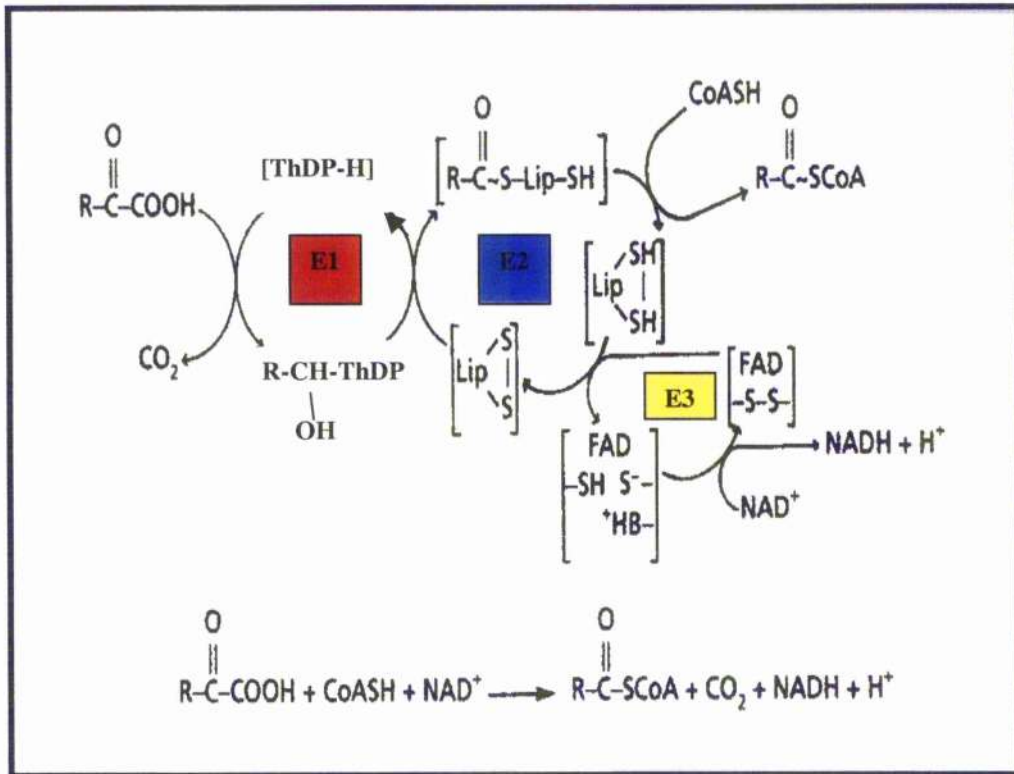
Figure 1.10. Catalytic Mechanism of the 2-Oxoacid Dehydrogenase Complexes and the Overall Reaction Summary

The oxidative decarboxylation of 2-oxoacid substrates by the individual enzyme components of the 2–oxoacid dehydrogenase complexes. R= CH_3 for PDC, R= CH_2CH_2COOH for OGDC, and R= $CH(CH_3)_2$, $CH_2CH(CH_3)_2$ or $CH(C_2H_5)CH_3$ for BCOADC. CoA= Coenzyme A, Lip = lipoic acid, ThDP = Thiamine diphosphate.

moiety of E2, progressing via an intermediate step in which two electrons from the dihydrolipoamide moiety are shared between the FAD and the reactive disulphide centre before being donated to NAD^+. *In vitro* it has been shown that E3 can also work in reverse, transferring reducing equivalents from exogenous NADH to E2, thereby reducing the lipoamide group.

1.10.5. E3-Binding Protein (E3BP)

E3BP may also participate in electron transfer; however its principal role is to facilitate E3 binding to the E2 core, hence its name. E3BP has a prominent multi-domain structure similar to that of E2. It contains only a single lipoyl domain although it does not exhibit acetyltransferase activity like E2.

1.10.6. 2-Oxoacid Dehdrogenase Complexes as Targets of Oxidative Stress

As mentioned previously (Section 1.4.2), studies were carried out to identify the principal enzyme targets of oxidative stress. The most susceptible enzymes were shown to be the 2-oxoacid dehydrogenase complexes, particularly OGDC. Indeed, OGDC inactivation by ROS is proposed to be responsible for the decrease in brain metabolism identified in several neuropathologies (Gibson *et al*, 2000). It is proposed that the lipoic acid group of E2 may be the target of such oxidation. To confirm this, a polyclonal antibody that recognises the lipoic acid group of E2 was raised. A corresponding decrease in recognition of the lipoic acid group with an increase in carbonyl content of E2 was observed, suggesting that it is the main target of oxidation (Cabiscol *et al*, 2000).

A more indirect SP-22 function with respect to E3 and E2 could be to serve to scavenge the RSS generated as a result of thiol damage or scavenge the free radicals that target the thiol groups. SP-22 could function to protect such damage with respect to the 2-oxoacid dehydrogenase complexes and other proteins containing vulnerable chemical groupings. E1 contains reactive cysteines and E2 and E3 contain reactive sulphydryl groups, which are potential targets for oxidative damage and can be detected using N-ethyl $(2,3,-^{14}C)$ maleimide (NEM), shown in Fig.1.11 (Hodgson *et al*, 1986). The reactive cysteines of E1 were

detected in the absence or presence of substrate pyruvate or NADH; however the sulphydryl groups of E2 and E3BP were only available for modification when these components were present. This is due to the requirement that E2 and E3BP are in their reduced form for the sulphydryl groups of the lipoic acid cofactors to be accessible to the NEM. Although E3 employs reactive disulphide for catalysis its sulphydryl groups were not labelled by the NEM, implying that they are buried within the structure, preventing their modification.

Trx is reported to activate the 2-oxoacid dehydrogenase complexes by forming specific protein–protein interactions, suggesting a clear involvement in their regulation (Bunik *et al*, 1999). The thiol-disulphide oxidoreductase activity of Trx is vital for activation of the complexes as demonstrated by site-directed mutagenesis. It has been suggested in one report that both PDC and OGDC have the same Trx isoform preference, indicating E3 component involvement common to both complexes. Furthermore reports have suggested that Trx is competitive with E3 oxidation of the dihydrolipoamide intermediate, and can also oxidise E2.
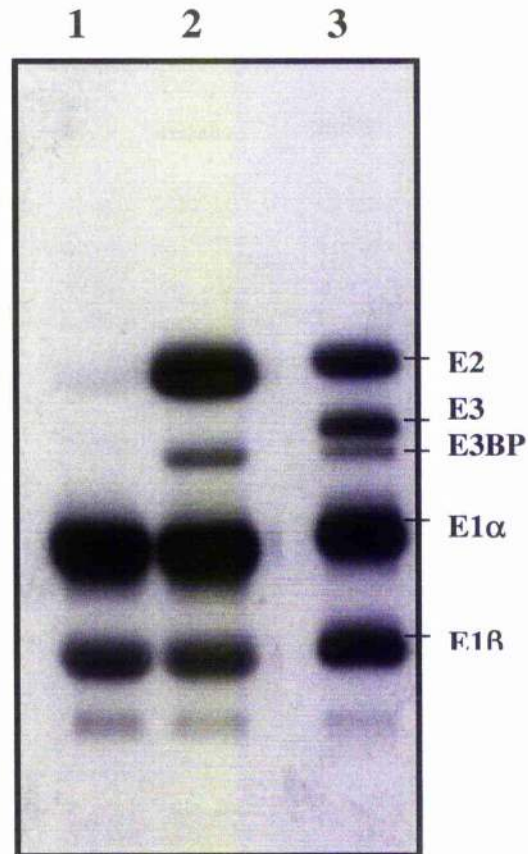
Figure 1.11. Identification of the Reactive Sulphydryl Groups of the Components of PDC as Potential Targets of Oxidative Damage

PDC purified from bovine heart was pre-treated for varying lengths of time with N-ethyl (2,3-^{14}C) maleimide, in the absence (**Lane 1**) or presence (**Lane 2**) of NADH. **Lane 3** shows the radiolabelled, denatured complex as a marker for all the individual enzymes. (Adapted from Hodgson *et al.*, 1986).

1.11. Project Aims

There are three principal areas of investigation considered in this thesis: the structure and function of SP-22, and the elucidation of any possible interaction between SP-22 and E3 of PDC. To address these questions, it was necessary to generate high yields of pure SP-22. This was achieved, constructing SP-22 as a histidine-tagged recombinant fusion protein (Chapter 3).

Analysis by non-reducing SDS-PAGE demonstrated that the building unit of SP-22 is a dimer, containing two intermolecular disulphide bonds. Site-directed mutagenesis and Ellman's assay were carried out to establish the cysteines responsible for dimerization (Chapter 3). An additional oligomeric form, corresponding either to a decameric or dodecameric toroid, was established by gel exclusion chromatography and transmission electron microscopy (Chapter 5). Analytical ultracentrifugation (AU) was adopted to obtain a more accurate molecular weight than gel exclusion chromatography. Circular dichroism (CD) and fluorimetry were used to ascertain the stability of SP-22, in addition to the influence of the disulphide interactions on oligomer integrity (Chapter 4).

In the available literature the activity of SP-22 (purified from bovine sources) was assessed by monitoring its protective activity towards several free-radical-sensitive enzymes. This thesis reports the reproduction of these protection assays for recombinant SP-22 using enolase, native bovine E3, PDC and OGDC as the susceptible targets (Chapter 6).

To make clear whether a physical SP-22/E3 interaction occurs, Isothermal Titration Calorimetry (ITC) and Surface Plasmon Resonance (SPR) were used (Chapter 7). Furthermore, the functional significance of such an interaction is discussed in more detail.

Chapter 2

2.1.0. Molecular biology materials

2.1.1. Bacterial Strains

Escherichia coli DH5α (Stratagene, Amsterdam, The Netherlands) and *Escherichia coli* DE3 pLysS (Novagen, Nottingham, UK) bacterial strains were used for propagation of plasmid vectors and the expression of recombinant proteins employing the pET vector system, respectively.

2.1.2. Chemicals

Duchefa (Haarlem, the Netherlands) supplied the chemicals for the bacterial media. Roche Diagnostics Ltd., East Sussex, UK, supplied the agarose. Ampicillin was purchased from Sigma Chemical Co, Poole, Dorset, UK. Diaminoethanetetra-acetic acid (EDTA) and isopropyl-β-D-thiogalactopyranoside (IPTG) were bought from Melford Laboratories Ltd, Suffolk, UK. Sodium dodecyl sulphate (SDS) was purchased from BDH Laboratory Supplies, Poole, Dorset, UK. The PCR nucleotide mix was purchased from Promega, Southampton, UK. All standard chemicals and buffers were of analytical grade or above.

2.1.3. Enzymes

Restriction endonucleases and calf intestinal alkaline phosphatase (CIAP) were purchased from Roche. T4 DNA ligase, *Pfu* DNA polymerase, and Dpn I were purchased from Promega.

2.1.4. Plasmid Vectors

PET-14b was purchased from Novagen. Recombinant human E3/pET-14b was previously cloned and kindly provided by Dr. Audrey Brown (see Fig. 2.1 for the pET-14b vector map).
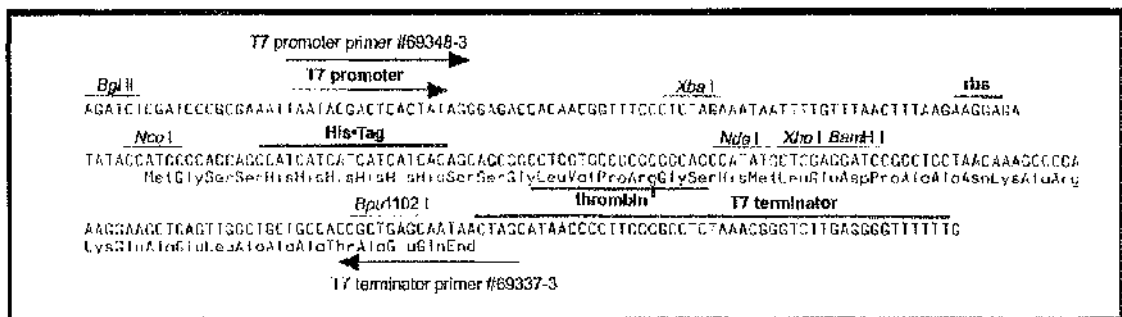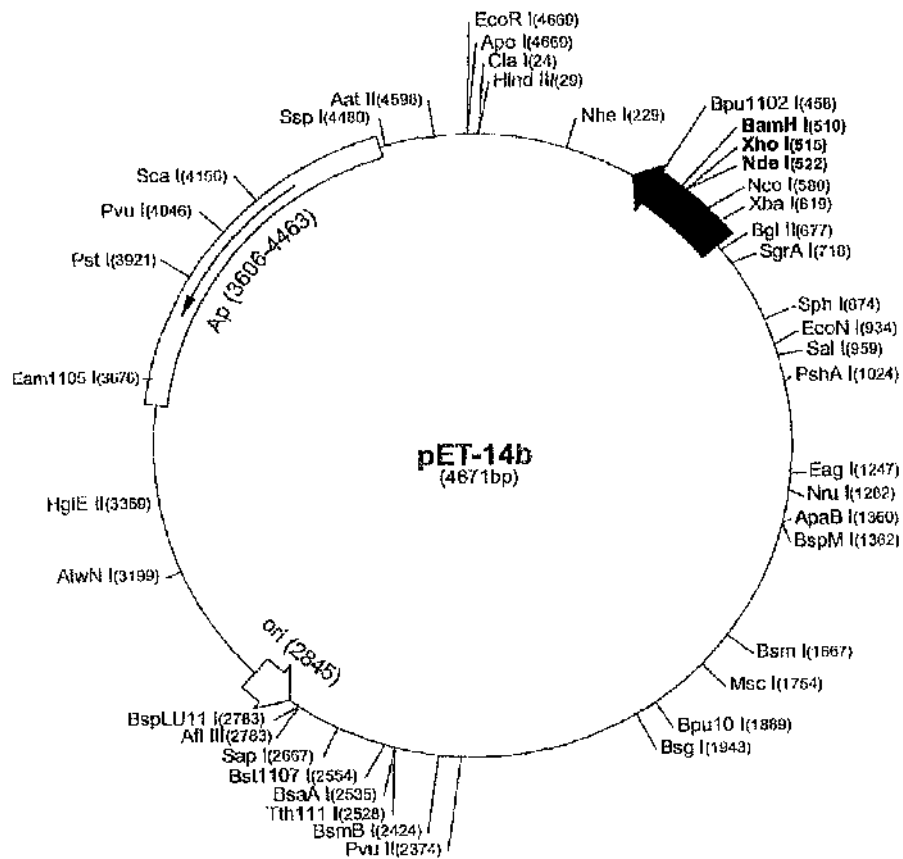
pET-14b
(4671bp)

Figure 2.1. Circular Map and Cloning/Expression Region of the pET-14b Vector

There is an N-terminal His-tag® sequence followed by a thrombin site, and three cloning sites (BamHI, XhoI and NdeI). The cloning/expression region transcribed by T7 RNA polymerase is shown in the box, numbered using the pBR322 convention; therefore the T7 expression region on the circular map is reversed.

2.1.5. Synthetic Oligonucleotides

Primers for gene amplification by PCR were designed in the laboratory and synthesized on the 50nmole scale by GIBCO BRL, Paisley or GenoSys Biotechnologies (Europe) Ltd., Cambridgeshire. Mutagenic primers were also designed in the laboratory and synthesized by Sigma (50nmole scale) including a PAGE purification step.

2.1.6. Plasmid DNA Purification Kits

Wizard® *Plus* Mini Preps and Maxi Preps DNA purification systems were purchased from Promega. The QIAquick Gel Extraction kit for DNA purification was purchased from QIAGEN Ltd. The QuikChange™ Site-Directed Mutagenesis Kit containing *Pfu Turbo* DNA polymerase was obtained from Stratagene.

2.1.7. DNA Molecular Weight Markers

The 1kb DNA Step Ladder, supplied with Blue/Orange Loading Dye (6X) was purchased from Promega. Low DNA Mass™ Ladder was obtained from Invitrogen™ Ltd, Paisley.

2.1.8. Photographic Equipment

Photographs were taken using a Polaroid DS34 direct screen-imaging camera and recorded on MITSUBISHI K65HM-$_{CE}$ glossy thermal paper supplied by Amersham Pharmacia Biotech.

2.1.9. Nucleotide Accession Numbers

The nucleotide and protein sequence for SP-22 was obtained from the Entrez Nucleotide database (http://www.ncbi.nlm.nih.gov/entrez), accession number D82025.

2.2.0. Molecular Biology Methods

2.2.1. Growth of Bacterial Cells

Luria Broth (LB) (1% (w/v) bacto-tryptone, 1% (w/v) NaCl, 0.5% (w/v) yeast extract; pH 7.2) or LB/agar plates (LB containing 1% (w/v) Agar) were the growth media of choice for all bacterial strains. When appropriate, media was supplemented with ampicillin at $50\mu g/ml$.

SOC media, prepared immediately before use, was used in all transformation reactions. SOC media was filter-sterilized following the addition of 0.02% (w/v) glucose to sterile SOB media (2% (w/v) bacto-tryptone, 0.5% (w/v) yeast extract, 0.05% (w/v) NaCl, 10mM $MgCl_2$, 10mM $MgSO_4$; pH 7.0).

2.2.2. Bacterial Cell Storage

Cells could be stored for 1-2 weeks as colonies on agar plates at 4°C. Cells present in LB media could be stored for longer periods of several months at -80°C, when mixed with an equal volume of 20% (v/v) glycerol.

2.2.3. Initiating Bacterial Growth

Small volumes of frozen or liquid cultures, removed with a sterile loop were used to inoculate growth media or agar plates. Growth was achieved by overnight incubation (16h maximum) at 37°C.

2.2.4. Competent Cell Preparation

Bacterial strains were made competent for cloning and subsequent expression of target genes. Bacteria were grown overnight at 37°C on sterile LB/agar plates. A single colony was used to inoculate 5ml of LB media, and grown overnight at 37°C with shaking. The overnight culture was used to inoculate 100ml sterile LB, incubating at 37°C with shaking until an absorbance of 0.5 at 550nm was reached. The cells were transferred to a sterile polypropylene tube and cooled on ice for 15 min before harvesting by centrifugation at 3,500rpm for 15 min at 4°C in a

Beckman Allegra™ 6R centrifuge. The supernatant was decanted and the pellet resuspended in 20ml ice-cold, filter-sterilized buffer 1 (30mM potassium acetate, 100mM RbCl$_2$, 10mM CaCl$_2$, 50mM MnCl$_2$ and 15% (v/v) glycerol; pH 5.8). The tube was incubated for 5 min on ice prior to centrifugation as before. The supernatant was decanted and the pellet resuspended in 2ml ice-cold filter-sterilized buffer 2 (10mM MOPS, 75mM CaCl$_2$, 100mM RbCl$_2$ and 15% (v/v) glycerol; pH 6.5), then cooled on ice for 15 min. Aliquots of 20µl were stored at –80°C for several months.

2.2.5. Transformation of Bacterial Cells

Competent cells (50µl) were thawed on ice immediately prior to use. Typically 10-50ng of plasmid DNA was added to the bacteria, then mixed by gentle agitation and incubated on ice for 15 min. The sample was heat pulsed for 90 s at 42°C and placed on ice for 2 min. SOC medium (450µl) (see section 2.2.1) was added to the transformation mix and grown at 37°C for 45 min. Following incubation the cells were harvested by centrifugation for 1 min at 14,000rpm in a bench top microfuge. The supernatant was decanted and the pellet resuspended in 200µl SOC medium. The cells were spread evenly on an LB/agar plate containing the appropriate antibiotic for the plasmid vector and incubated overnight at 37°C.

2.3.0. DNA Techniques

2.3.1. DNA Gel Electrophoresis

DNA fragments were separated by agarose gel electrophoresis, prepared by dissolving the required amount of agarose, typically 0.7-2.5% (w/v) in (1X) TAE buffer, pH 7.6. TAE buffer was prepared as a (10X) stock in 1litre (11.4ml glacial acetic acid, 20ml 0.5M EDTA and 48.8g Tris-HCl, pH 8.0). The gel was placed in an electrophoresis tank and submersed in TAE buffer (1X). In general, 3µl loading buffer (50% (v/v) glycerol, 0.01% (w/v) SDS, 0.01% (w/v) bromophenol blue) was added to 5µl of DNA prior to electrophoresis which was carried out at 100 volts (V) and 250 mAmps (mA). DNA fragments were visualized on

ethidium bromide (EtBr) staining in distilled water (0.5-1µg/ml in dH₂O) for 30 min with shaking at room temperature. The gel was rinsed in dH₂O to remove background stain, and then visualized under 320nm UV light. Photographs were taken with a Polaroid DS34 direct screen-imaging camera, and recorded onto K65HM-$_{CE}$ glossy thermal film. Where necessary, linear DNA fragments were excised from the gel using a scalpel, and subsequently purified using a Qiagen DNA gel extraction kit.

2.3.2. Polymerase Chain Reaction (PCR) Amplification of Precursor and Mature Forms of SP-22

Precursor SP-22 previously cloned into the pCRScript plasmid vector was used as the template for the PCR reaction, catalyzed by *Pfu* DNA polymerase. The PCR reaction contained 5µl reaction buffer (10X), 1µl dNTP mix (0.25mM each of dATP, dCTP, dGTP, and dTTP), 1µl forward and reverse specific primers (Fig. 2.2.), and 1µl *Pfu* DNA polymerase (3U/µl) prepared in a total volume of 50µl with sterile dH₂O. Amplification was carried out in a PTC-100™ programmable thermocycler (MJ Research Inc.). The reaction cycle comprising six steps is shown below:

1. **2.** **3.** **4.** **6.**

60 s at 95°C→60 s at 95°C→60 s at 40°C→2 min at 72°C→ Hold at 4°C

5. 24 cycles
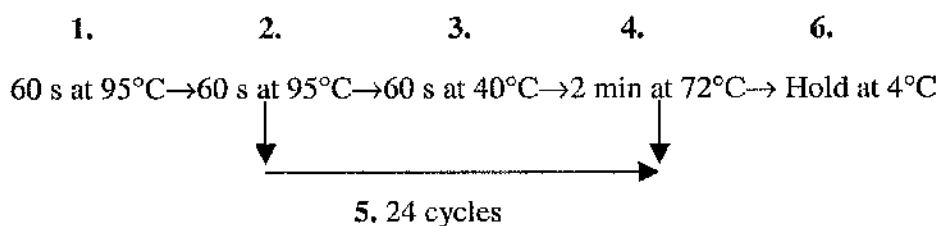
Successful amplification was determined by agarose gel electrophoresis.

Precursor SP-22 5' Primer:

5' - CAT AAC GGA TCC GGC GGC CAC GGC GGG - 3'

Mature SP-22 5' Primer:

5' - TTC CTC GGA TCC TGC CCC TGC CGT CAC CC - 3'

Reverse SP-22 3' Primer:

5' - CCG CCC GGA TCC CTA CTG ATT TAC CTT CTC - 3'

Figure 2.2. Specific Oligonucleotide Primers Designed for Amplification of the Precursor and Mature Forms of SP-22

BamH1 restriction endonuclease recognition sites are indicated in blue font. Start and stop codons are underlined.

a) **C47S 5′ Primer:** 5′-GATTTCACCTTTGTGAGTCCTACAGAAATC-3′

C47S 3′ Primer: 5′-CTAAAGTGGAAACACTCAGGATGTCTTTAG-3′

b) **C66S 5′ Primer:** 5′-CACGATGTGAACAGGGAAGTTGTGGCAGTG-3′

C66S 3′ Primer: 5′-GTGCTACACTTGTCGCTTCAACACCGTCAC-3′

c) **C168S 5′ Primer:** 5′-GCCCATGGAGAAGTCAGCCCAGCCAACTGG-3′

C168S 3′ Primer: 5′-CGGGTACCTCTTCAGTCGGGTCGGTTGACC-3′

Figure 2.3. Oligonucleotide Primers for Site-Directed Mutagenesis of Mature SP-22

The three forward and reverse primer pairs are shown in the 5′ to 3′ direction. The point mutations responsible for the conversion of a cysteine to a serine residue are highlighted in blue font and underlined.

2.3.3. Mutagenesis of SP-22

Using a QuikChange™ Site-Directed Mutagenesis Kit (Stratagene) the cysteine residues of SP-22 were mutated to serine residues. The oligonucleotide primers (Fig.2.3), each complementary to opposite strands of the recombinant SP-22/pET14b plasmid were extended during temperature cycling in a PTC-100™ programmable thermocycler, using *Pfu Turbo*™ DNA polymerase. *PfuTurbo* DNA polymerase is a mix of cloned *Pfu* DNA polymerase and a novel thermostable factor which enhances PCR product yields, without compromising DNA replication fidelity. *Pfu* DNA polymerases generally have lower error rates (1.3×10^{-6}) than other enzymes such as *Taq* DNA polymerase. The reaction mix contained 20ng SP-22/pET-14b template, 125ng each primer, 1µl dNTP mix (0.25mM each of dATP, dTTP, dCTP, and dGTP), 5µl reaction buffer (10X), and 1.5µl *Pfu Turbo*DNA polymerase (3U/µl), prepared to a total volume of 50µl with sterile dH$_2$0. The cycling parameters for the mutagenesis reaction were as follows:

1.	**2.**	**3.**	**4.**	**6.**

30 s at 95°C→ 30 s at 95°C→ 1 min at 45°C→ 12 min at 68°C→ Hold at 4°C

5. 12 cycles
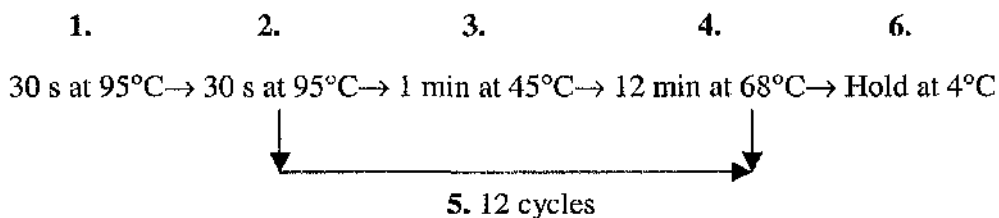
The annealing temperature (step 3) was 45°C for C47S and C66S, and 55°C for C168S. Following temperature cycling, the reaction mix was cooled on ice for 2 min. To determine whether amplification was successful, 10µl PCR product was analyzed by agarose gel electrophoresis. The parental (non-mutated) DNA template was removed by digestion, using the enzyme *Dpn* I which is specific for methylated and hemimethylated DNA. As DNA isolated from *E. coli* is generally methylated, it is a suitable substrate for *Dpn* I. Digestion of the PCR product was carried out with 1µl Dpn 1 (10U/µl) by incubating for 1h at 37°C. The mutant constructs produced contain nicks in their circular DNA which are repaired

following transformation into *E. coli* DH5α cells; 1μl of the reaction mix was added to 50μl competent cells (see section 2.2.5). Colonies containing the mutant constructs were selected according to their ampicillin resistant properties. Mutated plasmid DNA was purified from a 5ml LB/Amp overnight culture using a Wizard® *Plus* Mini Preps kit.

2.3.4. Restriction Endonuclease Digestion of SP-22 and Plasmid Vectors

Following PCR amplification of SP-22, the BamHI restriction endonuclease was used to generate sticky ends for subsequent ligation with pET-14b. Both insert and vector DNA (approx. 5μg) were digested in a reaction containing 3μl of the appropriate SuRE/Cut Buffer (10X), and 3μl BamHI (10U/μl) made up to a total volume of 30μl with sterile dH$_2$O. Digestion was carried out at 37°C for 3h. The restriction enzyme NcoI was also used to determine correct SP-22 insert orientation. Reaction conditions for NcoI digestion were the same as for BamHI.

To prevent re-joining of the vector DNA during ligation, the 5′ protruding termini were dephosphorylated immediately following restriction digestion. This was carried out by incubating the linear vector with calf intestinal phosphatase (CIAP) for 30 min at 37°C, followed by heat inactivation at 65°C for 15 min. The treated vector was then cleaned up using the QIAquick® Gel Extraction Kit, purifying directly from the reaction mix. After each purification step, 5μl of the insert DNA was analyzed on a 1.5% (w/v) agarose gel.

2.3.5. Ligation of SP-22 PCR Product into pET-14b

Following BamHI treatment, the DNA encoding SP-22, and pET-14b were joined via the actions of T4 DNA ligase. Three ratios of plasmid to vector were prepared (1:1, 1:3 and 1:7), in a reaction mix containing 2μl reaction buffer (10X), 1.5μl T4 DNA ligase (3U/μl) diluted to 20μl with sterile dH$_2$O).

2.3.6. Plasmid Propagation and Purification

Vector and recombinant plasmid DNA amplified in *E. coli* DH5α cells was purified from 5ml overnight cultures using a Wizard® *Plus* Mini Preps DNA purification kit. Purified DNA (5μl) was analyzed by agarose gel electrophoresis. For DNA sequencing, large-scale (250-500ml) bacterial cultures were grown to obtain increased quantities of plasmid DNA. Large-scale DNA purifications were carried out using a Wizard® *Plus* Maxi Prep purification kit.

2.3.7. Preparation of DNA for Sequencing

Following purification of plasmid DNA as stated above, the band of interest was gel purified to ensure high purity for subsequent sequencing. The concentration of DNA obtained was determined following agarose gel electrophoresis against 4μl Low DNA Mass™ Ladder. The Molecular Biology Sequencing Unit (MBSU), University of Glasgow performed the sequencing reactions requiring 600-800ng double-stranded DNA, and 3.2μM of T7 promoter and terminator primers per reaction.

2.3.8. Expression of Recombinant Protein in Bacteria

Expression of target proteins was achieved following transformation into *E. coli.* BL21(DE3) pLysS cells. Overnight cultures (5ml) were used to inoculate 50ml of LB media containing ampicillin (50μg/ml). Cultures were incubated at 37°C with shaking until an A_{600} of 0.5 was reached. Induction of heterologous protein expression was initiated by addition of 1mM IPTG. Induction temperatures varied according to the protein of interest. Bacterial growth was monitored, samples (1ml) were removed at the point of induction and at regular intervals thereafter, and their absorbance recorded at 600nm. Cells were harvested by centrifugation in a bench top microfuge for 2 min; the pellet was resuspended in Laemmli sample buffer (10% (w/v) sucrose, 2% (w/v) SDS, 62.5mM Tris-HCl, pH 6.8 and a small amount of Pyronin Y dye), adding 10μl per 0.1-absorbance unit. Successful overexpression was determined following reducing SDS-polyacrylamide gel electrophoresis (PAGE) analysis (section 2.5.6).

2.3.9. Bacterial Cell Lysis

Bacterial cells from small (50ml) cultures were harvested by centrifugation and resuspended in 5ml appropriate buffer. Lysis was achieved by four freeze-thaw cycles, followed by four 10 s sonication bursts. To optimize the yield of soluble protein, the cell extract was then incubated with 0.1% (v/v) NP-40 for 30 min at room temperature with shaking. For large (500ml) cultures, bacterial cells were harvested and the pellet resuspended in 15ml of appropriate Buffer. The bacterial extract was passed four times through a French Pressure Cell Press (AMINCO) at a pressure of 950Psi, to lyse the cells. Insoluble and soluble fractions were separated from the cell extract by centrifugation at 10,000rpm for 15 min in a JA-17 rotor in Beckman J2-MC Centrifuge.

2.4.0. Protein Materials

2.4.1. Chemicals

The following chemicals were purchased from Sigma Chemical Co, Poole, Dorset, UK: acetyl coenzyme A (lithium salt), coenzyme A (lithium salt), benzamidine, DL-6,8-thioctic acid amide (DL-lipoamide, oxidized form), 5,5'-dithionitrobenzoic acid (DTNB), ferric chloride ($FeCl_3$), guanidinium chloride (GdmCl), hydrogen peroxide (H_2O_2), N-(2-hydroxyethyl)piperazine-N'-(4-butanesulphonic acid) (HEPES), imidazole, leupeptin, β-nicotinamide adenine dinucleotide (oxidized form β-NAD$^+$) and the reduced form (β-NADH), 2-oxoglutaric acid (sodium salt), phenylmethylsulphonyl fluoride (PMSF), D(+) 2-phosphoglyceric acid (2-PGA), polyethylene glycol 6000 (PEG), potassium phosphate (KH_2PO_4), pyruvic acid (sodium salt), sodium fluoride (NaF), thiamine diphosphate (ThDP), trichloroacetic acid (TCA) and urea. DTT was bought from Melford Laboratories Ltd., Suffolk, UK. All chemicals were at least of analytical grade.

2.4.2. Proteins and Enzymes

Bovine catalase (50mg), rabbit muscle enolase (50U), bovine E3 (500U), human recombinant thioredoxin (500μg) and *E. coli.* thioredoxin reductase (250μg) were purchased from Sigma. Thrombin protease (50U) was bought from Amersham Pharmacia Biotech Ltd. Immunoglobulin G (IgG) and Protein Assay Dye Reagent concentrate were obtained from BIO-RAD.

2.4.3. Biological Tissues

Bovine hearts for isolation of PDC and OGDC were obtained from Paisley Abbatoir, Sandyford Road, Paisley, UK. Hearts were maintained and transported on ice following removal before storage at –80°C in aliquots of 300g. Tissue was thawed overnight at 4°C prior to use.

2.4.4. Molecular Weight Markers and Equipment

1) The Low Molecular Weight Marker Kit was purchased from Amersham Pharmacia Biotech UK Ltd, for molecular weight determination of proteins run on denaturing SDS-PAGE. The calibration mix was supplied as a lyophilized sample containing six highly purified proteins with a M_r range of 14,400-94,000. The calibration mix (250μg) was resuspended in 250μl Laemmli sample buffer (section 2.3.8) to give a 1X concentration, and 10μl was routinely loaded on a gel. The molecular weight of the protein of interest was determined by comparing its electrophoretic mobility with that of the molecular weight standards'.

2) The MW-GF-1000 molecular weight marker kit was obtained from Sigma and contained a protein mixture, exhibiting a molecular weight range from 29,000-669,000 M_r. Cytochrome-c (M_r 12,400) was additionally purchased from Sigma. The protein standards were prepared in 50mM KPi buffer, pH 7.0 containing 150mM NaCl to concentrations advised in the maker's instructions.

3) A pre-packed HiPrep (16mm x 600mm), Sephacryl S-300 High Resolution column was purchased from Pharmacia with a bed volume of 120ml and

fractionation range of 1×10^4- 2×10^6 M_r. The column was run using a BioCAD® 700E Perfusion Chromatography® Workstation.

4) The BioCAD® SPRINT™ and BioCAD 700 Series Perfusion Chromatography® Workstations and SelfPack POROS 20 Metal Chelate Affinity Packing were purchased from PerSeptive Biosystems, Framingham, MA, U.S.A. Chelating Sepharose® Fast Flow gel matrix was purchased from Amersham Pharmacia Biotech.

2.4.5. Spectrophotometric Equipment

All spectrophotometric measurements for enzyme assays, protein concentration determination, and Ellman's assay, were recorded using a UV-2101 PC scanning spectrophotometer (SHIMADZU). UV Quartz cuvettes (1ml, Jencons) with a 10mm light pathlength were routinely used.

2.5.0. Protein Methods

2.5.1. Preparation of the Metal Affinity Column

Metal affinity chromatography used to purify His-tagged proteins was carried out using a BioCAD® SPRINT™ Workstation. A column (10mm x 100mm) with a bed volume of 8.5ml was packed with SelfPack POROS 20 Metal Chelate Affinity Packing according to the manufacturer's instructions. Zinc ions (Zn^{2+}) were loaded onto the matrix by passage of 20 column vol of 0.1M $ZnCl_2$ at a low pH of 4.5-5.0 to minimize precipitation of metal hydroxide complexes. The column was then washed with 5 column vol of dH_2O to remove excess zinc ions followed by 5 column vol of 0.5M NaCl to remove non-specifically bound metal ions. To improve selectivity and recovery of the His-tag protein, the column was saturated with elution buffer (0.5M imidazole, 1.0M NaCl, 20mM KPi or HEPES buffer, pH 6.0). The metal chelate column was primed with 5 column vol of starting buffer (0.5mM imidazole, 1.0M NaCl, 20mM KPi or HEPES buffer, pH 8.0) prior to protein loading. The starting buffer for wild type and mutant SP-22

was changed from KPi to HEPES due to problems with irreversible binding to the metal column. The starting buffer for purification of human E3 was KPi.

2.5.2. His-Tag Purification of Wild Type, Mutant SP-22 and E3.

Bacterial cultures (500ml) were routinely employed in purification of high yields (20-30mg) of protein per single purification. Following bacterial lysis (section 2.3.9) the pellet was resuspended in 15ml starting buffer (section 2.5.1). The clarified supernatant resolved from the cell extract was maintained on ice until required.

Three 5ml injections steps were incorporated into the BioCAD elution protocol to load the 15ml sample onto the metal chelate affinity column. An increasing imidazole gradient, from 0.5mM - 0.5M over 5 column vol was carried out, eluting the His-tagged protein in 2ml fractions. Column regeneration was achieved by stripping with 1.0M NaCl containing 50mM EDTA, or alternatively using 1.0M NaOH for more tightly bound proteins followed by a water wash. The column was stored in dH$_2$O or 20% (v/v) ethanol for longer time periods. Fractions were stored at 4°C.

2.5.3. Preparation of BioCAD Protein Fractions for SDS-PAGE

Following elution of the His-tag recombinant protein, aliquots (100μl) of peak fractions were removed for TCA/acetone precipitation. Fractions containing 10% (w/v) TCA were placed on ice for 30 min, prior to centrifugation at 10,000rpm in a GS-15R Beckman centrifuge for 10 min at 4°C. The supernatant was discarded and the precipitate was resuspended in 500μl ice-cold acetone (100%) and incubated on ice for a further 30 min. The samples were centrifuged as before and the pellet resuspended in 40μl Laemmli sample buffer (section 2.3.8) supplemented with DTT (150mM) for subsequent SDS-PAGE analysis.

2.5.4. Protein Dialysis and Concentration

Peak fractions following metal chelate chromatography were pooled and dialyzed routinely into 10l of dialysate (5 x 2l changes) at room temperature or 4°C. Dialysis tubing had a molecular weight cut-off of 10,000 M_r. The dialysate was typically 150mM NaCl, 50mM KPi, pH 7.2 for the majority of experiments. Exceptions were for circular dichroism (150mM sodium fluoride (NaF), 50mM KPi, pH 7.2, and BIAcore analysis (HBS buffer which contains 10mM HEPES pH 7.4, 15mM NaCl, 3.4mM EDTA and 0005% (v/v) surfactant P20).

2.5.5. Protein Concentration Determination

Protein concentration was determined according to the Bradford Assay (Bradford, 1976). Absorbance readings at a wavelength of 595nm for known concentrations of IgG were used to generate a standard curve. The concentration of the unknown protein was determined by extrapolating from the standard curve. For more accurate concentration determination, the absorbance of the protein at 280nm was measured. To determine the A_{280}, it was necessary to derive an extinction coefficient for the protein under investigation. The protein was analyzed in the far UV spectrum over 200–340nm, using buffer only as the reference. The extinction coefficient was calculated using the following equation:

$$\frac{\text{No. of Tryptophan Residues} \times 5690 + \text{No. of Tyrosine Residues} \times 1280}{\text{Monomeric molecular weight of Protein}}$$

The A_{280} divided by the extinction coefficient enabled protein concentration determination. The extinction coefficient used for 1mg/ml of SP-22 and the cysteine mutants was 0.73, and 0.42 for E3.

2.5.6. SDS-PAGE

Electrophoresis of protein samples was carried out in SDS, according to the method of (Laemmli, 1970). Each gel comprised a 3% stacking gel and a 10-15% resolving gel depending on the molecular weight of the protein of interest.

Polymerization of the gel was achieved on addition of 0.03% (v/v) TEMED, and 0.05% (w/v) ammonium persulphate (APS) to a 30:0.8 ratio of acrylamide:bisacrylamide. Typically a 10μl sample was loaded per well. Electrophoresis was carried out at a constant voltage (400V) and 50mA/gel in 1X SDS running buffer prepared from a 10X stock (144g glycine, 10g SDS and 29.8g Tris-HCl, pH 8.8 prepared to 1l with distilled water). Protein bands were stained with Coomassie Brilliant Blue G250 in 50% (v/v) methanol and 10% (v/v) glacial acetic acid shaking for 30 min at room temperature. The gel was immersed in an appropriate volume of destain (10% (v/v) methanol and 10% (v/v) glacial acetic acid) to remove excess stain and enable clear band visualization.

For superior resolution when necessary, samples were run on pre-cast 4-12% NUPAGE®Novex Bis-Tris gels (Invitrogen) held within a XCell *SureLock*™ Mini-Cell. The preparation of protein samples for electrophoresis was the same as for SDS-PAGE. Electrophoresis was carried out in 1X NUPAGE® MES SDS Running buffer at constant voltage (200V) and 110mA/gel. The staining procedure was as for polyacrylamide gels.

2.5.7. Immunoblotting

Protein transfer from a protein blot to a Hybond™ ECL™ nitrocellulose membrane (Amersham Pharmacia Biotech Ltd.) was carried out overnight at room temperature in a Trans-Blot™ Cell (BIORAD) at 400V/40mA. Transfer buffer was prepared as a 10X stock (30.3g Tris-HCl, pH 8.3, 144g glycine and 2g SDS, prepared to 2.5l) and was used at a 1X dilution. Immunoblotting apparatus was assembled with the nitrocellulose membrane facing the anode, and the gel facing the cathode. Successful transfer was established following staining with Ponceau Red stain. Non-specific binding sites were blocked with Blocking Solution (20mM Tris-HCl, pH 7.2, 15mM NaCl, 5% (w/v) non-fat milk and 0.2% (v/v) Tween 20) overnight at 4°C with shaking. The membrane was subsequently incubated overnight at 4°C with a polyHis Antibody (Qiagen), diluted 1 in 2000 with 20mM Tris-HCl, pH 7.2, containing 1% (w/v) non-fat milk and 0.1% (v/v)

Tween 20. Four 30 min washes in large volumes of 20mM Tris-HCl, pH 7.2, containing 15mM NaCl and 1% (w/v) non-fat milk were carried out to remove the primary antibody solution. Protein blots were developed according to the maker's instructions onto Hyperfilm™ ECL™ using an ECL™ detection Kit, supplied by Amersham Pharmacia Biotech Ltd.

2.5.8. Silver Staining

Silver staining of proteins run by SDS-PAGE was carried out according to the method of Wray *et al.* (1981). All staining steps were carried out at room temperature with constant agitation. Protein gels were immersed in 50% (v/v) methanol for 2h followed by staining for 15 min with Solution C, prepared immediately prior to use by adding Solution A (0.8g silver nitrate dissolved in 4ml dH$_2$O) drop-wise to Solution B (21ml 0.36% (w/v) NaOH and 2.1ml ammonia) and diluted to 100ml with dH$_2$O. The gel was washed for 5 min with dH$_2$O and bands were developed with addition of Solution D (2.5ml 1% (w/v) citric acid and 0.25ml 0.38% (v/v) formaldehyde made up to total volume of 500ml with dH$_2$O). The gel was closely observed until optimal band visualization after which the gel was kept in 50% (v/v) methanol. Pictures were taken immediately as bands continue to develop.

2.5.9. Cleavage of His-tag from SP-22

The serine protease thrombin, supplied as a lyophilized powder, was used to cleave recombinant fusion proteins containing a His-tag. Cleavage was achieved by overnight incubation at room temperature with the protein (1U cleaves $\geq$ 90% of 100µg protein). Proteins with intact His-tags were removed by metal affinity chromatography using a PD-10 column prepared with 2ml of Chelating Sepharose® Fast Flow (Amersham Pharmacia Biotech Ltd.) employing immobilized zinc ions according to the manufacturer's instructions. Successfully cleaved protein was collected in 1ml fractions by washing through with buffer containing 150mM NaCl, 50mM KPi, pH 7.0.

2.5.10. Ellman Assay for Thiols

Protein samples of known concentration were prepared in 150mM NaCl, 50mM KPi, pH 7.0 in the presence and absence of 6M GdmCl. The amount of nitrothiobenzoate (NTB) released upon reaction of a thiol with DTNB was measured by monitoring the absorbance at 412nm. The absorbance was set to zero with a 1ml protein sample. To the protein sample, 25µl 10mM DTNB prepared in 0.1M KPi, pH 7.0 was added and inverted to mix. The absorbance was recorded over 40 min at room temperature. The absorbance difference between the plateau of the protein sample and the buffer only control was measured. The molar absorbance of the TNB anion (ε_{412} = 13,700/M cm in 6M GdmCl, 14,150/M cm in its absence) produced was used to calculate the molar concentration of the thiols present:

$$\mu M\ SP\text{-}22\ \times\ \varepsilon_{412} = \text{Expected A}^{412nm}\text{ per thiol.}$$

2.5.11. Gel Filtration

Gel exclusion chromatography was performed at room temperature using a pre-packed HiPrep 16/60 Sephacryl S-300 High Resolution column connected to a BIOcad® 700E Perfusion Chromatography® Workstation. The flow rate was 1ml/min and the volume of protein loaded was 1ml (recommended < 2% of bed volume). Fractions (1.5 ml) were collected between 0.3-0.9 column vol. All buffers were filtered through a 0.2µm vacuum filter (Millipore). The column was equilibrated with 2 column vol of the appropriate buffer, washed with 2 column vol of dH$_2$O between runs and stored in 20% (v/v) ethanol for longer periods.

2.5.12. Purification of PDC and OGDC from Bovine Heart

The purification of PDC and OGDC was based on the method of Stanley and Perham (1980) with modifications described by De Marcucci et al. (1986). All steps, unless otherwise stated, were carried out at 4°C and using either a JA-17 or JA-14 rotor in a Beckman J2-MC centrifuge. Bovine heart (300g), previously sectioned with the fat and connective tissue excised, was removed from storage at −80°C and thawed overnight at 4°C prior to use. Final thawing was carried out at

room temperature. The tissue was placed in a Waring blender and covered with 700ml ice-cold extraction buffer (50mM MOPS, pH 7.0, 3% (v/v) Triton X-100 (TX-100), 0.1% (v/v) silicon anti-foam, 1mM DTT, 1.5μM leupeptin, 1mM PMSF plus 1mM benzamidine and homogenized on low for 3 min. The homogenate was centrifuged at 10,000rpm for 20 min at 4°C. The pH of the cell/nuclear free supernatant was adjusted to 6.45 with 10% (v/v) acetic acid prior to the first PEG precipitation step which involved 0.12 vol of 35% (w/v) PEG 6000 being added drop-wise to the supernatant. To ensure complete precipitation the solution was stirred on ice for 30 min. The pelleted material was recovered following centrifugation at 14,000rpm for 15 min. Pellets were resuspended in a total volume of 100ml 1% (v/v) TX-100 buffer (50mM MOPS, pH 6.8, 1.5μM leupeptin, 1mM PMSF and 1mM benzamidine) using a Teflon homogeniser. The supernatant was clarified following centrifugation at 17,000rpm for 40 min and fat droplets were removed by filtration through eight layers of muslin. 0.013 vol of 1.0M $MgCl_2$ and 0.05 vol. of 1.0M NaPi, pH 6.3 were added to the supernatant, maintaining the pH above 6.8 with 0.5M NaOH. The pH was then lowered to 6.45 with 10% (v/v) acetic acid, and for the second PEG precipitation step, 0.12 vol of 35% (w/v) PEG 6000 was added drop-wise, stirring for a further 30 min. Pellets were recovered by centrifugation at 16,000rpm for 10 min and resuspended by homogenization in 80ml 1% (v/v) TX-100 buffer as before. The suspension was stored overnight at 4°C in the presence of protease inhibitors.

Next day, the suspension was homogenized briefly and then centrifuged at 17,000rpm for 1h. The pH of the supernatant was lowered to 6.45 with 10% (v/v) acetic acid and an aliquot was removed to assess PDC/OGDC activity. The third PEG precipitation step involved the addition of 0.05 vol of 35% (w/v) PEG 6000 to the supernatant stirring for a further 30 min. Another aliquot was removed and spun at 13,000g in a bench-top microfuge before re-assaying the supernatant for PDC/OGDC activity. If the OGDC activity was $\geq$ 5% of the previous activity, another 0.01 vol of 35% (w/v) PEG 6000 was added, stirring for 30 min. The supernatant was spun at 17,000rpm for 10 min and the pellets were resuspended in

50mM KPi, pH 7.0. OGDC was diluted to ≤ 10mg/ml and purified complex for immediate use was stored at 4°C; otherwise it was aliquoted and stored at –80°C in 50% (v/v) glycerol. The clarified supernatant was transferred into Ti70 tubes and centrifuged at 40,000rpm for 2h in a Beckman L7 model Ultracentrifuge. The pellets were resuspended in a minimal volume of 50mM KPi, pH 7.0. PDC was diluted to 10mg/ml and stored at 4°C or in 50% (v/v) glycerol at –80°C, for longer periods. EDTA was omitted from the TX-100 buffers due to its chelating effect on the iron in the free radical generating system used in future experiments.

2.5.13. E3 Assay

Bovine and recombinant human E3 activity was measured spectrophotometrically following the oxidation of DHL which is coupled to the formation of NADH and detected by an increase in absorbance at 340nm. All assays were carried out at 30°C. Bovine E3 was dialyzed into 0.1M KPi, pH 7.0 (4 x 1l changes at 4°C) to remove buffer components included in the enzyme mix which had a protective effect on the enzyme. Purified E3 (5-50µg) in 0.1M KPi, pH 7.0 was added to 670µl solution A (50mM KPi, pH 7.6, 3.0mM NAD^+, 2.0mM $MgCl_2$, 0.2mM ThDP) and the absorbance set to zero. The reaction was initiated by addition of 14µl fresh DHL (2.0mM in 70% (v/v) ethanol). The substrate DHL for the E3 assay was prepared in the laboratory from DL-lipoamide according to the method of Kochi and Kikuchi (1976).

2.5.14. Enolase Assay

Enolase activity was assessed by observing the increase in absorbance at 240nm corresponding to the conversion of the substrate 2-PGA to phosphoenol pyruvate (PEP). 2-PGA (1mM) was prepared in 30mM Tris-HCl, pH 7.0 containing 1mM $MgSO_4$. Substrate solution (1ml) was used to set the absorbance to zero. The reaction was initiated with addition of enolase (1-2µg) and the reaction monitored over 45s.

2.5.15. 2-Oxoacid Dehydrogenase Assays

The 2-oxoacid dehydrogenase complexes, PDC and OGDC were assayed by recording the absorbance increase at 340nm corresponding to the generation of NADH 45s (Brown & Perham, 1976). Complexes were purified from bovine heart and prepared in 0.1M KPi buffer, pH 7.0 as described in section 2.5.12. Purified enzyme (1-5μg) was added to 670μl solution A (50mM KPi, pH 7.6, 3.0mM NAD^+, 2.0mM $MgCl_2$, 0.2mM ThDP) and 14μl solution B (0.13M cysteine-HCl, 0.13mM Li_2CoASH), pre-warmed to 30°C and the absorbance set to zero. The reaction was initiated by addition of 14μl solution C (100mM pyruvic acid for PDC or 100mM 2-oxoglutarate for OGDC).

2.5.16. Hydrogen Peroxide Inactivation of PDC, OGDC and E3

As inhibition of the 2-oxoacid dehydrogenase complexes and E3 by the artificial free radical generating system was minimal, the effect of adding hydrogen peroxide directly was assessed. The particular enzyme was incubated with 1, 5, and 10mM hydrogen peroxide at 30°C and, at increasing time intervals, the remaining enzymatic activity was assessed according to the particular enzyme.

2.5.17. SP-22 Protection Assay

The activity of SP-22 was routinely determined by monitoring its ability to protect enolase from inactivation, in the presence of a thiol/Fe^{3+}/O_2 free radical-generating system (FRS). Enolase was dialyzed into 50mM KPi, pH 7.0 containing 150mM NaCl (4 x 1l changes at 4°C) to remove components supplied in the enzyme mix that had potential stabilizing effects on enolase. Assays were performed in 120μl incubation mix containing 33μg enolase, 30μM $FeCl_3$, 30mM DTT, 50mM imidazole-HCl, pH 7.2 and 3-66μg SP-22. Controls for each component of the FRS were also carried out in the absence of SP-22. The FRS and SP-22 were pre-incubated together for 5 min at 30 °C prior to addition of the enolase. At various time intervals, 20μl assay mixture was removed and added to 20μl 2mM EDTA. A sample (30μl) was then removed and assayed in a total volume of 1ml containing 30mM Tris-HCl, pH 7.0, 3mM $MgSO_4$ and 1mM of 2-

PGA. The absorbance was monitored at 240nm over 45s indicating the successful conversion of 2-PGA to PEP.

2.5.18. Assessment of Hydrogen Peroxide Removal

Hydrogen peroxide removal by catalase and SP-22 was measured by monitoring the reduction in absorbance at 240nm over 85s. Hydrogen peroxide (50mM) was prepared in 50mM KPi buffer, pH 7.0 and 1ml was pre-heated to 30°C in a quartz cuvette prior to addition of bovine catalase (30μg) or SP-22 (300μg). Experiments were also carried out in the presence of 20mM DTT as the peroxidase activity of SP-22 requires a source of thiol groups to be reduced for subsequent catalytic cycles.

2.5.19. Circular Dichroism (CD) of SP-22 and the Cysteine Mutants

CD measurements were taken in the near and far UV regions of the spectrum, using a JASCO J-600 spectropolarimeter. For unfolding experiments, SP-22 (0.5mg/ml) was chemically denatured over a range of urea concentrations (0-9M) prepared in 50mM KPi, pH 7.0 containing 150mM NaF and equilibrating overnight at room temperature. Urea was prepared fresh and experiments were carried out immediately before urea breakdown could occur. To assess the role of the disulphide bonds in structural integrity, unfolding experiments were also carried out in the presence of 20mM DTT. Circular dichroism experiments were carried out by Dr. S. Kelly in the laboratory of Prof. N.C. Price, Department of Chemistry, University of Glasgow, UK.

2.5.20. Fluorimetry

Fluorimetry experiments were carried out using a Perkin Elmer LS 50B Fluorimeter. Following chemical denaturation of SP-22 (0.5mg/ml) for CD unfolding experiments (section 2.5.19), the sample was excited at 295nm and the absorbance was measured over 300-400nm in a 500μl quartz cuvette. Results were expressed as an average of the three scans taken over this range. Fluorimetry

was carried out by myself and Dr. S. Kelly in the laboratory of Prof. N.C. Price, Department of Chemistry, University of Glasgow, UK.

2.5.21. Analytical Ultracentrifugation (AUC)

For sedimentation equilibrium analyses, protein samples were dialyzed into 50mM KPi, pH 7.2 containing 150mM NaCl. To assess the occurrence of aggregation protein samples were diluted from the stock sample to a range of A_{280} ranging from 0.1-0.5 in 0.05 increments. The procedure was carried out at 4°C at three rotor speeds of 5, 7 and 10K in a Beckman Optima XL-A analytical ultracentrifuge (Beckman Instuments Inc., Palo Alto, California). Recordings at 3K were taken to allow back calculation of the sample concentration and centrifugation at 47K was also carried out to generate a baseline free from macromolecular species. All experiments were carried by Gordon Campbell in the laboratory of Dr. O. Byron, Division of Infection and Immunity, University of Glasgow, UK.

2.5.22. Transmission Electron Microscopy (TEM)

Purified protein samples (1ml) were eluted on a Sephacryl-300 16/60 HR gel filtration column as described previously. Peak fractions were selected for negative staining maintaining them on ice until use. The single droplet method described by Harris J.R., (1991) was adopted. Typically 3µl 50-100µg/ml of protein was immobilized to a continuous carbon support film. Grids were washed with dH_2O, stained with a single drop of 1% (w/v) uranyl acetate and air-dried. All electron micrographs were generated using a JEOL 1200 Transmission Electron Microscope recording at 30,000X magnification onto S0163 film (Kodak). Projection averages were calculated from top-views of SP-22 rings using the SPIDER image-processing package (Frank *et al*, 1996). All EM work and image processing was carried out by Dr. David Bhella of the Department of Virology, University of Glasgow, UK.

2.5.23. Isothermal Titration Calorimetry (ITC)

Mrs Margaret Nutley performed all ITC experiments in the laboratory of Prof. Alan Cooper, Dept. Chemistry, University of Glasgow using a VP-ITC microcalorimeter (MicroCal Inc., Northampton, MA, USA. SP-22 and human recombinant E3 were dialyzed into 0.1M KPi buffer pH 7.0 containing 0.15M NaCl in the same container to ensure the buffer characteristics of both protein samples were identical. The dialysate was placed in the ITC reference cell for the experiments. SP-22 ($10\mu M$) was placed in the ITC sample cell and E3 ($200\mu M$) was placed in the syringe of the microcalorimeter. Typically twenty-six, $10\mu l$ injections of E3 into SP-22 were made per experiment and were carried out at controlled temperature (25°C). The heat of binding was measured continuously by the microcalorimeter and the data analyzed using Origin software (OriginLab Corporation).

2.5.24. Surface Plasmon Resonance (SPR)

SPR studies were carried out using a BIAcore 2000 machine (Pharmacia Biosensor AB, Uppsala, Sweden). A CM-5 sensor chip was activated using 0.1M NHS (N-hydroxysuccinimide) and 0.1M EDC (N-ethyl-N'-[3-(dimethylamino) propyl] carboiimide hydrochloride), followed by immobilization of bovine E3 ($50\mu g/ml$) prepared in 0.1M sodium acetate pH 4.5 using the Wizard program provided with the BIAcore software. It was aimed to couple approx. 1500 response units (RU) of E3 to the chip via this amine coupling method. Free binding sites were blocked using 1M ethanolamine and the chip was equilibrated with HBS buffer. When not in use the sensor chip was stored at 4°C in a sterile plastic tube containing HBS buffer.

Peak fractions of SP-22 following His-tag purification were dialyzed at room temperature into 10mM HEPES buffer pH 7.4 containing 15mM NaCl and 3.4mM EDTA over five 2l changes. The dialyzed sample was concentrated to approx. 10mg/ml. SP-22 was diluted to the appropriate concentration with HBS buffer (10mM HEPES pH 7.4, 15mM NaCl, 3.4mM EDTA and 0005% (v/v) surfactant

P20). 60μl injections of the various SP-22 concentrations were passed over the chip surface at a flow rate of 20μl/min representing the association phase. The flow of HBS over the chip surface was continued for a further minute constituting the dissociation phase. Between injections 10μl 1M NaCl was passed over the chip surface to regenerate it for future runs.

Chapter 3
Section 1

3.1.0. Introduction

SP-22 was initially isolated from bovine adrenal cortex and to date has not been produced as a recombinant protein. For structural studies it is not practical or cost-effective, to isolate SP-22 from natural sources as yields are generally low and impurities are frequent. To facilitate the elucidation of the structure and function of a specific protein it is necessary to obtain it in large quantities in a highly purified state. To achieve this, the primary aim was to clone and overexpress the precursor and mature forms of bovine SP-22 as N-terminal His-tagged fusion proteins using the pET (plasmid for expression by T7 RNA polymerase) system vectors. This system enables high-level expression of cloned genes in *E. coli* and is presently the preferred choice of prokaryotic system for heterologous expression. The bacteriophage T7 RNA polymerase and its cognate promoter tightly control the pET system. Expression of T7 RNA polymerase is induced in *E. coli* BL21 (DE3)pLysS cells on addition of IPTG.

The structures of several 2-Cys Prx members have been elucidated by X-ray crystallography and transmission electron microscopy. There are common structural characteristics occurring within this group, one of which is the presence of a basic dimeric unit with 2-fold symmetry. A common feature of the dimeric unit is the presence of intermolecular disulphide bonds. Generally, these interactions involve the N-terminal cysteine of one monomer and the C-terminal cysteine of the opposing subunit. The rat 2-Cys Prx, HBP23 and the human erythrocyte enzyme TPx-B are typical examples, forming dimers of two tightly associated monomers with a flattened ellipsoidal conformation.

Consequently, following the overexpression and purification of SP-22, one of only two mitochondrial 2-Cys Prxs identified to date, the second objective was to establish if SP-22 also forms a dimeric unit containing intermolecular disulphide bonds. The human mitochondrial 2-Cys Prx, PRDX5 does not form a dimer, and exists exclusively in monomeric form. If SP-22 forms a dimeric unit, it will be determined which of the conserved cysteine residues are involved in the interactions. To address this possibility the aim was to mutate each of the

cysteine residues to serine residues, and analyse the purified products by non-reducing SDS-PAGE. Generating SP-22 mutants will also be advantageous, in order to assess the roles of each of the cysteines for peroxidase activity as discussed further in Chapter 6.

Results

3.1.1. PCR Amplification of Bovine SP-22

The bovine SP-22 gene was previously amplified from a bovine brain cDNA library (Clonetech), and ligated using the pCR-Script vector Cloning Kit (Stratagene). This recombinant plasmid served as a template for further amplification of both precursor and mature forms of SP-22 by PCR as described in Materials and Methods section 2.3.2, using specific primers to the 5′ and 3′ ends of the gene (Fig. 2.2). It was necessary to incorporate an extra base immediately before the start codon of precursor and mature SP-22 to ensure that on ligation into pET-14b, the cDNA would be in the correct reading frame. BamHI restriction sites were incorporated flanking the gene-coding region enabling subsequent ligation into the pET-14b expression vector (Fig. 2.1). All primers terminated with either a guanine or cytosine nucleotide to reduce the occurrence of base mismatches. To minimise errors in base incorporation, the *Pfu* DNA polymerase was used in the PCR reaction. *Pfu* is a magnesium-dependent, thermostable enzyme with 3′→5′exonuclease proofreading activity.

PCR products were gel-purified and analysed on a 1.5% (w/v) agarose gel, alongside a 1kb DNA Step Ladder (Materials and Methods section 2.3.1). Bands of ~750bp and 500bp were observed, corresponding to the precursor and mature forms of bovine SP-22, respectively (Fig. 3.1).

3.1.2. Cloning of SP-22, and Selection of Positive Clones

The purified SP-22 insert and pET-14b vector were BamHI-treated to generate complementary sticky ends. To prevent recircularization of the linearized vector during ligation, the phosphate groups from both 5′-termini were removed by treatment with CIAP as described in Materials and Methods section 2.3.4. SP-22

inserts were ligated into pET-14b at a range of vector to insert ratios (Materials and Methods section 2.3.5). A control ligation, containing vector only was also prepared to determine the efficiency of the dephosphorylation step. Following amplification in *E. coli* DH5α cells, colonies were observed at all three vector to insert ratios. As expected, the vector only control plate was clear. Two precursor (P1 and P2), and three mature SP-22 (M1-M3) clones were selected. The plasmid DNA purified from 5ml overnight cultures as described in section 2.3.6 of Materials and Methods, was analysed on a 1.5% (w/v) agarose gel (Fig. 3.2). Clones P2 and M2 display a lower mobility on agarose gels than wild type plasmid, indicating the presence of an insert. Plasmids are largely supercoiled, with a small amount of relaxed circular DNA. Plasmid DNA obtained from the positive clones P2 and M2 were digested with BamHI to confirm the presence of an insert of the correct size (Fig. 3.3) as described in Materials and Methods section 2.3.4. Digestion of pET-14b and the negative clones was carried out for comparison. As expected P2 and M2 both contained inserts of the correct size, ~750bp and ~500bp, respectively. All other clones were linear, wild type vector (4700bp).

3.1.3. Determination of Insert Orientation

As the cloning procedure was not directional, there are two possible insert orientations; only the correct one will enable protein expression. To establish insert orientation P2 and M2 were digested with the restriction endonuclease NcoI (Materials and Methods section 2.3.4). NcoI cuts pET-14b at position 580 and position 225 in the insert. P2 and M2 were both correctly orientated, generating fragments of approx. 5000 and 200 (mature) or 350 (precursor) base pairs (results not shown).
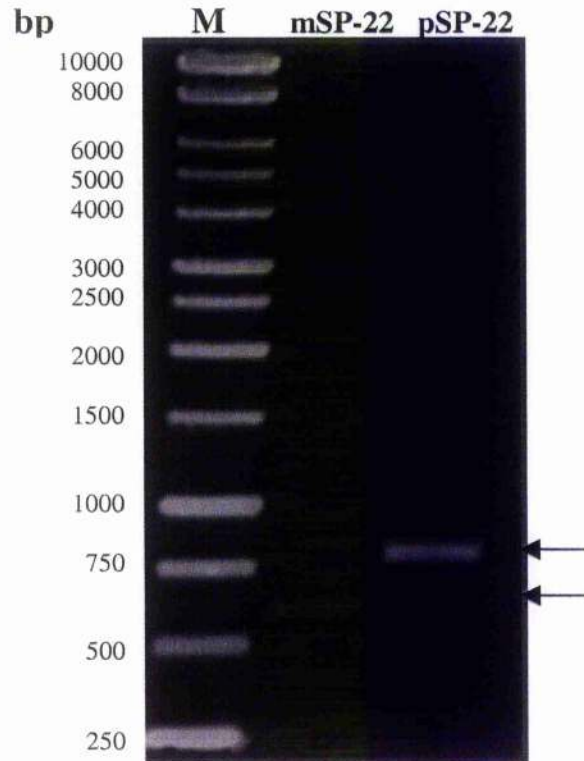
Figure 3.1. Amplification of Precursor and Mature SP-22

Following PCR amplification of SP-22 from the SP-22/pCR-Script template, 5µl was analysed on a 1.5% (w/v) agarose gel. Bands were stained with ethidium bromide, and sizes were determined by comparison with a 1kb DNA Step Ladder (M), shown to the left of the gel, with units in base pairs (bp). Lanes contain PCR products for precursor SP-22 (pSP-22), and mature SP-22 (mSP-22). Arrows indicate the PCR products.
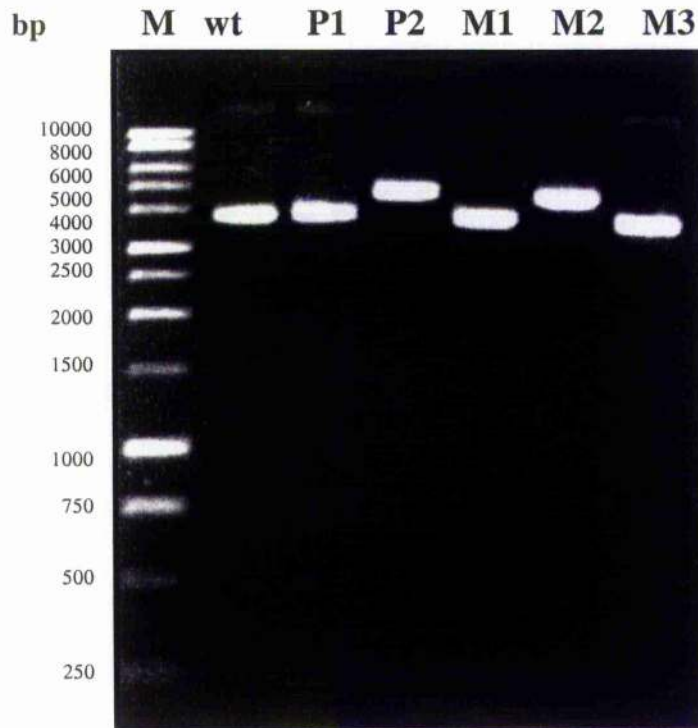
Figure 3.2. Isolation and Identification of Recombinant SP-22 Plasmids

pET14-b and SP-22 insert ligation reactions were amplified in DH5α *E. coli* cells. Plasmid DNA was purified from overnight inoculations (5ml) and analysed on a 1.5% (w/v) agarose gel. Bands were stained with ethidium bromide. Sizes, expressed in base-pairs (bp) were determined using a 1kb DNA Step Ladder (M), shown to the left of the gel. Uncut pET-14b is represented by Wt; P1 and P2 are precursor SP-22 clones, and M1-M3 are mature SP-22 clones.
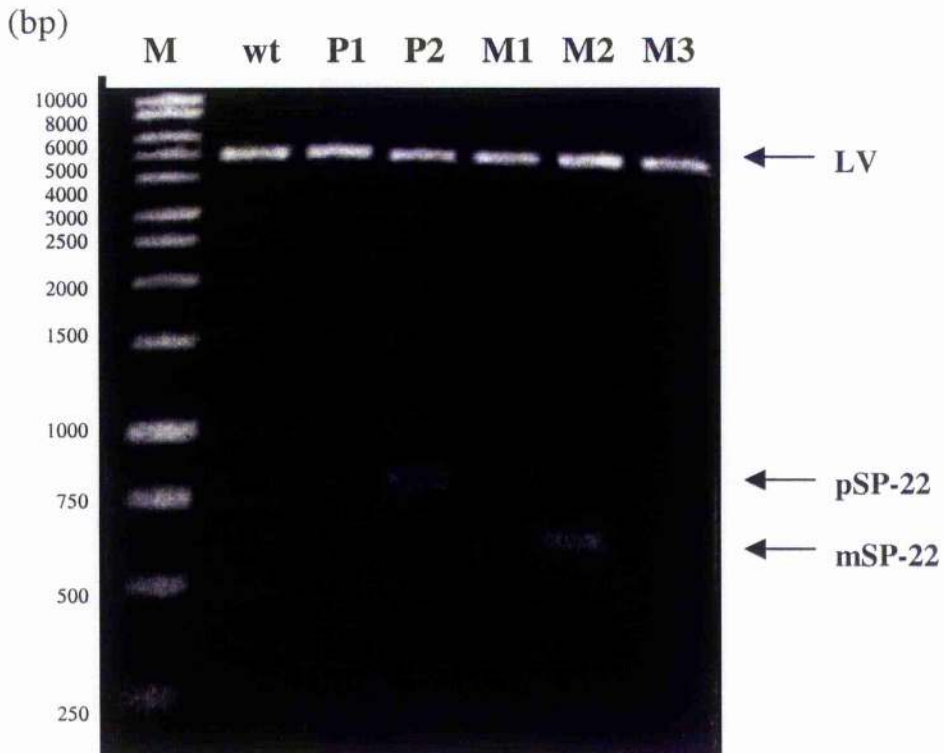
Figure 3.3. BamH1 Restriction Analysis of the SP-22/pET-14b Recombinant Clones (P2 and M2)

Clones P1, P2, M1-M3 and wild type pET-14b were digested with BamH1 to confirm the presence of an insert and analysed on a 1.5% (w/v) agarose gel. Bands were stained with ethidium bromide. The 1kb DNA Step Ladder (M) is shown to the left of the gel, sizes in base-pairs (bp). Linear vector (LV), precursor SP-22 (pSP-22) and mature SP-22 (mSP-22).

3.1.4. Protein Expression of SP-22

The heterologous expression of SP-22 was carried out in Epicurian Coli BL21(DE3)pLysS cells (see Materials and Methods section 2.3.8). Following reducing SDS-PAGE (Materials and Methods section 2.5.6), bands at 27-28kDa, and 24-25 kDa were observed, corresponding to the predicted M_r values of the precursor and mature forms of the protein respectively, complete with His-tag and adjacent vector regions (Fig. 3.4). Levels of expression were maximal after a 3h induction period. The solubility of SP-22 was assessed at three induction temperatures: 22°C, 30°C, and 37°C. Bacterial cell lysis is described in Materials and Methods section 2.3.9. Precursor SP-22 was insoluble at all three temperatures, indicating that the mitochondrial presequence interferes with correct folding of the protein. Typically proteins correctly fold following cleavage of the targeting sequence after arrival of the nascent polypeptide at the mitochondrion. No further work was carried out on the precursor form.

In contrast, the solubility of mature SP-22 was found to be dependent upon induction temperature. There was a corresponding decrease in protein solubility with an increase in induction temperature (Fig. 3.5). The amount of soluble mature SP-22 as a percentage of total SP-22 in the cell extract was approx. 100%, 75% and 25%, at 22°C, 30°C and 37°C respectively, as judged by visual inspection. It is proposed that by lowering the induction temperature, the rate of translation is reduced, allowing more time for the protein to fold correctly. Furthermore, by slowing translation and thus the levels of protein produced in a given time, the possibility of protein aggregation and entry into inclusion bodies is minimised. Optimal expression of mature soluble SP-22 was routinely achieved at 22°C inducing for 5h to ensure maximal levels of protein were attained.

3.1.5. His-tag Purification of SP-22

SP-22 was routinely purified from large-scale (500ml) bacterial cultures by metal chelate affinity chromatography using a BioCAD® SPRINT™ Workstation
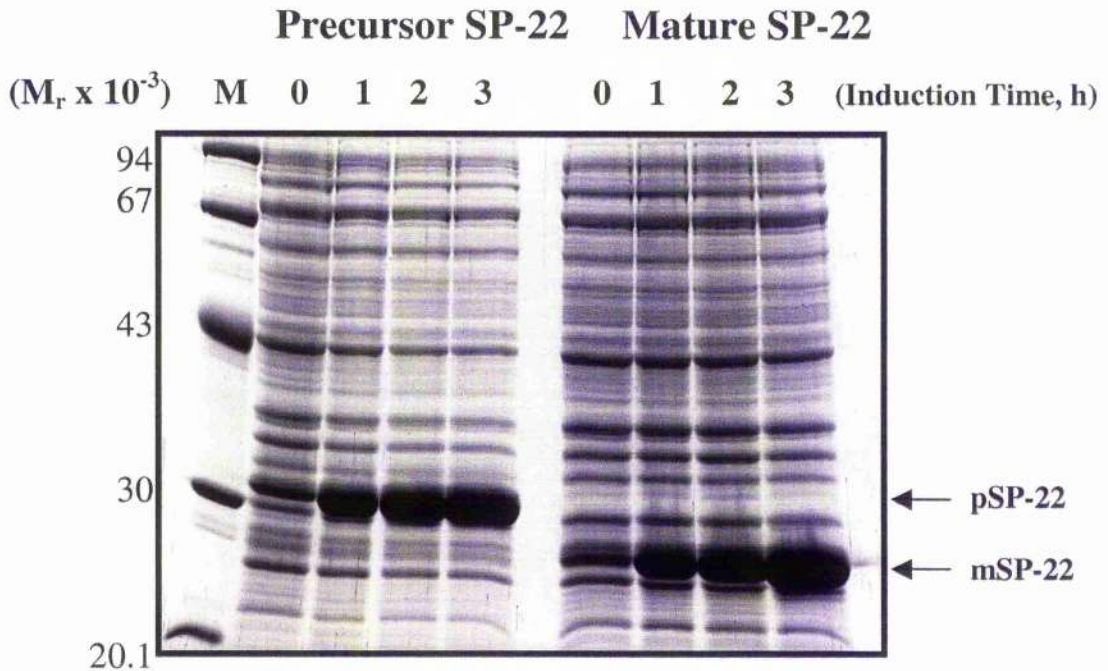
Figure 3.4. Overexpression of Precursor and Mature SP-22

Precursor and mature SP-22 were overexpressed at 37°C in BL21(DE3)pLysS cells, by induction with 1mM IPTG. Samples (1ml) were removed at the point of induction and hourly intervals thereafter for 3h. Bacterial pellets were resuspended in Laemmli sample buffer (10μl/0.1 absorbance unit), and denatured for 5 min at 100°C in the presence on DTT (150mM). Samples were analysed on a 10% SDS/polyacrylamide gel, and stained with Coomassie Brilliant Blue. Precursor SP-22 (pSP-22), and mature SP-22 (mSP-22) expression is shown in the lanes indicated. Molecular weight markers (M) are shown to the left of the gel.
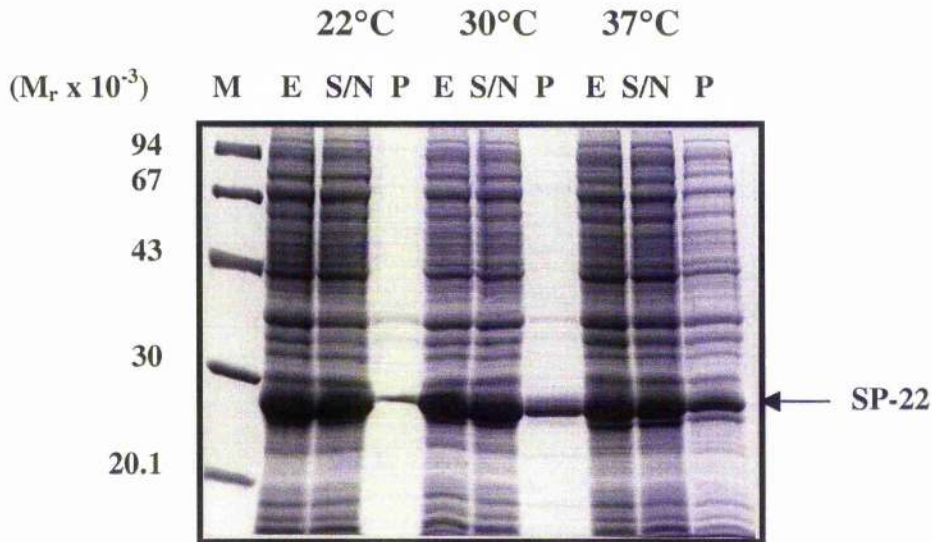
Figure 3.5. Assessment of Mature SP-22 Solubility at Different Induction Temperatures

Mature SP-22 was overexpressed in BL21(DE3)pLysS cells by addition of 1mM IPTG at induction temperatures of 22°C, 30°C, and 37°C. The bacterial culture (50ml) was centrifuged and the pellet resuspended in 5ml 50mM KPi buffer, pH 7.0 containing 150mM NaCl. Cells were lysed with repeated freeze-thaw cycles followed by sonication (four x 10 s bursts) and incubation with 0.1% (v/v) NP-40 at room temperature for 30 min. The cell extract (E) was separated into its soluble (S/N), and insoluble (P) fractions by centrifugation. Samples were diluted with an equal volume of Laemmli sample buffer, supplemented with DTT (150mM) and denatured for 5 min at 100°C, prior to loading on a 10% SDS/polyacrylamide gel. Bands were stained with Coomassie Brilliant Blue. Molecular weight markers (M) are shown on the left of the gel.

(Materials and Methods section 2.5.2). Aliquots of the peak fractions were TCA/acetone precipitated (Materials and Methods section 2.5.3) and analysed by SDS-PAGE to assess sample purity (Fig. 3.7). This system was extremely efficient in producing high yields of pure SP-22 (20-30mg/500ml culture). Insignificant levels of contaminating *E. coli* proteins were detected; therefore no other purification steps were deemed necessary. A typical protein elution profile is illustrated in Fig. 3.6.
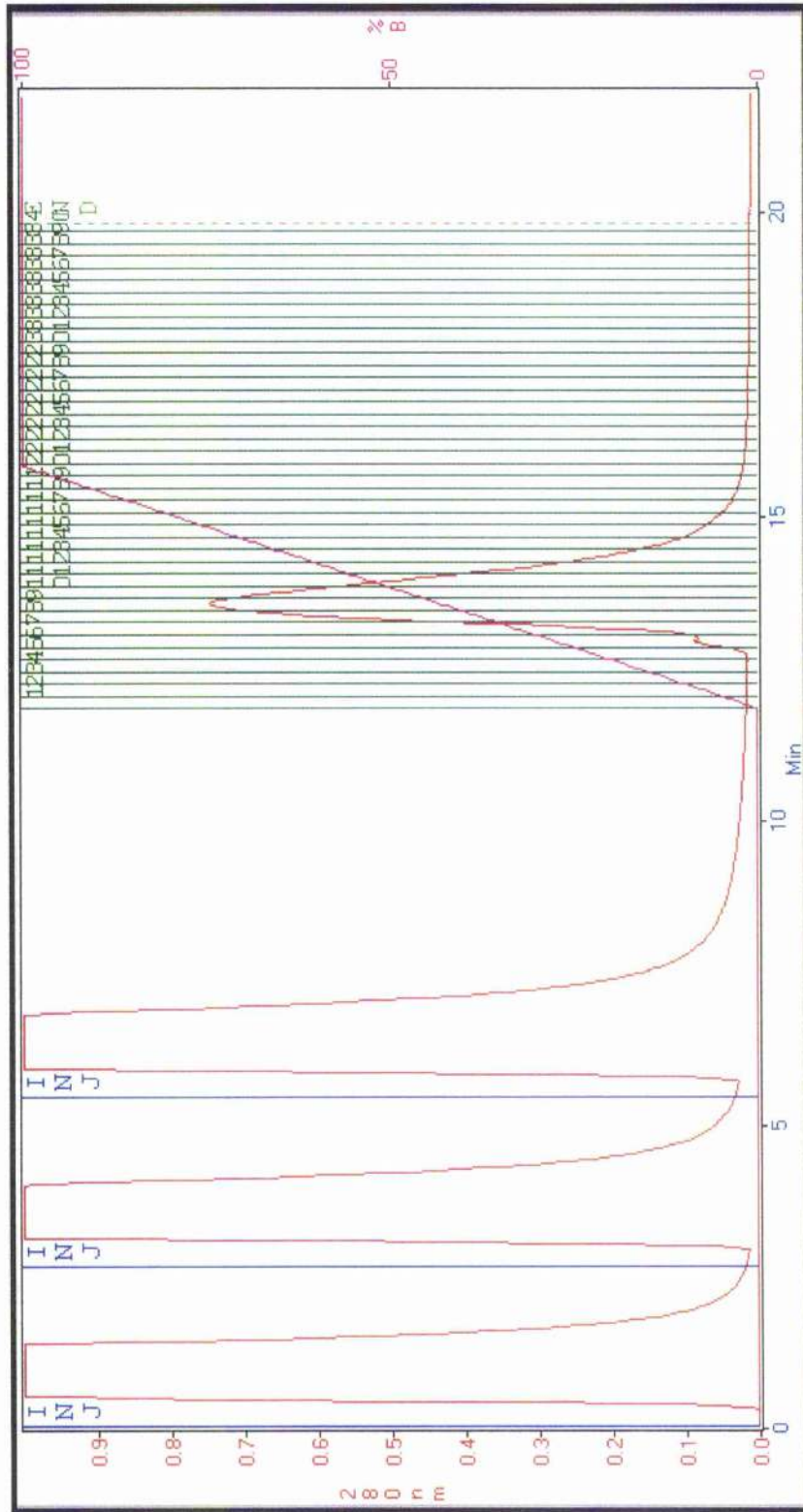
Figure 3.6. A BioCAD Elution Profile of Mature SP-22

The soluble fraction (15ml) of a 500ml bacterial culture containing overexpressed SP-22 was loaded onto a zinc metal chelate column via three 5ml injection stages (INJ) shown in the profile above. The protein was eluted over an increasing imidazole gradient (0.5mM-0.5M) shown in magenta. The A_{280} of SP-22 (x-axis) is recorded over time in minutes (y-axis). Fraction numbers are highlighted in green.
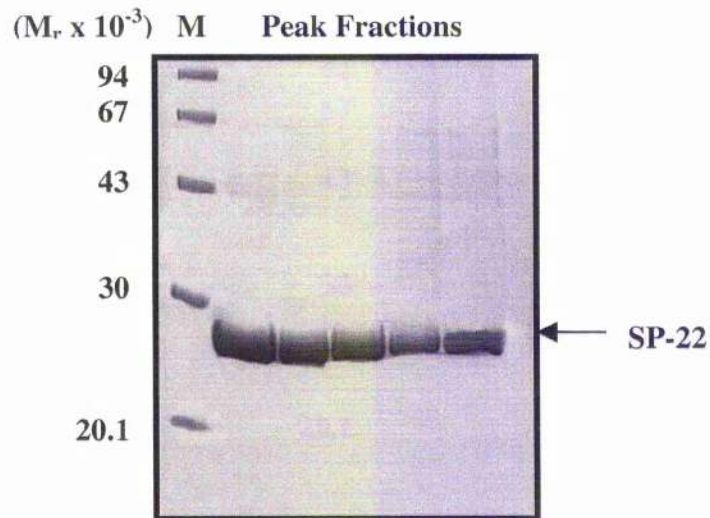
Figure 3.7. BioCAD Fractions of Purified SP-22

Aliquots of the peak fractions from a single His-tag purification run were TCA/acetone precipitated before final resuspension in Laemmli sample buffer. Samples were denatured for 5 min at 100°C in the presence of DTT (150mM). Samples were analysed on a 10% SDS/polyacrylamide gel and stained with Coomassie Brilliant Blue. Molecular weight markers (M) are shown to the left of the gel.

3.1.6. Non-Reducing SDS-PAGE Analysis of SP-22

To establish whether any inter- or intramolecular disulphide bonds were present involving any of the three conserved cysteine residues, SP-22 was subjected to non-reducing SDS-PAGE. Denaturation of purified SP-22 (5µg) in Laemmli sample buffer at room temperature (RT), 37°C, 70°C and 100°C for 5 min was assessed in the absence and presence of the reducing agent DTT (Fig. 3.8.). At each denaturation temperature, in the non-reduced sample lanes, a strong band was observed at approx. 47kDa, equivalent to a SP-22 dimer (D1). At the highest temperature (100°C), there was slight degradation of the dimer into its monomeric form likely to be non-specific reduction, as it is not observed at the lower temperatures. In contrast, in the presence of DTT, only the monomeric form (M1) of SP-22 was observed at all temperatures.

To establish whether any intermediate states of SP-22 exist between the monomeric and dimeric forms, SP-22 was denatured at increasing DTT concentrations (0-10mM). In the absence of DTT there is a major dimeric band (D1), evident until around 1mM DTT, at which point dissociation into its cognate monomers (M1) gradually increases with increasing DTT concentration (Fig. 3.9.). The protein bands appear diffuse and with lighter loading, major and minor bands corresponding to the monomeric state of the enzyme were observed between 1mM–10mM DTT. These two forms probably result from non-specific intramolecular disulphide bond formation during denaturation, altering the migration of the protein through the gel. The two monomeric forms are more easily observed with silver staining shown in chapter 5, Fig. 5.7. An additional band corresponding to tetrameric SP-22 (T1) was also detected between 0-1mM DTT, a likely consequence of dimer aggregation. Due to the oxidative properties of the NOVEX gradient gel, non-specific disulphide bonds can potentially form.
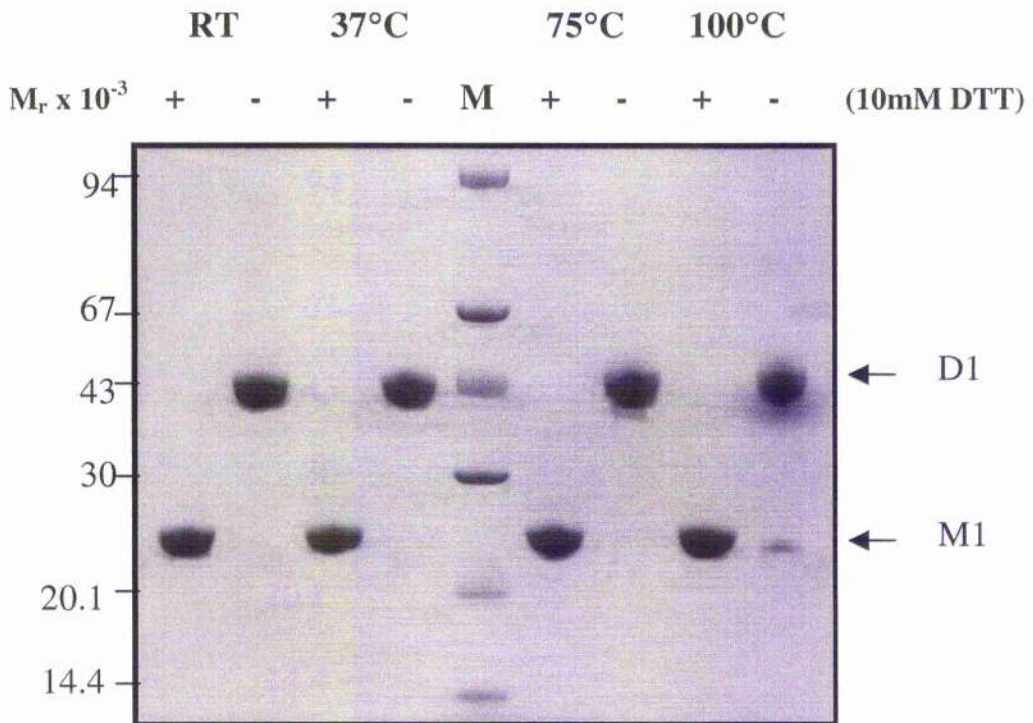
Figure 3.8. Non-reducing and Reducing SDS-PAGE Analysis of SP-22 with Increasing Denaturation Temperature

Samples of SP-22 (5µg) were run in reducing (150mM DTT) and non-reducing (-DTT) conditions on a 10-12% NOVEX gradient gel, following denaturation for 5 min as indicated. After staining with Coomassie Brilliant Blue, two forms of SP-22 were observed; the dimeric species (D1); and the monomeric species (M1). Molecular weight markers (M) are shown in the centre of the gel.
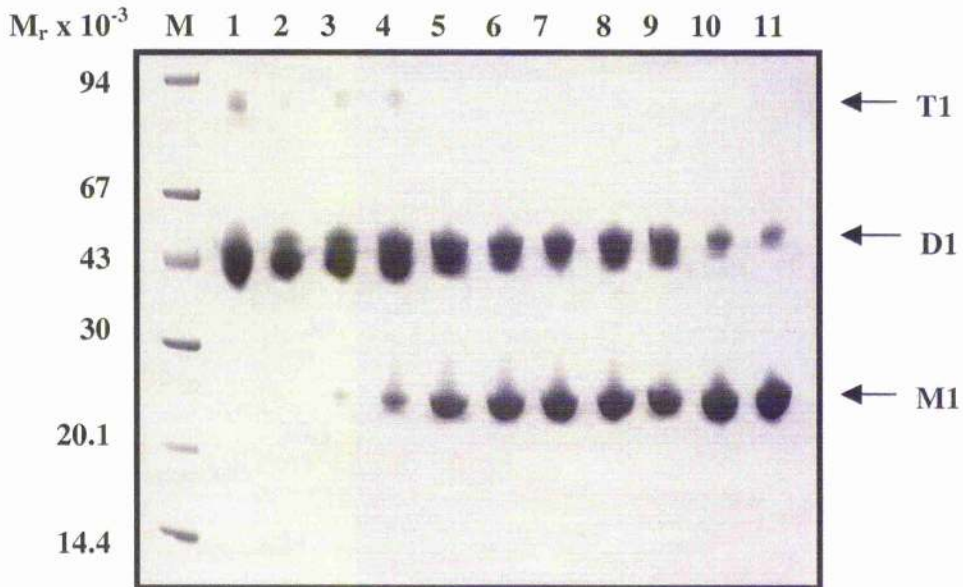
Figure 3.9. Progressive Reduction of SP-22 with Increasing DTT Concentration

Purified SP-22 (5µg) was analysed on a 10-12% NOVEX gradient gel, following denaturation for 5 min at 75°C, and progressive reduction with increasing DTT concentration (0-10mM). Bands were visualised with Coomassie Brilliant Blue staining. D1 and M1 indicate the dimeric and the monomeric forms of SP-22, respectively. T1 indicates the putative tetrameric form. Molecular weight markers (M) are shown on the left of the gel. Lanes 1-10 indicate the concentration of DTT present (mM). **Lane 1** (no DTT), **2** (0.5mM), **3** (0.75mM), **4** (1mM), **5** (2mM), **6** (3mM), **7** (3.5mM), **8** (4mM), **9** (6mM), **10** (8mM) and **11** (10mM).

Chapter 3

Section 2

3.2.0. Introduction

In the previous section it was established that there are disulphide bonds present within the basic dimeric unit of SP-22. In order to identify the key cysteine residues involved, and to determine their roles in maintaining the structure and function of SP-22, three mutants were generated (C47S, C66S, and C168S). Single point mutations were incorporated into the wild type plasmid converting each cysteine to a serine residue. Mutagenesis requires an oligonucleotide primer complementary to the region of the gene containing the target residue to be mutated. The two strands of the plasmid template are separated by thermal denaturation, enabling the mutagenic primers to anneal to their complementary regions. A DNA polymerase enzyme then elongates the primer before the duplex DNA is religated by DNA ligase. Amplification of the mutant constructs in bacterial cells yields two products: one mutated strand, and one parental (non-mutated) strand. To remove the parental strand prior to amplification, the DNA is digested with an endonuclease (*Dpn* I), which specifically recognises methylated and hemi-methylated DNA, leaving behind the unmethylated, mutated strand.

Mutagenesis will enable the elucidation of the roles of the cysteine residues in structural assembly and peroxidase function of SP-22. It has been proposed that C47 is the catalytic residue due to the presence of a sulphenic acid moiety, functioning as a 2-electron redox centre; however mutational studies have yet to be carried out. The C47S mutant should also serve as an effective negative control for functional studies. This is discussed in more detail in chapter 6.

Results

3.2.1. Generation of the Cysteine Mutants

The SP-22/pET-14b recombinant plasmid was used as a template for the mutagenesis PCR reaction. Specific oligonucleotide primers complementary to opposite strands of the vector regions to be mutated were designed (Fig. 2.3). These primers were extended upon amplification using the *Pfu Turbo* DNA polymerase system according to the protocol described in Materials and Methods section 2.3.3. The mutant constructs were amplified in DH5α *E. coli* cells and

selected according to their ampicillin resistance (Materials and Methods section 2.2.5. Several colonies were selected, and the mutant plasmid DNA was isolated from 5ml overnight cultures as described in Materials and Methods section 2.3.3, and analysed on a 1% (w/v) agarose gel (results not shown). Successful mutagenesis of the cysteine residues was confirmed by sequencing the DNA obtained from a large culture (see Materials and Methods section 2.3.7).

3.2.2. Expression and Purification of the Mutant Constructs

Each of the mutant constructs were transformed into competent BL21(DE3)pLysS cells for heterologous expression. For optimum solubility of wild type SP-22, expression was carried out at 22°C; therefore this temperature was also selected for the mutants. High levels of expression were achieved after a 5h induction period (Fig. 3.10). Cells from a 50ml bacterial culture were lysed (Materials and Methods section 2.3.9). Analysis by SDS-PAGE on a 10% polyacrylamide gel demonstrated that the degree of solubility varied between the mutants (Fig. 3.11). As a percentage of the total SP-22 in the cell extract, the extent of solubility for C47S, C66S and C168S was estimated to be approx. 75%, 50% and 65% respectively as judged by visual inspection. As soluble protein levels in all cases were sufficient for future experiments, no additional attempts were made to improve solubility.

The mutants were purified as for wild type SP-22 using a BioCAD® SPRINT™ Perfusion® Chromatography Workstation (Materials and Methods section 2.5.2). Peak fractions were TCA/acetone precipitated (Materials and Methods section 2.5.3) and analysed on a 10% gel by SDS-PAGE as described in Materials and Methods section 2.5.6 (results not shown). The C47S mutant demonstrated a weaker binding affinity than C66S and C168S. The peak fractions were pooled and dialysed into the required buffer (Materials and Methods section 2.5.4). This

80
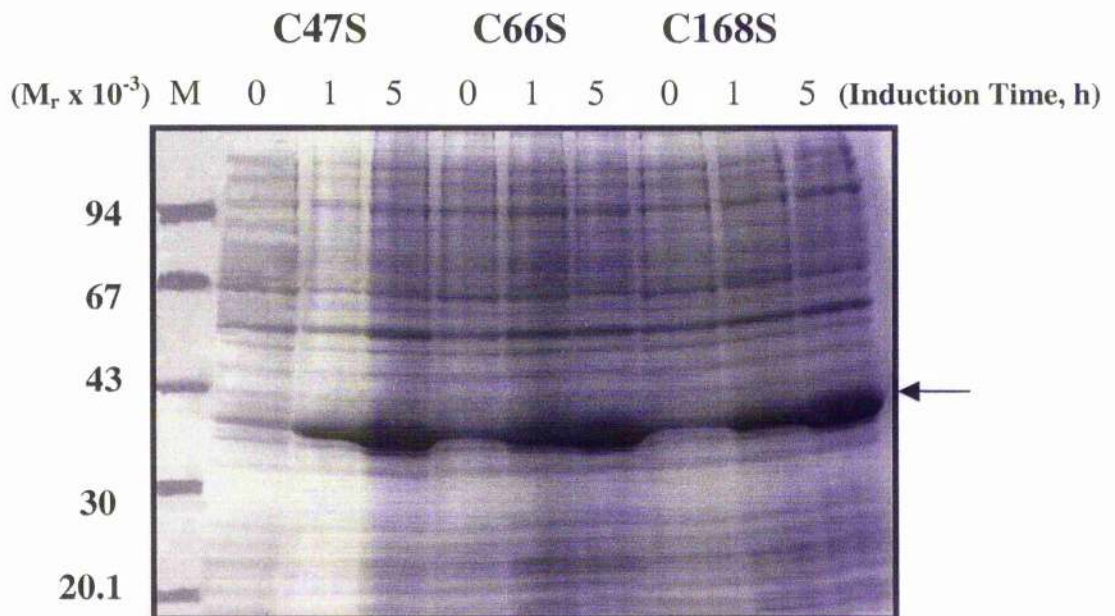
Figure 3.10. Overexpression of the Cysteine Mutants

Proteins were expressed over 5h at 22°C in *E. coli* BL21(DE3)pLysS cells. Samples were denatured in the presence of DTT (150mM) at 100°C for 5min prior to analysis on a 10% SDS/polyacrylamide gel. Protein bands were stained with Coomassie Brilliant Blue. Molecular weight markers (M) are shown to the left of the gel. The arrow on the right of the gel denotes overexpressed recombinant protein.
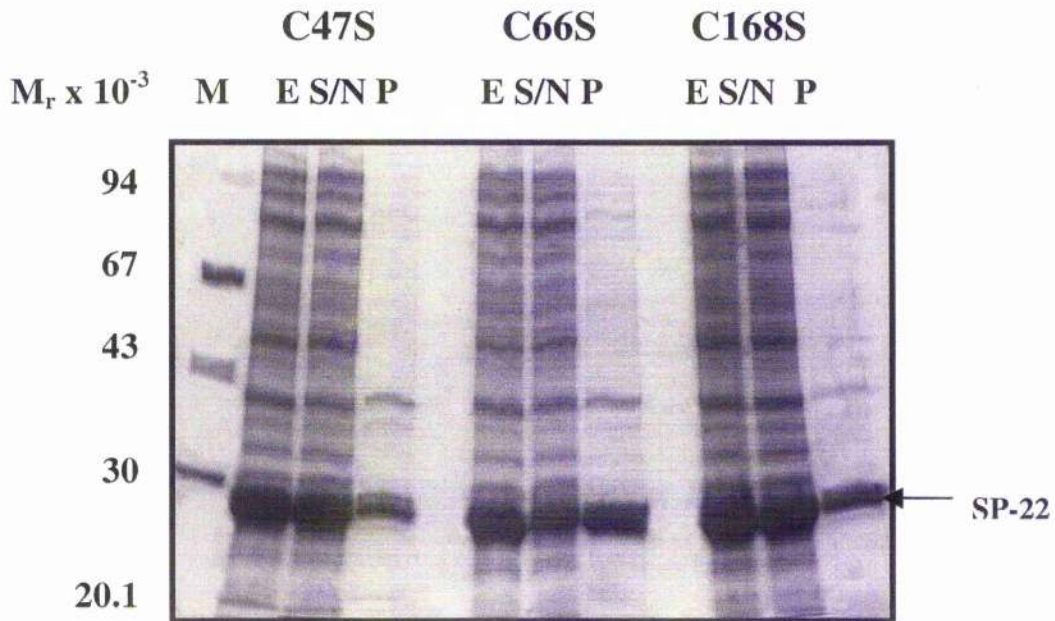
Figure 3.11. Solubility Assessment of Mutant SP-22s

Following protein overexpression of the mutant SP-22s (C47S, C66S and C168S) at 22°C for 5h, the bacterial culture (50ml) was centrifuged and the pellet resuspended in 5ml 50mM KPi buffer pH 7.0 containing 150mM NaCl. Cells were lysed with repeated freeze-thaw cycles, followed by sonication (four x 10s bursts) and incubation with 0.1% (v/v) NP-40 at room temperature for 30 min with shaking. The cell extract (E) was separated into its soluble (S/N) and insoluble (P) fractions by centrifugation. Samples were prepared in Laemmli sample buffer and denatured for 5 min at 100°C in the presence of DTT (150mM), prior to loading on a 10% SDS/polyacrylamide gel. Bands were stained with Coomassie Brilliant Blue. Molecular weight markers (M) are shown to the left of the gel. The arrow indicates mutant SP-22 protein.

one-step procedure yielded 5-10mg/ml of extremely pure protein per 500ml culture. No further purification steps were deemed necessary.

3.2.3. Determination of the Specific Cysteines Involved in Disulphide Bond Formation

In the first section it was established that SP-22 is formed from a basic dimeric unit containing one or more disulphide bonds. To pinpoint the cysteine residues that participate in these interactions, each of the mutants was analysed by non-reducing SDS-PAGE (Materials and Methods section 2.5.6). For comparison, reduced samples containing DTT were also prepared. In non-reducing conditions, disulphide bonds of wild type SP-22 remain intact and SP-22 is dimeric. Fig. 3.12 confirms that both C47 and C168 are involved in the formation of these disulphide bonds as in the absence of DTT these mutants still remain in their monomeric form (M1). However C66S is dimeric; therefore this cysteine does not participate in subunit association. Therefore, it can be concluded that the disulphide bonds form between the N-terminal cysteine of one monomer and the C-terminal cysteine of the opposing subunit.

3.2.4. Accessibility Determination of the Cysteines using Ellman's assay

Ellman's assay was used to confirm which cysteines were accessible to thiol modification by the reactant 5,5'-dithionitrobenzoic acid (DTNB) under native and non-native conditions. The number of thiols accessible to DTNB was assessed by measuring the A_{412} of the nitrothiobenzoate (NTB) product released during the reaction. The chemical reaction also gives rise to a mixed-disulphide product coupled to the release of the NTB anion. The A_{412} of native purified wild type and mutant SP-22 was measured over 40 min following addition of DTNB as described in Materials and Methods section 2.5.10. No cysteine residues were accessible in the fully folded wild type SP-22; however following denaturation in 6M GdmCl, one cysteine became accessible (results not shown). This cysteine is C66, as the N- and C-terminal cysteines are involved in disulphide bond formation confirmed in the previous section. This implies that in the native protein C66 is buried in the overall structure. To confirm that the accessible
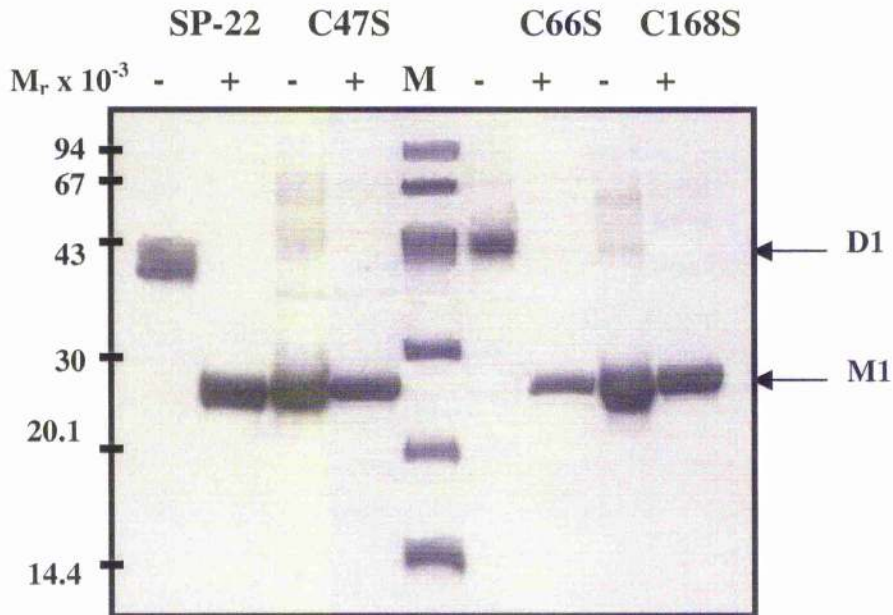
Figure 3.12. Reducing and Non-reducing SDS-PAGE of the SP-22 Mutants

Purified samples (5μg) of wild type SP-22, C47S, C66S and C168S prepared in Laemmli sample buffer were denatured at 75°C for 5 min. Samples were analysed on a 10% SDS/polyacrylamide gel in the presence (+), or absence (-) of 150mM DTT. Protein bands were stained with Coomassie Brilliant Blue. Molecular weight markers (M) are shown in the centre of the gel. Arrows indicate the dimeric (D1) and monomeric (M1) forms of SP-22 respectively.

cysteine residue is C66, Ellman's assay was repeated for the three cysteine mutants (results not shown). As expected no cysteines were accessible in the C66S mutant, in both native and denaturing conditions. For C47S and C168S however, an increase in the A_{412} was observed corresponding to thiol modification by DTNB. These findings reiterate that the N- and C-terminal cysteines participate in disulphide bond formation and also show that in the native wild type protein, C66S is buried within the structure and is not susceptible to modification by DTNB.

3.2.5. Summary and Discussion

In this chapter the first successful overexpression of SP-22 as a recombinant protein is reported. Precursor and mature forms of bovine SP-22 were cloned into the expression vector pET-14b and overexpressed as N-terminal His-tag fusion proteins in *E. coli*. Both forms exhibited high levels of expression; however their solubility properties differed. The precursor form was totally insoluble, while mature SP-22 solubility increased with a reduction of induction temperature. Proteins containing leader peptides are generally insoluble as they maintain the nascent polypeptide in its unfolded state to enable its successful translocation to the target organelle. The presequence is subsequently cleaved by a specific protease, thus allowing the protein to fold into its native, active state. As our interest resides in the active form of the enzyme, no further attempts to solubilize precursor SP-22 were made.

High levels of extremely pure mature SP-22 were obtained following a one-step method of metal chelate affinity chromatography, facilitating future structural analysis. Following non-reducing SDS-PAGE of the purified enzyme it was established that SP-22 forms a dimeric unit, containing two intermolecular disulphide bonds. This conforms to results generated from other studies on mammalian 2-Cys peroxiredoxins. Using mutagenesis to replace each of the three conserved cysteine residues with serine residues, and analysing each of the mutants by non-reducing SDS-PAGE, it was established that the disulphide interactions occur between the N-terminal (C47) cysteine of one monomer and the

C-terminal (C168) cysteine of the opposing subunit. These findings were supported using Ellman's assay which confirmed that only one cysteine residue (C66) was accessible to DTNB in the native protein, suggesting the other two (C47 and C168) are participating in disulphide bond formation. These results were also typical for other 2-Cys peroxiredoxin members.

Although not discussed, the human form of SP-22 was also amplified and cloned into pET-14b as for bovine SP-22. Human SP-22 exhibits >90% primary sequence identity with the bovine form. Using the bovine SP-22 nucleotide sequence, a search of a human expressed sequence tag (EST) database (www.ncbi.nlm.nih.gov/BLAST/) was conducted. Clones displaying high homology with bovine SP-22 were selected, and specific oligonucleotide primers were designed to the N- and C-terminal region of the protein. Due to low expression levels, only detectable with an anti-His-tag monoclonal antibody, and time considerations, structural and functional studies were carried out with the bovine isoform. Investigating alternative *E. coli* strains and heterologous expression systems to increase production of the human isoform will be advantageous to enable future structural and functional studies. As human E3 has been cloned as a His-tag fusion protein, and one of the major aims of this work is to determine whether E3 and SP-22 interact, it would be ideal to utilise the human isoform in interaction studies.

Chapter 4

Section 1

4.1.0. Introduction

Analytical ultracentrifugation (AUC) was employed to determine the exact molecular weight of SP-22, to establish if it forms a larger oligomeric structure comparable with other 2-Cys Prx members. There are two main experimental approaches: sedimentation equilibrium (SE) analysis and sedimentation velocity (SV) analysis (Laue and Stafford, 1999). SE provides information on the mass and stoichiometry of macromolecules in solution and can also determine association/dissociation constants for protein-protein interactions. SV gives information on the shape and stoichiometry of a macromolecule. There are three principal forces exerted on a molecule that are used in the calculation of the sedimentation coefficients obtained from AU: the centrifugal force, buoyancy of a molecule and the frictional force. The buoyant and frictional forces are in opposition to the centrifugal force. An analytical centrifuge is equipped with an optical system that allows the measurement of one or more optical signals as a function of radial position of the molecule held within a specially designed cell located within the centrifuge rotor. Relatively slow centrifugal speeds are selected so that the diffusion flow and the sedimentation flow of a macromolecule are at equilibrium at any radial position in the cell.

AUC is a rapid and non-destructive technique requiring low sample concentrations; therefore is a useful tool for the assessment of oligomeric structure prior to the application of high-resolution techniques such as X-ray crystallography and nuclear magnetic resonance (NMR).

Results

4.1.1. Size Determination of SP-22

Purified SP-22 prepared in 50mM KPi pH 7.2 containing 150mM NaCl was diluted to give 9 samples covering an A_{280} range of approx. 0.1-0.5 to allow the possible determination of aggregate formation. The equilibrium run was carried out at 4°C at three rotor speeds of 5,7 and 10K to allow detection of species within the 80-1000 kDa range (Materials and Methods section 2.5.21). Recordings at 3K were taken to allow back calculation of the sample

concentration and centrifugation at 47K was also carried out to generate a baseline free from macromolecular species. Results from the 10K run were discarded as this speed was too fast, resulting in complete sedimentation of the SP-22. Figure 4.1 shows the apparent whole cell weight average mass (M_w,app), against the A_{280} of SP-22 at rotor speeds of 5 and 7K. The distribution data obtained from the equilibrium runs fitted well to a single ideal species model. Moreover, at the time of the equilibrium experiments it was assumed that the SP-22 oligomer existed as a single species. The M_w,app varied slightly with the concentration of SP-22 contained within the cell, and even more so between the two different rotor speeds. A mass of 615-635kDa was determined for SP-22, corresponding to 25-26 monomers. A slight decrease in apparent whole cell weight average mass with increasing protein concentration was observed at both rotor speeds.

4.1.2. Summary and Discussion

The sedimentation equilibrium results confirm that SP-22 does have an alternative high M_r oligomeric form consistent with other mammalian Prxs, with an average molecular weight of 615-635kDa. This equates to approx. 25-26 SP-22 monomers, much larger than the other mammalian Prxs. Our initial hypothesis was that SP-22 might exist as a double toroid containing 10 or 12 subunits per ring. It becomes evident following electron microscopy (Chapter 5 section 2) that SP-22 is toroidal like the other mammalian Prxs. Furthermore it can also form stacks of two and three rings. Therefore, it is possible that there is a dynamic equilibrium occurring between the various oligomeric forms of SP-22. This would account for larger-than-expected estimated mass of SP-22 determined by this technique. There is slight deviation from non-ideality, indicated by a slight decrease in apparent whole cell weight average mass with increasing protein concentration. This may be due to the presence of a central cavity within the SP-22 oligomer, as in solution they would not be able to pack so tightly together resulting in a larger excluded volume than for a perfect compact sphere.
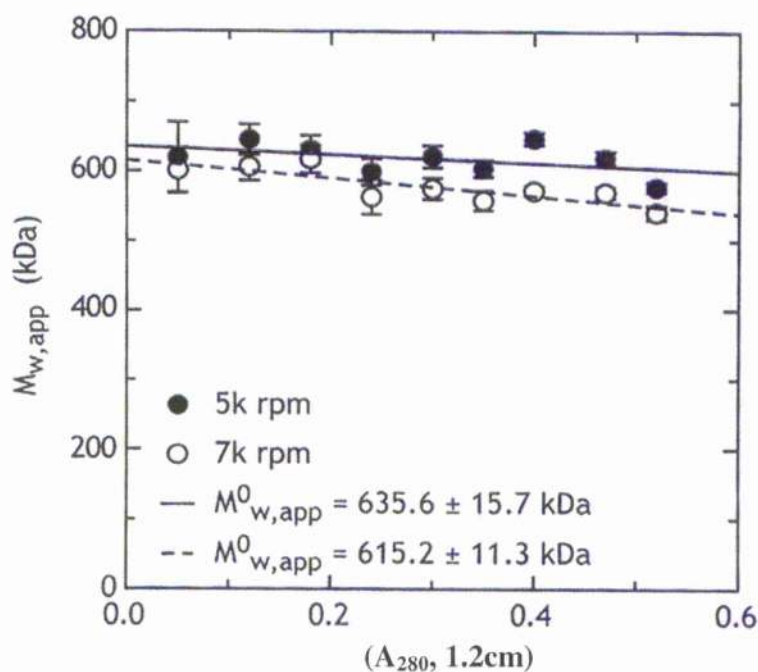
Figure 4.1. Estimation of the Molecular Weight of SP-22 by Sedimentation Equilibrium Ultracentrifugation

Purified SP-22 prepared in 50mM KPi pH 7.2 containing 150mM NaCl was diluted to give 9 samples covering an A_{280} range of approx. 0.1-0.5. The equilibrium run was carried out at in a Beckman Optima XL-A analytical ultracentrifuge at 4°C. Centrifugation at 47K was also carried out to generate a baseline free from macromolecular species. The results at rotor speeds of 5 and 7K are plotted as apparent whole cell weight average mass (M_w,app), against the A_{280} of SP-22.

Studies were also carried out in the presence of 20mM DTT to assess the effects of the disulphide bonds on oligomer integrity. Although the DTT interfered with the optics of the ultracentrifuge and were inaccurate, it was clear that the integrity of the complex was not dependent on disulphide bond formation, with the molecular weight of the oligomer remaining in the $\geq$500kDa range. As an alternative means of investigating the contribution of the disulphide bonds equilibrium studies were also carried out for the C47S mutant. This protein appeared to form large aggregates of approx. 1500kDa, which following assessment by electron microscopy in Chapter 5, were recognised to be genuine.

Chapter 4

Section 2

4.2.0. Introduction

There are several techniques available to probe the structural conformations of proteins including NMR, X-ray crystallography and circular dichroism (CD) (Price, 2000) . CD is a form of light absorption spectroscopy used to analyse the general characteristics of protein and nucleic acid conformations (Kelly and Price, 2000). This technique involves the measurement of the differential absorption of left- and right-circularly polarised light instead of the more frequently measured isotropic light. If one of the components is absorbed to a greater extent, an ellipse is generated on recombination (dichroism). Ellipticity (θ) is typically used as the unit of CD, and is defined as the tangent of the ratio of the minor to major elliptical axis ($\theta = \tan^{-1}$). CD measurements are recorded using an instrument called a spectropolarimeter. The macromolecule of interest must be an inherently asymmetric chromophore or a symmetrical chromophore in an asymmetric environment.

CD spectra can provide low resolution, yet reliable, secondary structural information on a protein. In the far UV region (240-180nm) the principal absorbing species is the peptide bond, therefore CD studies in this region can be used to estimate the proportion of α-helix, β-sheet and β–turn (Sreerama et al, 1999). The most common secondary structural motif in proteins is the α-helix, displaying a CD spectrum with distinctive minima at 208 and 222nm. This structural motif is easily identified as it produces the largest CD signal magnitude. β-sheet content is not so easily determined due to its decreased signal and the various arrangements of the β-sheets, parallel or anti-parallel, and varying lengths and widths. These are all factors that may hinder the accurate determination of β-sheet content of a protein. Furthermore the absorption of a third structural feature called the random coil also absorbs in a similar region to that of the β-sheet. 'Random coils' represent the regions of a protein that do not encompass the major secondary structural motifs. An additional secondary structural feature called the coiled-coil, comprising α-helices wrapped around each other, is ubiquitously identified in a large number of proteins. Coiled-coils are well defined and mainly

consist of seven-residue repeats called heptads, the number of which varies between proteins.

There are several computer programs available to estimate the secondary structural content of a protein, from the properties of their CD spectra. The majority of these programs offer an accurate determination of α-helical content, provided data is submitted down to at least 190nm. Databases containing the spectra of approximately 40 reference polypeptides (globular) with resolved structures, are used as models to estimate the various secondary structural contributions within the unknown protein.

Tertiary structural information can also be obtained by recording CD spectral changes in the near UV region (320-260nm), where the contribution of the aromatic amino acids (phenylalanine, tyrosine and tryptophan), prominently reflect more global and three-dimensional characteristics of the protein. Tryptophan is responsible for the most intense transitions in the near UV region, compared with the other aromatic amino acids, exhibiting a maximal extinction coefficient at 290nm (Kelly and Price, 2000). Disulphide bond transitions can also contribute to the overall absorbance in this region between wavelengths of 250-270nm. Any protein conformational changes and significant unfolding or folding events can be traced by monitoring the change in ellipticity with progressive chemical denaturation. In general, urea and guanidinium chloride (GdmCl) are the chemical denaturants of choice, prepared in a suitable buffer.

Following *in vivo* translation, the nascent polypeptide is transported to its target intracellular compartment where it folds into the native, active form. Attainment of a mature tertiary structure is a complex process that may involve several folding steps, and additional enzymes (molecular chaperones) or other protein co-factors are often required to mediate the folding process. Understanding folding pathways can aid the optimisation of expression of soluble recombinant proteins

in the laboratory and can provide an improved insight into a number of pathologies that arise from protein misfolding.

In this section, CD was used to determine the secondary structure of SP-22. Furthermore the stability and mechanism of SP-22 oligomer unfolding was investigated, monitoring changes in CD spectra in the far UV region during gradual denaturation in urea. The contribution of the disulphide bonds to complex stability was also assessed, by comparing the denaturation profiles of wild type and mutant SP-22 in the presence and absence of the reducing agent DTT.

Results

4.2.1. The CD Spectrum of Wild Type SP-22

Purified SP-22 (0.2mg/ml) was prepared for CD analysis as described in Materials and Methods section 2.5.19. Figure 4.2 shows the CD spectrum obtained for wild type SP-22 in its native state. The CD spectrum was produced following the subtraction of the baseline (buffer only) spectrum from the sample spectrum. Using the SELCON procedure (Sreerama and Woody, 1993) the secondary structure estimates were calculated and are tabulated below:

Secondary Structure	Proportion Present in Overall Structure (%)
α-Helix	46.3
Anti-parallel β-Sheet	9.1
Parallel β-Sheet	6.6
β-Turn	13.8
Other	24.2

Table 1. Secondary Structure Estimates of Wild Type SP-22

It can be seen that the largest secondary structure contribution is attributed to the α-helical content, constituting nearly 50% of the overall secondary structure. Figure 4.3 shows the alignment of SP-22 with the 2-Cys Prxs HBP23, and TPx-B, complete with highlighted regions that encode the various secondary structural
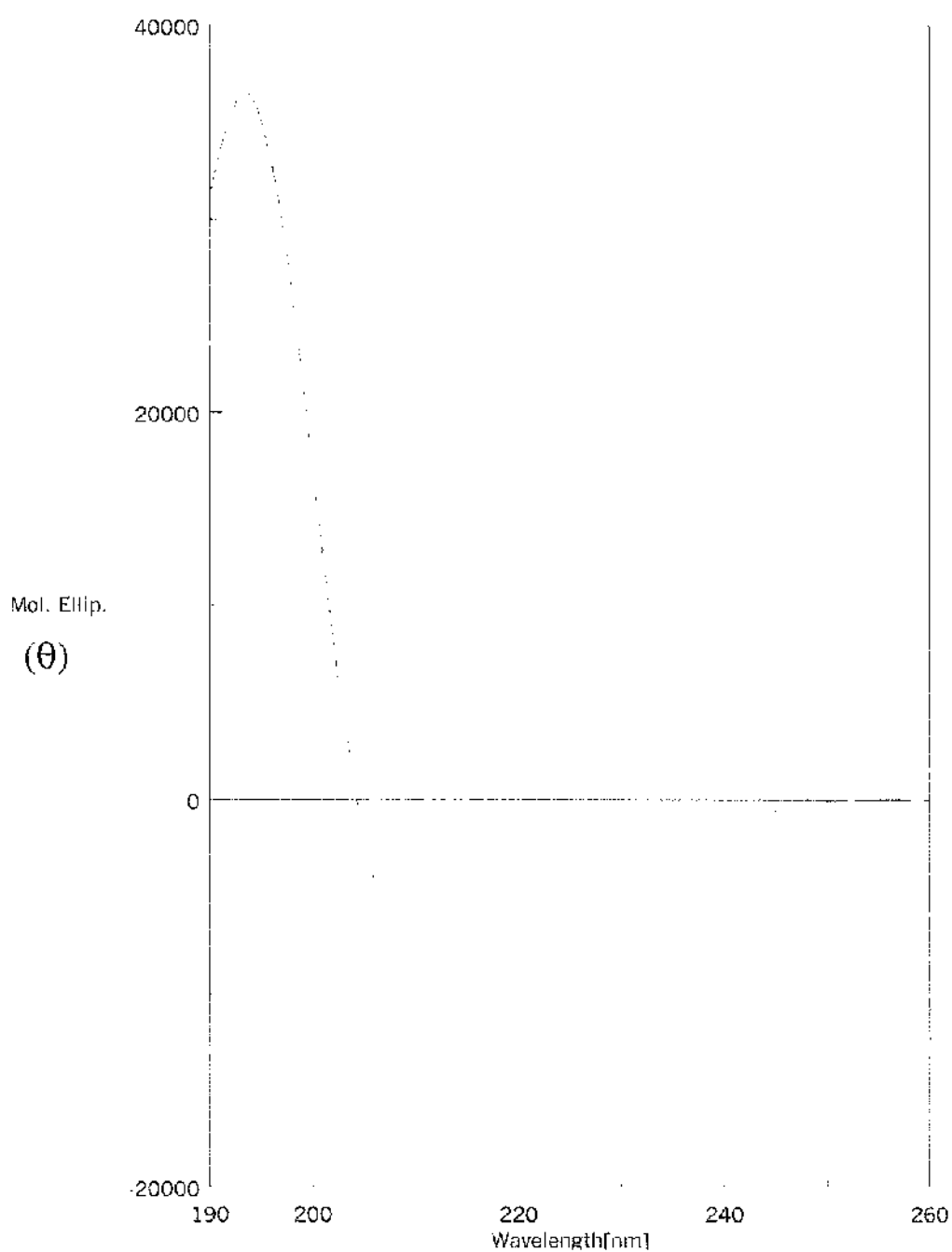
Figure 4.2. Secondary Structure Determination of SP-22

Measurements were recorded in a quartz cell with a pathlength of 0.02cm, containing purified SP-22 (0.2mg/ml) in 50mM KPi buffer, pH 7.2 containing 150mM NaF.

motifs. The sequence identity between the three proteins, and secondary structural similarity between HBP23 and TPx-B is extremely high. From the CD results, as for HBP23 and TPx-B, the α-helix is the predominant secondary structural component of SP-22. However, SP-22 is predicted to have a slightly greater α-helical content than the other two Prxs, particularly TPx-B, which contains less α-helix than HBP23. The 'other' secondary structural estimation encompasses any other structure not easily identifiable by CD because their contribution is usually masked by the α-helix and β-sheet contributions.

4.2.2. Assessment of SP-22 Stability

Urea was selected to assess SP-22 oligomer stability by chemical denaturation, and to establish the pattern of the unfolding profile. Purified SP-22 samples (0.5mg/ml) were prepared in increasing urea concentrations as described in Materials and Methods section 2.5.19. Denaturation was carried out at room temperature, incubating overnight to allow equilibrium to be reached. Despite this lengthy incubation period and choice of denaturant, complete unfolding was not achieved, indicating that SP-22 was extremely stable. Pilot studies had established previously that the routinely used, 15-min incubation period was insufficient to promote unfolding.

Figure 4.4 shows the unfolding profile of SP-22 with increasing urea concentration. The effect of urea on the protein conformation may account for the small increase in the profile between 0-3M urea. Between 4 and 6M urea there is a major unfolding event that is subsequently followed by gradual unfolding until 9.5M urea at which stage the oligomer still retains approx. 25% of native ellipticity. Overall results therefore indicate that the SP-22 oligomer is extremely stable and unfolding does not follow a simple two-state mechanism (native state→ unfolded state) characterised by a monophasic denaturation curve.
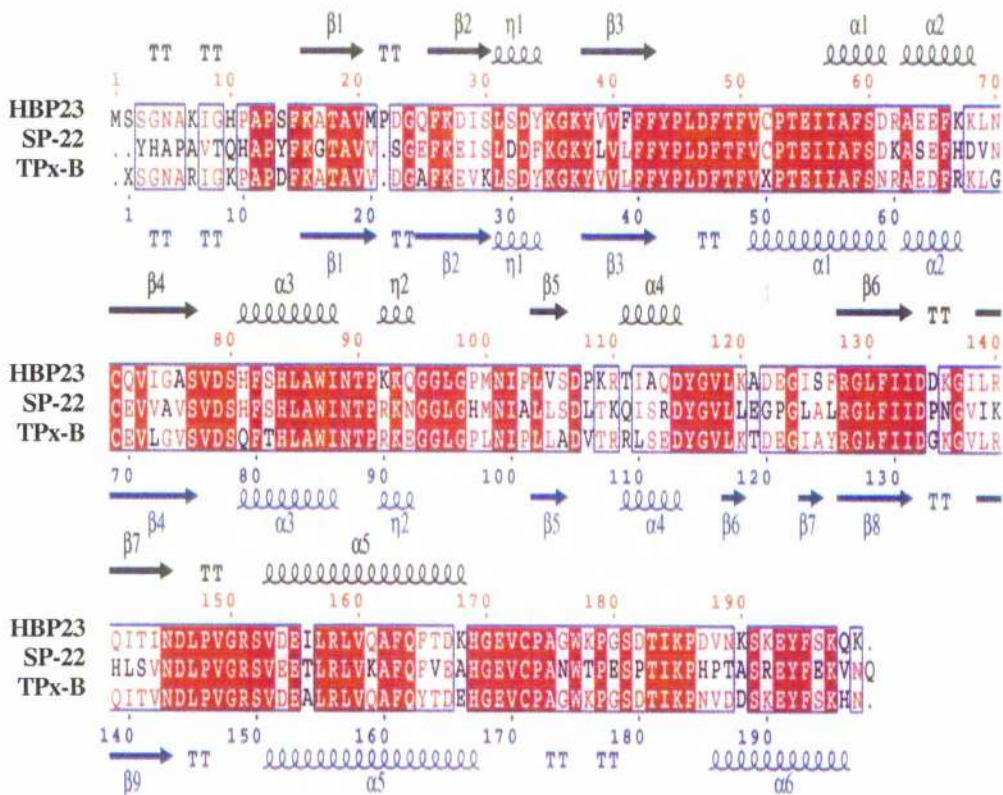
Figure 4.3. Alignment of SP-22 with HBP23 and TPx-B

SP-22 protein sequence alignment with rat haem-binding protein (HBP23) and human thioredoxin peroxidase-B (TPx-B). The secondary structural features for HBP23 and TPx-B have been resolved and are shown above the amino acid stretches where they occur. α-helices (α), β-sheets(β), coiled-coil (η), and TT (β-turns). Amino acid identity is highlighted in red.

To elucidate the effect of the disulphide bonds on oligomer stability and to prevent the formation of non-specific disulphide bond formation during unfolding, the experiment was also performed in the presence of 20mM DTT (Fig. 4.4). As expected, the reduced protein unfolds more readily in a co-operative manner with the most significant structural changes occurring between 4 and 6M urea, implying that the disulphide bonds are important in this stage of unfolding for stability. However as for non-reduced SP-22, unfolding is not complete and the protein displays approx. 25% native ellipticity at 9.5M urea.

Overall the integrity of the oligomer was maintained suggesting that the disulphide bonds are not required for assembly; however they do contribute to overall stability. To support this result, these experiments were repeated for the cysteine mutants.

4.2.3. Secondary Structural Determination of C47S

Secondary structural determination of C47S was carried out as for SP-22. Incorporating mutations into a protein may give rise to slight conformational changes in the complex; however, the far UV CD spectrum of C47S was super-imposable with the wild type SP-22 CD spectrum (results not shown). We can therefore conclude that cysteine 47 is not critical for maintaining any of the major secondary structural features within the protein.

4.2.4. Assessment of C47S Stability

The unfolding profile for C47S indicated that there is slightly reduced stability in comparison with wild type SP-22 at the lower concentrations of urea (2-4M), at which point gradual loss of secondary structural elements occurs until 9.5M urea (Fig. 4.5).
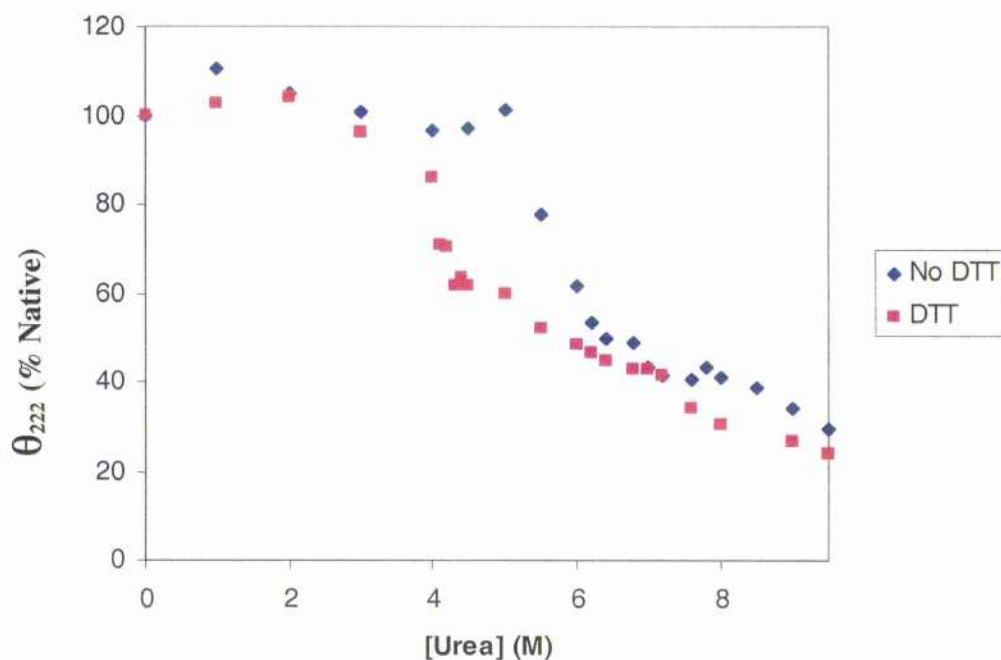
Figure 4.4. Unfolding Profile of SP-22 During Denaturation with Increasing Urea Concentration

Purified SP-22 (0.5mg/ml) was incubated overnight at room temperature at increasing urea concentration in the presence or absence of 20mM DTT. The fraction of folded protein was calculated as a percentage of the native state, using ellipticity readings recorded at 222nm in a cell with a pathlength of 0.05cm.
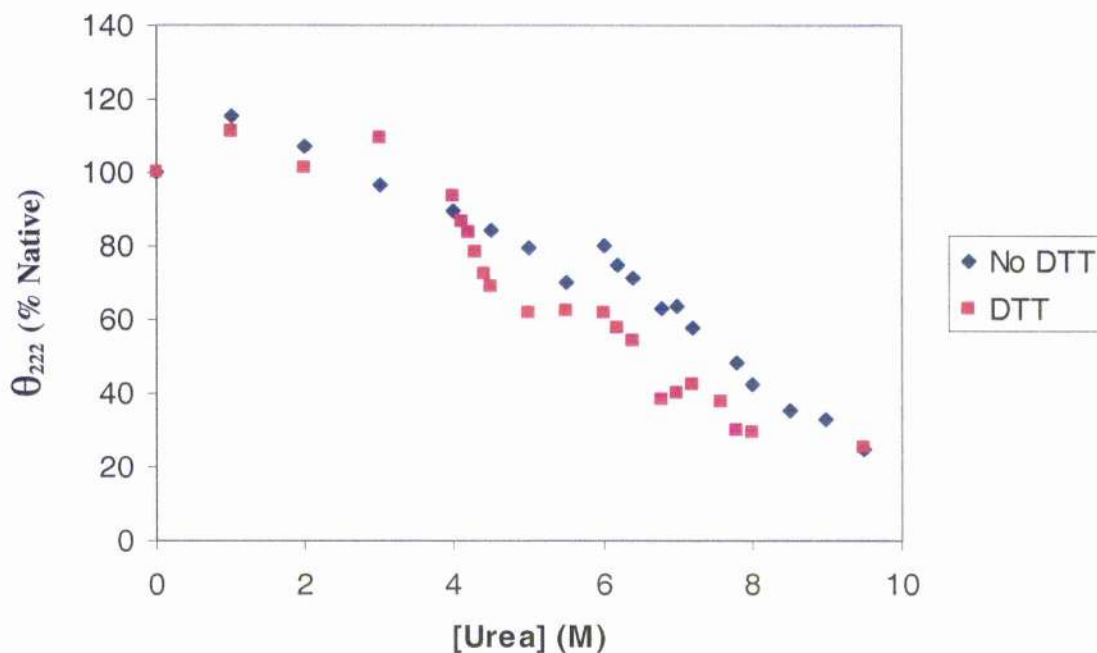
Figure 4.5. Unfolding Profile of C47S During Denaturation with Increasing Urea Concentration

Purified C47S (0.5mg/ml) was incubated overnight at room temperature at increasing urea concentration in the presence, or absence of 20mM DTT. The fraction of unfolded protein was calculated as a percentage of the native state, using ellipticity readings recorded at 222nm in a cell with a pathlength of 0.05cm.

Unfolding events commence slightly earlier than for wild type at approx 3.75M urea, after which gradual denaturation continues until ~20% of native ellipticity remains at 9.5M Urea. Therefore, the disulphide interactions do in fact influence overall oligomer stability.

The denaturation of C47S was also carried out in the presence of 20mM DTT to ensure that non-specific, stabilising disulphide bonds that could potentially form during unfolding, were not present (Fig. 4.5). In general the effects of DTT on C47S stability were less evident than for wild type SP-22. This is not unexpected given that mutating C47 prevents disulphide bond formation with C168.

4.2.5. Assessment of C66S Stability

Although C66 does not participate in dimerisation of SP-22 its role in overall stability remains to be investigated. Results suggest that C66 may contribute to oligomer stability; an increased resistance to unfolding is observed with only localised events occurring above 6M urea after which unfolding ensues (Fig. 4.6.). Complete denaturation was not achieved with approx. 30% of the native protein ellipticity remaining at 9.5M urea.

As for wild type SP-22 and C47S, the experiment was repeated in the presence of 20mM DTT. The destabilising effect of the DTT was more pronounced for this mutant than C47S and mirrored that of the wild type. This is not unexpected as disulphide bonds within the dimeric unit are intact in this mutant. The major unfolding step occurs at the same point (4–6M urea) as for wild type SP-22, implying that disulphide bond contribution to overall SP-22 stability is most important in this region. Approx. 25% of the native protein ellipticity is still present in 9.5M urea.
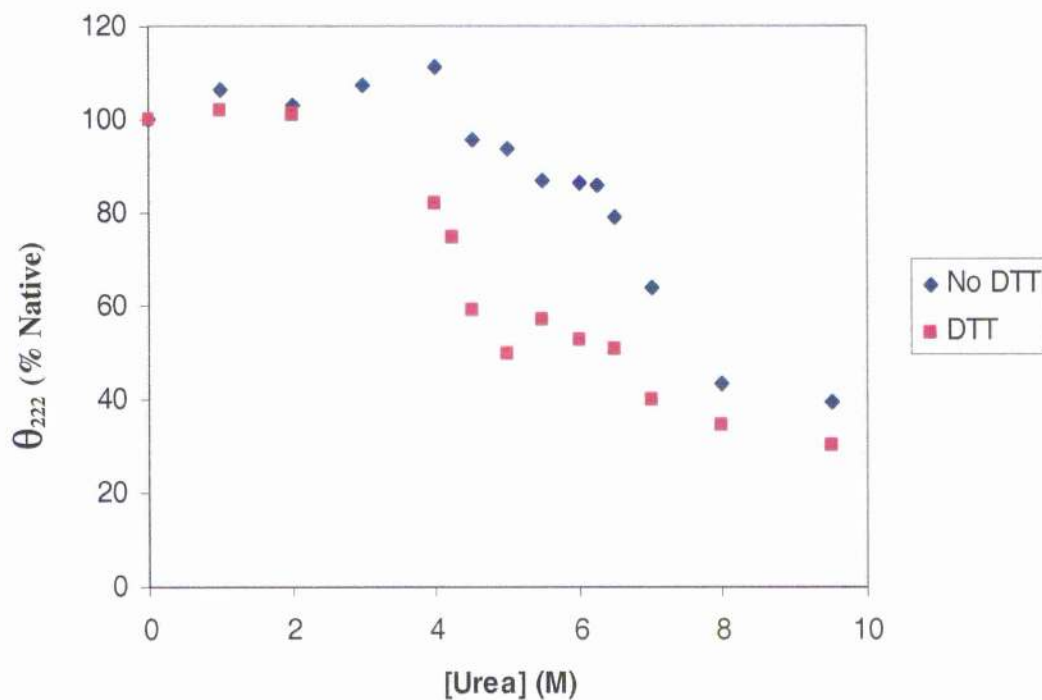
Figure 4.6. Unfolding Profile of C66S During Denaturation with Increasing Urea Concentration

Purified C66S (0.5mg/ml) was incubated overnight at room temperature at increasing urea concentration, in the absence, or presence of 20mM DTT. The fraction of unfolded protein was calculated as a percentage of the native state, using ellipticity readings recorded at 222nm in a cell with a pathlength of 0.05cm.
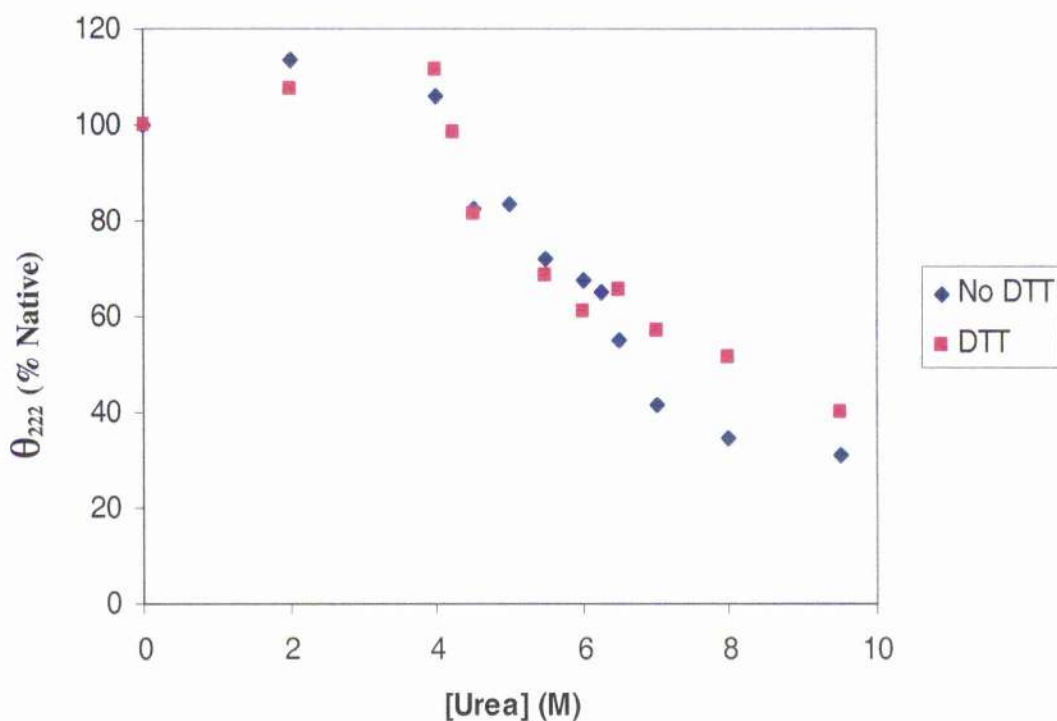
**Figure 4.7. Unfolding Profile of C168S with Increasing Urea Concentration**

Purified C168S (0.5mg/ml) was incubated overnight at room temperature at increasing urea concentration, in the absence, or presence of 20mM DTT. The fraction of unfolded protein was calculated as a percentage of the native state, using ellipticity readings recorded at 222nm in a cell with a pathlength of 0.05cm.

4.2.6. Assessment of C168S Stability

The unfolding profiles for C168S in the absence and presence of 20mM DTT were generated as for the others (Fig. 4.7). The unfolding profile was most similar with that of C47S, not unexpected given the involvement of C47 and C168 in disulphide bond formation. The non-reduced protein unfolds in a manner similar to that of C47S with gradual unfolding occurring until 9.5M urea at which point protein remaining retains approx. 25% of the native protein ellipticity.

DTT-treatment does not have a significant destabilising effect above 4M urea which was observed for wild type and C66S proteins. There is a slight reduction in stability at higher urea concentrations (6-9.5M). As for C47S, these minor effects of DTT treatment on C168S stability may be attributed to random disulphide bond formation occurring during the unfolding process.

4.2.7. Summary and Discussion

Analysis of the far UV CD spectra indicates that the predominant secondary structure is the α-helix, constituting nearly 50% of the overall structure. This value is slightly higher than the resolved rat 2-Cys HBP23 and human TPx-B, with which SP-22 has >90% sequence identity. The CD spectrum generated for C47S was super-imposable on that for wild type SP-22, implying mutation of this residue did not influence secondary structure to any significant extent.

It was established that the SP-22 oligomer is very stable, exhibiting marked resistance to chemical denaturation and does not fully unfold even following overnight incubation in maximal concentrations of urea. This is not surprising given the size of the assembly and the presence of disulphide bonds. There are two disulphide bonds per dimeric unit, and with an estimated M_r of 500,000-600,000, this correlates to approx. 40 disulphides per oligomer, which together would act to stabilise the structure. Indeed the reduction of the disulphides by addition of DTT was demonstrated to reduce global stability, although complete loss of structure was still not observed.

The CD denaturation profiles of wild type and mutant SP-22s in the presence absence of DTT showed some differences. Wild type SP-22 and C66S profiles were comparable with a pronounced unfolding step occurring in the range of 4-6M. Furthermore, the unfolding profiles for C47S and C168S were most similar, lacking any obvious unfolding stages. These comparisons indicate that the disulphide bonds contribute to oligomer stability within the region of structure that unfolds between 4-6M urea. Therefore it can be concluded that the cysteine mutants adopt the same stable structure as wild type SP-22, and the disulphide bonds contribute to overall oligomer stability, but not oligomer formation.

Chapter 4
Section 3

4.3.0. Introduction

To complement the CD analyses, fluorescence spectroscopy was also carried out. This technique is one of the most extensively used spectroscopic methods, and can be used to provide valuable information on protein conformation, and protein-protein interactions (Kelly and Price, 2000). When a molecule absorbs electromagnetic radiation, its electrons are promoted from a 'ground' state to an 'excited' state. To return to the ground state, the molecule must lose energy, usually as heat, or in the case of fluorogenic molecules, as radiation. The macromolecule of interest must be intrinsically fluorescent or have an extrinsic fluorescent probe attached to it. Proteins containing aromatic amino acids (tyrosine, tryptophan and phenylalanine) are intrinsically fluorescent and therefore extremely useful for studying protein conformational changes. Tryptophan (Trp) is an indole amino acid of particular importance as it exhibits greater fluorescence than tyrosine or phenylalanine, and many proteins have limited numbers of Trp residues present, therefore the behaviour of this residue can be easily examined. Proteins lacking a Trp can have one incorporated by mutagenesis, an extremely useful tool to study protein structure. Trp residues are typically buried within the hydrophobic core of a protein or at the interface between two interacting proteins. With protein unfolding, the Trp residue becomes exposed, giving rise to either an increase or decrease in Trp fluorescence, and the emission wavelength is 'red-shifted' to around 255nm, depending on the degree of exposure. Therefore Trp fluorescence is a useful tool in the elucidation of protein unfolding pathways, and an effective probe in binding studies.

Excitation spectra are typically recorded for investigating mixtures of substances. It involves selecting a single wavelength in the fluorescence spectrum, and keeping it constant throughout whilst recording the excitation spectra. The wavelength used to selectively excite Trp residues is 295nm to prevent contributions from tyrosine residues.

Fluorimetry was used to probe the unfolding pathway of the SP-22 oligomer by monitoring the changes in tryptophan fluorescence during denaturation in urea.

For easier interpretation, ideally a protein should contain only one or two Trp residues; however it is still possible to obtain information from a protein containing more depending on their positions in the native protein. If Trp residues are in too close proximity to one another they may interact and the resulting emission spectrum will be affected. SP-22 contains two Trp residues positioned near the middle of the sequence (position 82) and near the C-terminus (position 172). Although they are well separated in the sequence, it is not known how close they are in the tertiary structure.

Results

4.3.1. Fluorescence Spectrum of Native and Denatured SP-22

Purified SP-22 (0.5mg/ml) was prepared for fluorimetry as described in Materials and Methods section 2.5.18. The fluorescence spectrum was obtained for native SP-22, and protein denatured in increasing concentrations of urea until 9.5M. The results for the native and protein denatured in 9.5M urea are shown in Fig. 4.8. A shift to longer wavelengths in the spectrum is observed at 355nm for denatured SP-22 owing to the exposure of buried tryptophan to the bulk aqueous solvent. Only minor changes in fluorescence were observed, interestingly there was no increase in fluorescence with denaturation; this may be due to the fact that quenching of the signal is occurring, discussed in more detail in section 4.3.2. This was observed for the mutants too.

4.3.2. Summary and Discussion

In this section, fluorimetry results were attempted to complement the CD results, and perhaps help elucidate any discrete unfolding events that may occur during unfolding of the SP-22 oligomer. For example, detection of the dissociation of the oligomer into its basic dimeric units would be possible by monitoring changes in tryptophan fluorescence if Trp was located at the interface between adjacent subunits. A denaturation profile could potentially be generated as for CD, using the fluorescence readings at suitable wavelength to estimate the fraction of protein remaining folded, as a percentage of the native. This profile would theoretically be similar, if not identical to the CD denaturation profile. However despite a shift

to a longer wavelength (355nm), there was not a significant increase in tryptophan fluorescence between the native and unfolded states of the protein. In contrast, the emission signal of the unfolded protein was lower than that of the native, and changes were extremely small. As the total change in emission following denaturation in 9.5M urea was minor and lower than that of the native structure, it was not possible to generate an unfolding profile. This reduced fluorescence signal is a likely consequence of fluorescence quenching.

Quenching is a term to describe reduction of the absorption intensity of a fluor such as Trp, occurring as a result of non-radiative loss of energy due to vibrational transitions, and internal/external quenching. There are two Trp residues per SP-22 monomer, which have the potential to interact with one another and transfer energy, resulting in a reduced fluorescence signal. Furthermore, contributions from amino acid side-chains and disulphide bonds have potential quenching effects on a Trp signal. Internal quenching arises due to structural rearrangement within a molecule e.g. denaturation etc. Interactions between structures and chemical groupings, normally prevented in the native macromolecule, may occur in the unfolded state. The disulphide bonds within SP-22 are examples of types of bonds that can promote internal quenching. There are two disulphides per dimeric unit, therefore during denaturation there is increased potential for quenching. External quenching arises due to buffer contamination or addition of external molecules to the sample, for example the addition of DTT to SP-22. External molecules can collide briefly with the excited molecule, or they can form longer-lived associations, causing it to lose energy. As a result, it is more beneficial to use these fluorimetry results in conjunction with the other data obtained in future chapters, to gain insight into the nature of the SP-22 oligomer.
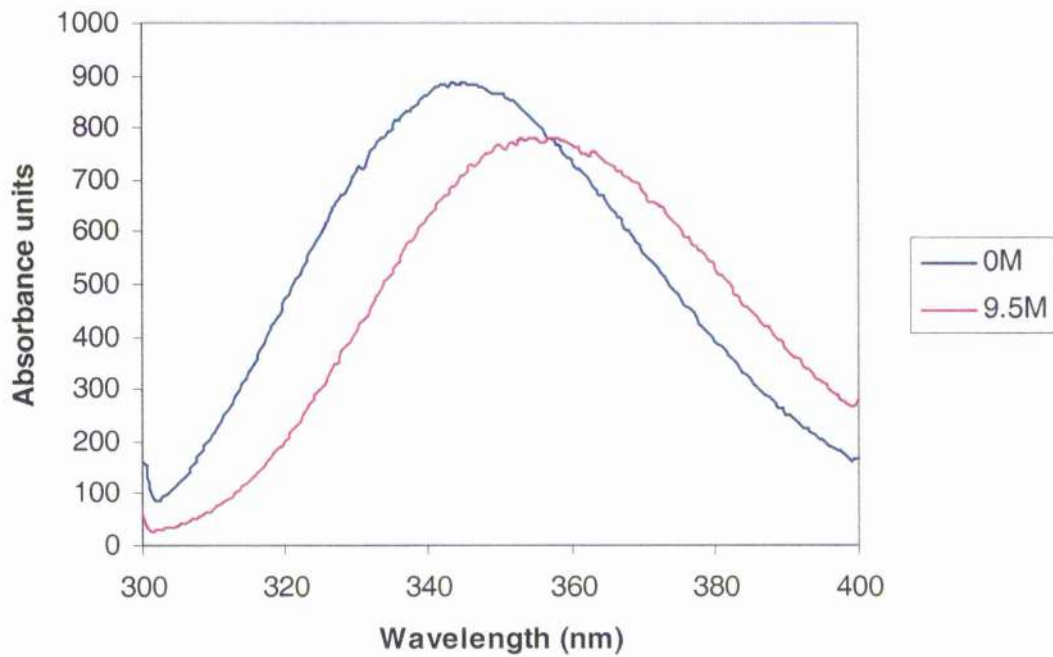
Figure 4.8. A Comparison of the Fluorescence Spectra of SP-22 in the Presence and Absence of Urea

Purified SP-22 (0.5mg/ml) was incubated in 0M and 9.5M urea overnight at room temperature. Samples were excited at 295nm and the fluorescence spectra recorded over 300-400nm in a Perkin Elmer LS 50B Fluorimeter.

Chapter 5
Section 1

5.1.0. Introduction

In the previous chapter it was established that SP-22 exists as a basic dimeric unit, containing two disulphide bonds formed between the N-terminal cysteine of one subunit, and the C-terminal cysteine of the opposing monomer. This feature is consistent with findings for other mammalian Prx members. Structural information available for several Prxs indicates the formation of a larger oligomeric assembly, comprising five dimers joined end-to-end in a toroidal arrangement. The central cavity of the decameric structure exhibits pentagonal symmetry. Dimers are proposed to associate with adjacent dimers via several types of interaction including hydrophobic interactions and hydrogen bonds.

Gel exclusion chromatography was utilised for a crude estimation of the overall molecular weight of SP-22 and the cysteine mutants, to establish if they too exist as larger oligomers. This technique is especially useful for monitoring alterations in the native structure of a protein over a wide variety of conditions including pH, temperature and ionic strength. The principle of this technique is to separate molecules present in solution according to their size by passage down a column containing a specialised gel matrix. The gel comprises a continuous liquid phase held within the pores of a continuous solid phase. Pore sizes can be varied depending on the size of the macromolecules in the solution to be resolved. Small molecules penetrate into the gel and consequently migrate down the gel at a reduced speed in comparison to larger molecules, which are excluded from the pores and elute more rapidly with the surrounding solution. Thus globular proteins are separated and eluted from the column in order of decreasing molecular weight.

The size of a protein of interest is determined by comparing the ratio of the elution volume (V_e) to the void volume (V_o) for the unknown protein, with the V_e/V_o of several protein standards of known molecular weight. The void volume is based on the elution volume of a large macromolecule usually with a M_r of $\geq 2 \times 10^6$. A calibration curve is generated using the logarithms of the known molecular weights of the protein standards, against their respective V_e/V_o values.

From this calibration curve the size of the unknown protein may be extrapolated, using its V_e/V_0 value.

Results

5.1.1.   Construction of the Calibration Curve for Molecular Weight Determination

A calibration curve was generated using a Molecular Weight Standard kit (Methods and Materials section 2.4.4), run on a HiPrep 16/60 Sephacryl S-300 High Resolution column, as described in Methods and Materials section 2.5.11. The V_0, determined by elution of the dye Blue Dextran (M_r of approx. 2×10^6) was 38.0 ml. Using this figure and the V_e value of the other protein standards, the V_e/V_0 for each was calculated. Table 2 illustrates the molecular weights and the V_e/V_0 values for each protein standard used to construct the calibration curve shown in Fig. 5.1.

Protein	Approx. MW	V_e (ml)	V_e/V_0
Alcohol dehydrogenase	150,000	62.8	1.65
β-amylase	200,000	60	1.58
Apoferritin	443,000	51.9	1.37
Bovine serum albumin	66,000	69.1	1.82
Carbonic anhydrase	29,000	80.4	2.1
Cytochrome c	12,400	88.3	2.32
Thyroglobulin	669,000	45.1	1.19

Table 2. V_e/V_0 Values of the Protein Standards Against Their Molecular Weights (MW)
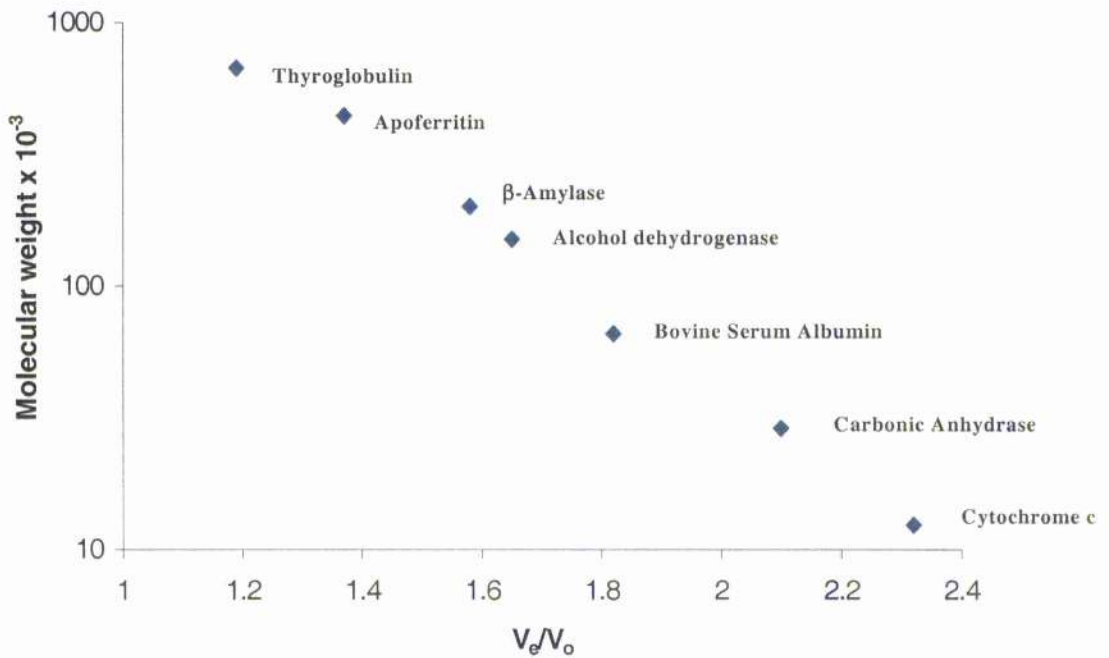
Figure 5.1. Calibration Curve for Size Determination of Wild Type and Mutant SP-22s

Calibration curve generated using a MW-GF-70 Kit (Sigma) run on a HiPrep 16/60 Sephacryl S-300 High Resolution column with a bed volume of 120ml and a flow rate of 1ml/min. The column was equilibrated with two column volumes of 50mM KPi (pH 7.0) containing 150mM NaCl.

5.1.2. Size Determination of Wild Type and Mutant SP-22

Wild type and mutant SP-22 (5mg/ml) prepared in 50mM KPi pH 7.0, containing 150mM NaCl was run on the column, previously equilibrated in 2 column vol of the same buffer. Fractions (1.5ml) were collected, and aliquots were TCA/acetone precipitated and analysed by SDS-PAGE to confirm the peaks represented the proteins of interest (Methods and Materials sections 2.5.3 and 2.5.6). Monodisperse, symmetrical peaks were generated from which the V_e was determined. Figure 5.2 illustrates the elution profile for wild type SP-22. The calculated V_e/V_o values and the molecular weight estimations, extrapolated from the standard curve are shown in Table 3.

Protein	V_e (ml)	V_e/V_o	Approx. MW
SP-22	50.0	1.31	500,000
C47S	Void volume	-	≥2,000,000
C66S	51.0	1.34	450,000
C168S	Void volume and 49.6	1.3	500,000

Table 3. Summary of Gel Filtration Results for Wild Type SP-22, C47S, C66S and C168S

Results imply that SP-22 forms a larger oligomer with a M_r of approx. 500,000. This corresponds to about 20 monomers. In some cases an additional peak at the void volume was observed, especially if samples were not fresh suggesting that aggregation may be occurring with time. The N-terminal cysteine mutant eluted entirely at the void volume indicating aggregate formation, confirmed later in this chapter in section 2. However, for C168S only a minor peak was observed at the void volume, corresponding to aggregated oligomers. The major peak produced corresponded to a M_r of 500,000 as for wild type SP-22. The C66S mutant eluted with a M_r of 450,000, corresponding to approx. 18 monomers. Due to the low resolution of the column in this M_r range, it is difficult to ascertain the exact subunit composition of SP-22, and the C66S and C168S mutants, although all
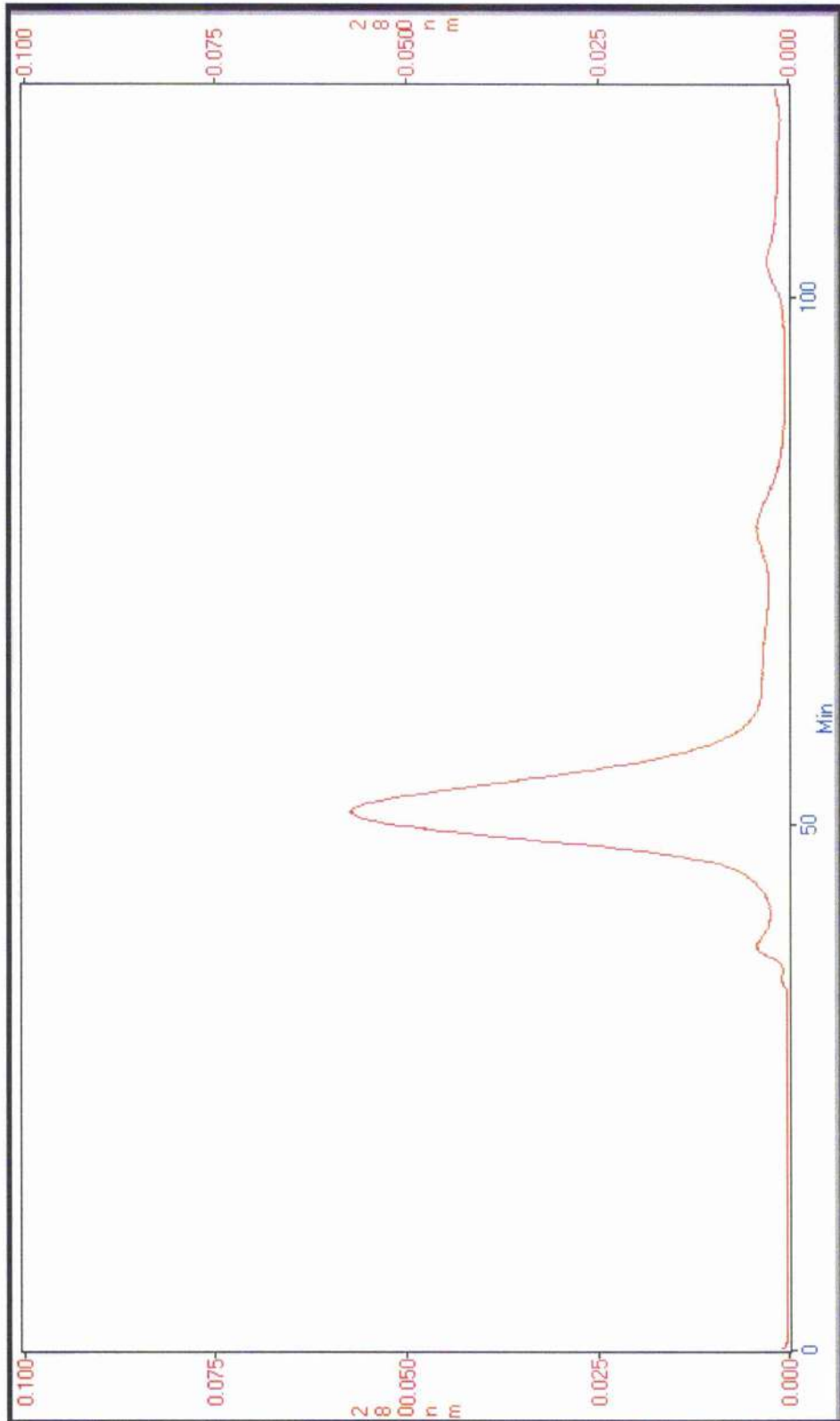
Figure 5.2. Gel Exclusion Chromatography Elution Profile for Wild Type SP-22

Purified SP-22 (5mg/ml) was passed down a HiPrep 16/60 Sephacryl S-300 High Resolution column with a bed volume of 120ml, and at a flow rate of 1ml/min. The profile above shows the A_{280} of the protein against time (min).

appear to have a molecular weight in the range of 450,000-500,000 corresponding to 18-20 monomeric units. The subunit composition of SP-22 and C66S may in fact be identical.

5.1.3. Assessment of the Structural Role of the Disulphide Interactions

Together with gel filtration results for the cysteine mutants, experiments were repeated in the presence of DTT (20mM) to determine if the presence of disulphide bonds was necessary for oligomer assembly. SP-22 was run as before, but this time it eluted at 52.6ml, corresponding to a M_r of approx. 400,000. This was significantly lower than the value obtained in the absence of DTT. However, its existence as a high M_r oligomer suggests that the disulphides are not required for structural integrity. A more significant structural role would be reflected in a large collapse of the assembly as indicated by a dramatic decline in M_r value. This was also observed for C47S which in the presence of DTT (20mM) did not disassemble, and eluted as before at the void volume.

5.1.4. Assessment of His-tag Involvement in Oligomer Assembly

Following purification of SP-22 by metal chelate chromatography, it is possible that some contaminating zinc ions are attached to the His-tags. It is also possible that these zinc ions may mediate the aggregation of SP-22 subunits via their His-tags (Linder *et al*, 1992). To remove this possibility, a gel filtration run was carried out in the presence of the chelating agent EDTA (10mM). SP-22 eluted this time at 51.4ml, corresponding to a M_r of 450,000. This result is consistent with previous sizes, and implies that oligomer assembly is not attributed to lateral aggregation via the His-tags. This result was further confirmed by a separate gel filtration run, analysing SP-22 with its His-tag removed. The His-tag was cleaved using the serine protease thrombin, which specifically recognises the thrombin cleavage site present in the SP-22 fusion protein, as described in Materials and Methods section 2.5.9. Thrombin-cleaved SP-22 produced a major peak at 52.1ml, corresponding to a M_r of 420,000. This slight decrease in size reflects the loss of the His-tags from each SP-22 monomer.

5.1.5. Summary and Discussion

SP-22, like several other Prx members was demonstrated to form a basic dimeric unit containing two intermolecular disulphide bonds. Furthermore it has now been established that SP-22 forms a larger assembly with an apparent M_r value of approx. 450,000. The estimated size of the SP-22 oligomer varied between sample preparations in the M_r range of 400-500,000; therefore the technique of gel filtration offered only a crude estimation of molecular weight. Gel filtration is an effective technique for accurate determination of the sizes of globular, regularly shaped proteins, but is of limited value for irregularly organised oligomers or polypeptides with large axial ratios. The resolution limits of the column are reduced when investigating proteins with sizes comparable to SP-22s. It becomes apparent in the following section that SP-22 adopts a toroidal conformation with a large central cavity like other mammalian Prxs. Therefore the effective diameter of the SP-22 oligomer is larger than the predicted value, resulting in the SP-22 oligomer being more rapidly eluted from the gel filtration column than expected. Furthermore it is possible that the formation of SP-22 is in a dynamic equilibrium between oligomeric states, therefore does not exist as a single species, a possibility that is discussed further in the following section. Based on the gel filtration results however, SP-22 would be predicted to contain 18-20 subunits. As every 2-Cys Prx member adopting a larger oligomeric form, has been identified to exist as a decamer, it may be postulated that SP-22 may form a double decamer or even triple decamers.

The disulphide bonds contained within the basic dimeric unit are not structural in character as determined by experiments carried out for mutant SP-22 constructs and for wild type SP-22 in the presence of DTT. These results are in agreement with findings for other Prx members. The human erythrocyte Prx, TPx-B, forms a decamer in which the disulphide-linked dimers join end-to-end via several types of interactions including hydrophobic interactions, hydrogen bonds and Van der Waals forces.

One interesting observation was the tendency for C47S but not C168S to aggregate. This may imply a possible conformational change induced by the alteration of C47 to a serine residue. This conformational change may result in the exposure of hydrophobic residues that can interact with other hydrophobic faces of adjacent

oligomers. In other Prxs, C47 is in fact located at the bottom of a hydrophobic pocket. The involvement of disulphide interactions in aggregation was removed by repeating the gel filtration experiments for C47S in the presence of DTT. Aggregate formation was still exclusive to this mutant even when reduced. As wild type and mutant SP-22s were generated as His-tag fusion proteins, it was thought possible that aggregation may be directed by these His-tags being tethered together via interactions with contaminating zinc ions from the purification procedure. This possibility was eliminated by repeating the experiments in the presence of the chelating agents EDTA and also DTT which can bind zinc ions, and by proteolytic removal of the His-tags.

Chapter 5

Section 2

5.2.0. Introduction

The 3D structure reconstruction of macromolecules has been facilitated by three widely used techniques: X-ray crystallography, NMR and Transmission Electron Microscopy (TEM). X-ray crystallography and NMR are particularly useful for structural resolution of small oligomers, or individual proteins to atomic detail. TEM in contrast, is beneficial for probing large oligomeric assemblies, for example virus particles, filaments and tubular structures. TEM avoids the necessity for complex molecular replacement programs required in X-ray crystallography, uses lower protein concentrations and is less time consuming.

There are two major procedures undertaken in TEM: negative staining and cryo-negative staining (also termed ice-embedding) (Adrian *et al*, 1998). Both methods provide information on the overall size and shape of the specimen.

Due to reduced equipment costs, speed and methodological simplicity, negative staining is typically attempted first. It was introduced by Brenner and Horne (1959) and has permitted the characterisation of numerous macromolecular assemblies at low resolution. The resolution capability is generally in the range 10 to 20Å, and involves immobilising the specimen onto a carbon support grid prior to staining with a heavy metal salt, usually a uranyl salt such as acetate or formate. The specimen becomes embedded in the stain and a footprint of its overall shape is generated. The stain has high electron scattering potential and forms microcrystals that can permeate surface modulations of the oligomer of interest, thereby producing a reliable 'cast' of the protein. A resolution limit of ≥ 10Å, the inability to observe internal structural features and damage to the specimen by dehydration are three major limitations of negative staining. In addition, this procedure only provides accurate results for rigid assemblies- large flexible domains and 'soft' structures cannot be observed.

To overcome some of the limitations of negative staining, ice-embedding or cryo-negative staining was developed. Cryo-negative staining offers higher resolution

limits with down to 3Å being reported in some cases (Avila-Sakar and Chiu, 1996). It uses the physiological properties of water, thus preventing the problem of specimen dehydration as in negative staining. Following application of the sample to the carbon grid, it is frozen rapidly by immersion in liquid ethane or propane. Water as a result, becomes trapped in an amorphous (vitrified) state, maintaining the specimen in a near-native environment. Cryoprotectants such as glycerol or DMSO are typically included when requiring high-resolution detail. The EM image in cryofixation is generated by the protein specimen itself, rather than the heavy metal salt cast surrounding the structure and can be used on non-rigid structures. Secondary and tertiary structural features, together with internal structural information can be obtained. Furthermore, due to the rapid freezing process, protein-protein interactions can be probed, as can conformational changes, therefore providing information on the functional mechanisms of the macromolecule. The limitations of this method are mainly attributed to the inherent limitations of electron microscopy rather than the sample preparation as for negative staining.

The simpler method of negative staining TEM was carried out to elucidate the structure of SP-22 and the cysteine mutants. Structure determination of the mutants was used to confirm the roles of the disulphide bonds in oligomer integrity. Decameric toroidal structures have previously been observed using this technique and X-ray crystallography, for TPx-B and HBP23. The number of subunits comprising the toroid was also determined by 3D reconstruction by angular reconstitution using crystallographic imaging software. The aim was to determine if SP-22 too conforms to the decameric toroidal structure adopted by the non-mitochondrial 2-Cys peroxiredoxins.

Results

5.2.1. Negative Staining of Wild Type SP-22

Purified SP-22 (5mg/ml) was eluted from a Sephacryl-300 16/60 HR gel filtration column (Methods and Materials section 2.5.11), and depending on the sample,

produced one or two peaks, corresponding to aggregates eluting at the void volume or a M_r of approx. 450,000, respectively. The purified SP-22 (50-100μg/ml) from each peak fraction, prepared in 50mM KPi buffer pH 7.0, containing 150mM NaCl, was immobilized on a continuous carbon support and stained with 0.1% (w/v) uranyl acetate (Materials and Methods section 2.5.22). Peak fraction 5 (void volume) showed that SP-22 is toroidal with the presence of long stacks comprising multiple rings aggregated in a lateral fashion, a predominant feature (Fig. 5.3). Analysis of SP-22 from fraction 13 (peak 2) showed single rings and stacks with two or three rings (Fig. 5.4). Stacking would account for the variation in M_r values obtained for gel filtration and sedimentation equilibrium ultracentrifugation experiments (Chapter 4). Furthermore, gel filtration is only useful for globular, regularly shaped proteins; therefore the mass of the SP-22 oligomer with a central cavity would not be easily determined. Interestingly side-views were prevalent in comparison with top views implying some interaction of the protein with the grid.

Image processing was carried out to investigate the ring structure of SP-22 from fraction 13 at higher resolution. It was not possible to determine the exact number of subunits per ring as they were very tightly packed, making it is more difficult for the stain to penetrate the structure. Estimations suggest that the toroid is decameric or dodecameric, the former being more likely given the structures of other mammalian 2-Cys Prxs. Out of 188 selected rings, each image was rotationally averaged to generate a radial density profile, and these profiles were in-turn averaged to generate a plot from which it was established that radius of the SP-22 toroid is ~ 7.5 nm, therefore the diameter including the central cavity is approx. 15nm (Fig. 5.5). Another feature of the rings, ubiquitously observed, was the presence of spikes radiating out from the outer surface (Fig. 5.6). They are proposed to be too ordered to be artefacts of the stain. Additionally, electron dense material was observed within the central cavity of the majority of rings. The material appears to be regularly organised, displaying distinct structural features.
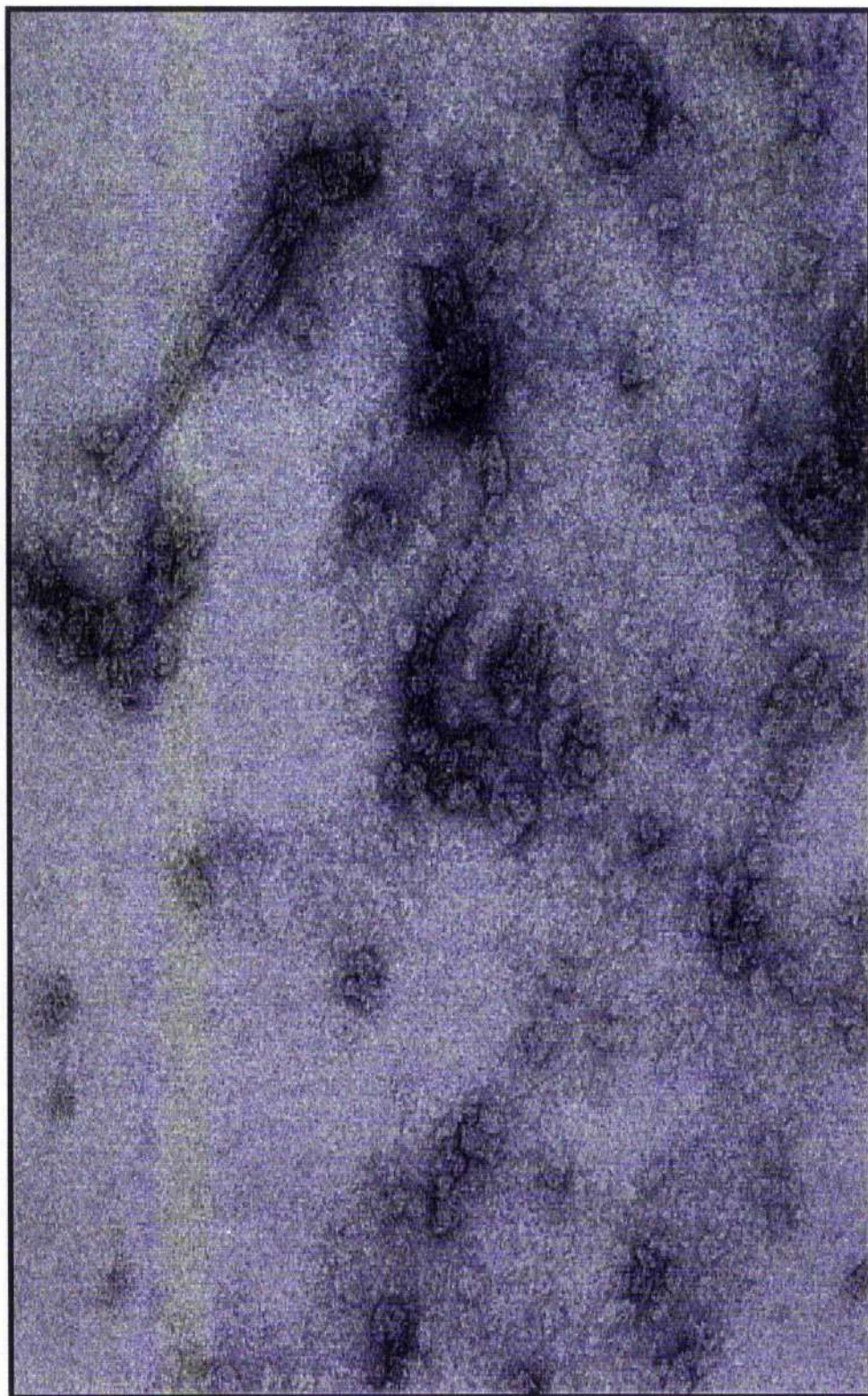
Figure 5.3. Low Resolution Electron Micrograph of SP-22 Void Volume Fraction

The SP-22 gel filtration peak (50-100µg/ml) corresponding to the void volume was immobilised onto a continuous carbon grid and negatively stained with 0.1% (w/v) uranyl acetate. Micrographs were generated using a JEOL 1200 Transmission Electron Microscope recording at 30,000X magnification onto S0163 film.
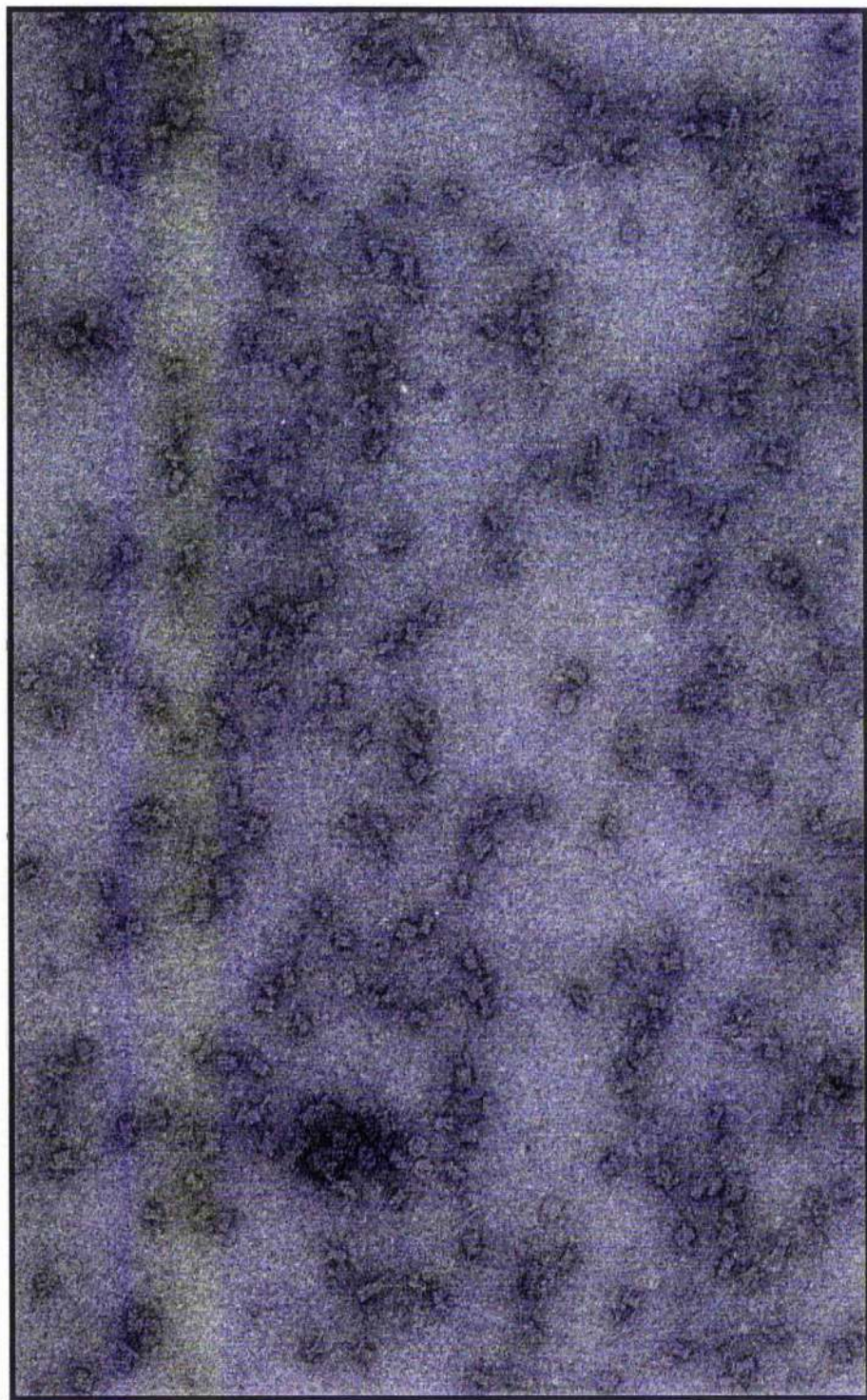
Figure 5.4. Low Resolution Electron Micrograph of SP-22 Peak Fraction 13

Purified SP-22 (50-100µg/ml) obtained from peak fraction 13, corresponding to a M_r of approx. 450,000 was immobilised onto a continuous carbon grid and negatively stained with 0.1% (w/v) uranyl acetate. Micrographs were generated using a JEOL 1200 Transmission Electron Microscope recording at 30,000X magnification onto S0163 film.
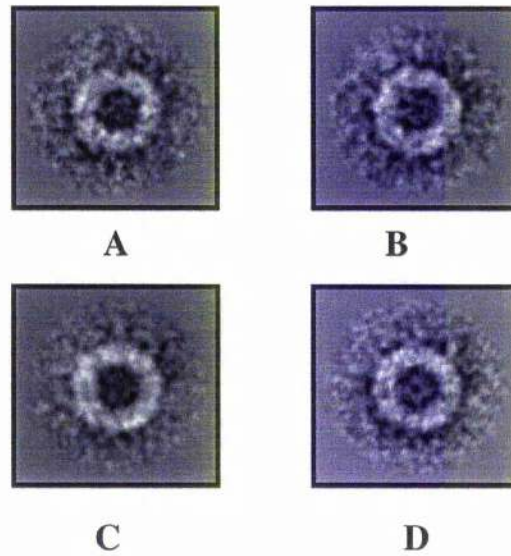
Figure 5.5. Electron Micrographs of SP-22 Toroids

Purified SP-22, (100-50µg/ml) eluted from a Sephacryl-300 16/60 HR gel filtration column was immobilised onto a continuous carbon grid and stained with 0.1% (w/v) uranyl acetate. Micrographs were taken using a JEOL 1200 Transmission Electron Microscope recording at 30,000X magnification onto S0163 film.

A. Double Stack

B. Triple Stack

C. Toroid exhibiting radial spikes
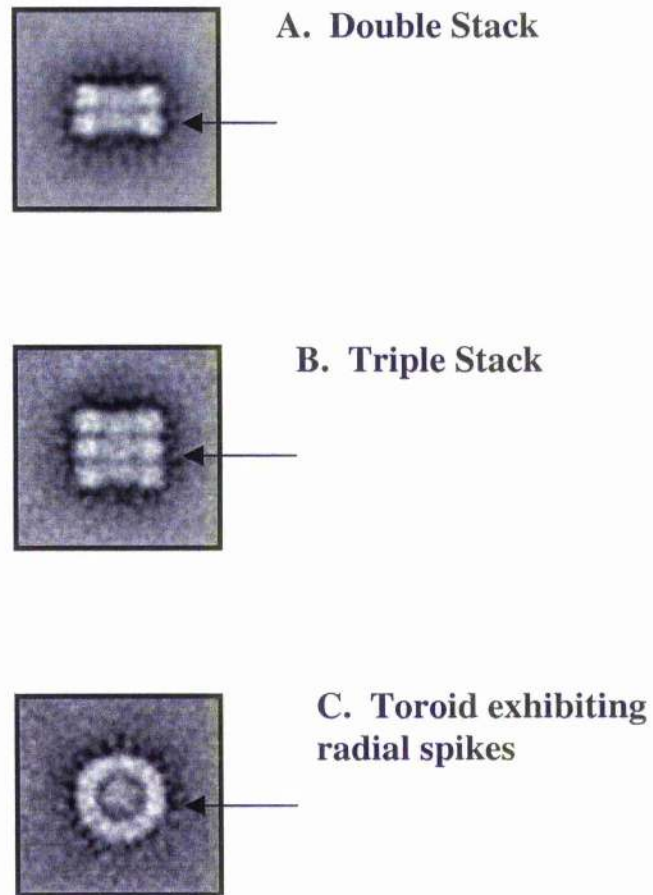
Figure 5.6. Side-views and Top View of SP-22 Illustrating Radial Spikes and Toroid Stacking

Electron micrographs of purified SP-22 (50-100µg/ml), immobilised onto continuous support carbon grids and stained with 0.1% (w/v) uranyl acetate, were visualised using a JEOL 1200 Transmission Electron Microscope recording at 30,000X magnification onto S0163 film.   Radial spikes are indicated by the arrows.

Silver staining established that this material is probably part of the SP-22 oligomer, as no contaminating *E. coli* proteins were detected in a sample of purified SP-22 run on a silver-stained 12% polyacrylamide gel (Materials and Methods section 2.5.8). Silver staining is approximately ten-fold more sensitive than Coomassie Brilliant Blue staining and established that no additional bands apart from the monomeric form of SP-22 were detected (Fig. 5.7). The two monomeric forms observed are likely to represent the intra-molecular disulphide bond intermediates that can adventitiously form during SDS-PAGE. To determine whether they were definitely SP-22 monomers, immunoblotting with a monoclonal antibody that specifically detects His-tag proteins was used (Materials and Methods section 2.5.7). Indeed, the bands highlighted by silver staining were detected by the polyHis-antibody, implying the material within the central cavity is part of the overall SP-22 structure and not contaminating *E. coli* proteins.

5.2.2. Negative Staining of Reduced Wild Type SP-22

To confirm the disulphide bonds are non-structural, the negative staining procedure was repeated for SP-22, this time in the presence of 20mM DTT. Reduced SP-22 is still toroidal confirming that the disulphides are not required for structural integrity. More top views and more single rings were observed however, and stacking was less frequent than for oxidised SP-22 (results not shown).

5.2.3. Negative Staining of C47S

C47S produced a gel filtration peak at the void volume, corresponding to a M_r of approx. 2×10^6. To elucidate the structure of this mutant, negative staining was repeated as for the wild type. This mutant was observed to form long stacks, with single toroids being extremely rare (Fig. 5.8). These structures were comparable to protein filaments, and it is proposed that they stack in a manner too ordered to be attributed to non-specific aggregation. To determine whether disulphide
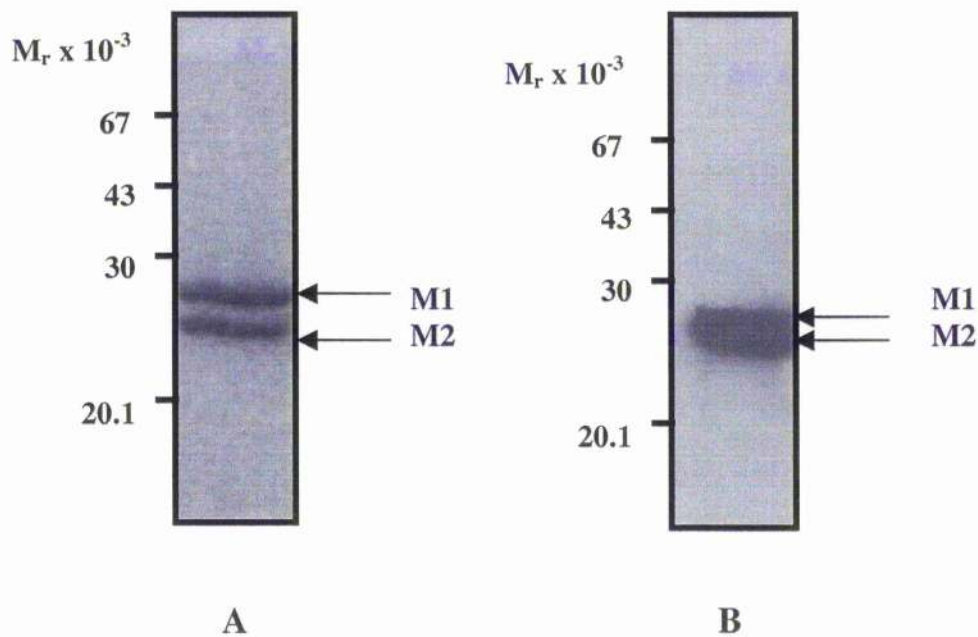
Figure 5.7. Comparison of Silver Stained Purified SP-22, and SP-22 Detection by Immunoblotting

(A) Purified SP-22 (5µg) was denatured for 5 min at 100°C in the presence of DTT (150mM), prior to analysis on a 12% SDS/polyacrylamide gel. Bands were detected by silver staining according to Materials and Methods section 2.5.8. (B) After SDS/PAGE analysis as in (A), bands were detected on immunoblotting with a polyHis-monoclonal antibody according to Materials and Methods section 2.5.7. Molecular weight markers are shown to the left of the gel. The two monomeric forms of SP-22 are indicated, corresponding to SP-22 monomers containing adventitious intramolecular disulphide bonds (M2) formed during denaturation, and the fully reduced monomeric form (M1).
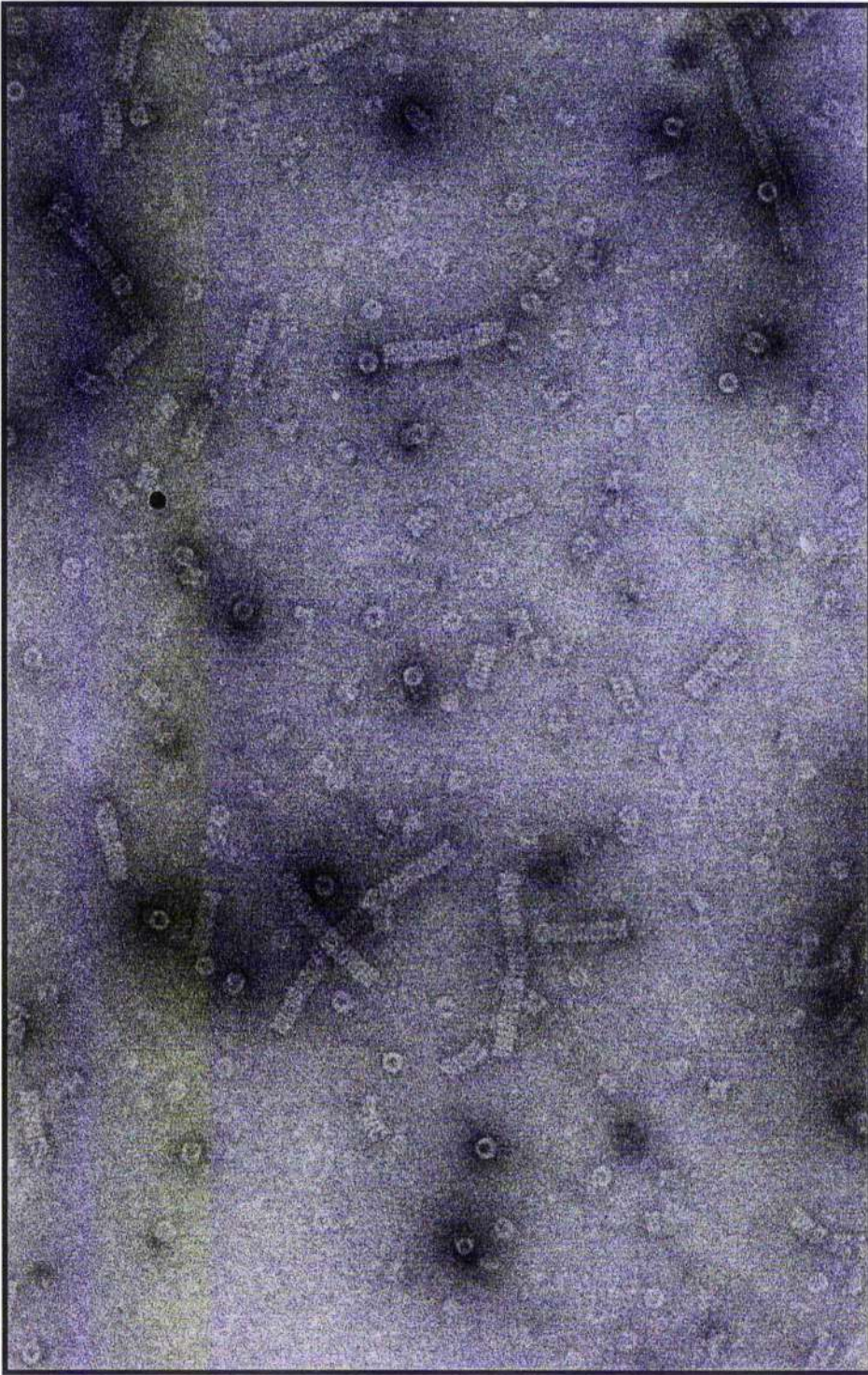
Figure 5.8. Low Resolution Electron Micrograph of C47S

Purified C47S (50-100μg/ml) was immobilised to a continuous carbon grid, and stained with 0.1% (w/v) uranyl acetate. Electron micrographs were generated using a JEOL 1200 Transmission Electron Microscope, recording at 30,000X magnification onto S0163 film.

interactions may mediate stacking, gel filtration was carried out in the presence of DTT (20mM). The elution peak generated was identical to that of non-reduced C47S, confirming that the disulphides are not involved in stacking, and large molecular weight aggregates were still forming.

5.2.4. Summary and Discussion

These results report the first structure elucidation of an oligomeric mitochondrial 2-Cys Prx member. The structure of the human mitochondrial Prx, PRDX5 has been resolved; however it is distinct from other 2-Cys Prxs in it does not form a dimeric unit; instead it exists completely as monomers (Declercq *et al*, 2001). Furthermore these results are the first to demonstrate that the recombinant protein assembles correctly. Negative staining of SP-22 confirms that it is toroidal with an external diameter of approx. 15nm, and a large central cavity. Preliminary results suggest SP-22 is a decamer or dodecamer. As all mammalian Prxs to date with the exception of PRDX5 are decameric, it is likely SP-22 also conforms to this model. Given the presence of a central cavity, together with the immense size of the SP-22 oligomer and its tendency to aggregate laterally, it is not surprising that difficulties were encountered in the determination of the exact number of subunits via gel filtration experiments (Chapter 5 section 1).

Material was observed within the central cavity in the majority of rings, confirmed to be SP-22 as no contaminating *E. coli* proteins were detected using the highly sensitive silver staining technique. Stacking was a common feature in the electron micrographs, particularly with respect to the C47S mutant, which formed stacks as long as fifteen rings. The factor mediating this process and whether it is important for SP-22 function remains to be elucidated. There may be a physiological relevance as TPx-B was also found to form double stacks (Harris *et al*, 2001). Interestingly, this 2-Cys protein has been demonstrated to convert between the dimeric and decameric form of TPx-B, the latter being the favoured form when the protein is in a highly oxidising environment. The process of toroidal stacking

is not limited to the Prx family and has also been observed for the bacterial molecular chaperone system comprising GroEL and GroES (Harris *et al*, 1994).

It is possible that time-dependent aggregation of rings is occurring, especially for wild type SP-22 where this feature was only occasionally observed, particularly in 'older' protein preparations. As SP-22 micrographs in the presence of DTT produced mainly single toroids, it is likely that some of the stacking, at least in wild type SP-22 involves Zn^{2+}. It has been reported that SP-22 purified from tissue sources displays lateral stacking too, therefore it is likely that the Zn^{2+}only increases the occurrence of stacking and does not direct it entirely (Wood *et al*, 2003).

The 2-Cys Prx tryparedoxin peroxidase (TryP) from the parasitic trypanosomatid *Crithidia fasciculate,* has been demonstrated to alternate between its decameric and dimeric states according to its redox state. Reduced TryP is decameric and able to perform its peroxidase function, however on oxidation, the enzyme is converted to an inactive, dimeric state (Alphey *et al*, 2000). Future work may look to investigate the physiological significance of the oligomeric form of SP-22 and the phenomenon of stacking. Unlike TryP, SP-22 exists as a large oligomer in both the reduced and oxidised states; therefore the significance of this with respect to its peroxidase function remains to be explored.

Chapter 6

Section 1

6.1.0. Introduction

To date, the activity of SP-22 has been measured with respect to its protective effect towards a number of free-radical sensitive enzymes, particularly glutamine synthetase, and enolase (Kim *et al*, 1988). All assays utilised SP-22 purified from native sources. Although the inactivation of these enzymes via oxidation is well reported, the actual mechanism remains to be elucidated. The mitochondrial enzymes involved in aerobic respiration are particularly vulnerable to oxidation, and are characteristically detected in a number of pathologies of which oxidative stress is contributory.

Glutamine synthetase is a dimeric enzyme, crucial in nitrogen metabolism and thus highly regulated by mechanisms including covalent modification and negative feedback inhibition. There are two steps involved in the inactivation of *E. coli* glutamine synthetase (Amici *et al*, 1989; Levine, 1983). The first stage involves the oxidation of one specific histidine residue (out of sixteen) that renders the enzyme inactive. The second stage involves the oxidation of a second histidine residue that renders the enzyme susceptible to proteolytic degradation. A model free radical-generating system (FRS) has been designed to study the oxidative modification of the histidine residue in glutamine synthetase (Kim *et al*, 1985). This system is proposed to mimic the various enzymatic systems that normally generate reactive oxygen species, for example the NAD(P)H oxidase or cytochrome P450 systems. The requirements for this artificial free-radical generating system are oxygen, a source of electrons e.g. ascorbate or DTT and trace metal, typically Fe^{2+}. Oxidation of the metal ion by molecular oxygen gives rise to the superoxide anion and the oxidised metal ion (**Reaction 1**). Superoxide anions ($^{\bullet}O_2^-$) as previously discussed in chapter 1, spontaneously undergo a dismutation reaction with other superoxide anions to form hydrogen peroxide (H_2O_2) (**Reaction 2**). Hydrogen peroxide is subsequently degraded into hydroxyl radicals (OH$^{\bullet}$) via the Fenton reaction catalysed by the reduced metal ion (**Reaction 3**). Ascorbate/DTT is required to recycle the oxidised metal ion (Fe^{3+}) back to its reduced state (Fe^{2+}).

Reaction 1: $Fe^{2+} + O_2 \rightarrow Fe^{3+} + {}^\bullet O_2^-$

Reaction 2: $2{}^\bullet O_2^- + 2H^+ \rightarrow H_2O_2 + O_2$

Reaction 3: $Fe^{2+} + H_2O_2 \rightarrow Fe^{3+} + OH^\bullet + OH^-$
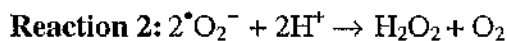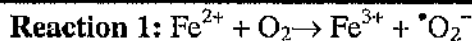
The oxidative modification of the second histidine residue introduces a carbonyl group into the enzyme that is specifically recognised by a protease that catalyses its subsequent degradation (Amici *et al*, 1989; Levine, 1983). The destructive effect of the FRS is prevented by catalase or peroxidase, suggesting that the principal contributor to oxidative damage is hydrogen peroxide. The requirement for metal ions is reinforced by the observation that chelating agents also display a protective effect against damage to glutamine synthetase. This suggests that hydrogen peroxide is not directly damaging, but required as a substrate for the Fenton reaction and subsequent hydroxyl radical production.

Enolase is also a dimeric enzyme, responsible for the conversion of 2-phosphoglyceric acid (2-PGA) to phosphoenolpyruvate (PEP). It is more susceptible to damage by ROS than glutamine synthetase. The mechanism and targets of inactivation of enolase is less well understood; however, it is proposed that at least one histidine residue per subunit is modified as a consequence of oxidative damage.

Enolase inactivation was used to assess the protective effect of SP-22 when subjected to a FRS. Enolase was selected rather than glutamine synthetase as its activity is more easily and accurately determined on a routine basis. To identify which of the conserved cysteine residues of SP-22 were required for activity, the protective effects of the cysteine mutants were also assessed. The N-terminal conserved cysteine of the 2-Cys Prxs is thought to be the catalytic residue. This together with the identification of a sulphenic acid group at C47 suggests that C47 of SP-22 is likely to be essential for peroxidase activity. Ascorbate was replaced with DTT due to the requirement of thiol groups for 2-Cys Prx activity. Not only does DTT recycle the metal ions, it is also necessary for reducing the oxidised/inactive form of the enzyme back to its reduced/active state.

Furthermore the ability of SP-22 to directly scavenge hydrogen peroxide was assessed in comparison with catalase, a well-established peroxidase.

Results

6.1.1. Protective Role of SP-22 Towards Enolase Inactivation

The activity of enolase was measured by recording the A_{240}, indicating the successful conversion of 2-PGA to the product PEP (Materials and Methods section 2.5.14). To assess the protective effect of SP-22, rabbit muscle enolase (33μg) was incubated at 30°C with the FRS (10μM FeCl$_3$, 30mM DTT) and 3-66μg SP-22 (Materials and Methods section 2.5.17). At regular time intervals, the remaining enolase activity was assessed. Enolase activity was less than 20% of the controls after 10 min, with inactivation to approx. 6% of the original activity being achieved after 30 min (Fig. 6.1). Incubating the FRS with 2mM EDTA prior to addition of the enolase prevented its inactivation implying that Fe^{2+} was essential for generating the reactive oxygen species involved in inactivation. Inactivation did not occur with DTT or FeCl$_3$ alone (results not shown).

At a ratio of 2:1 of SP-22: enolase, protection was approx. 100% after 20 min. The extent of protection was similar for lower SP-22: enolase ratios (Fig. 6.2). Even when four times the amount of enolase was present in comparison with SP-22, enolase activity was greater than 70% after 20 min.

Overall the extent of enolase protection is similar for all SP-22 concentrations, until the lowest proportion of SP-22: enolase (1:8) where the remaining enolase activity was only 30.9% after 20 min. To ensure protection was specifically due to SP-22 and not the presence of additional protein, controls were prepared using bovine serum albumin (BSA) and catalase. BSA present at maximal levels (66μg/assay) displayed no protective effect towards enolase as expected (results not shown). Catalase (66μg) did protect enolase, confirming that the ROS responsible for damaging enolase is hydrogen peroxide, possibly via its breakdown product, the hydroxyl radical generated via the Fenton reaction (Fig.

6.3). This could be investigated further by assessing the effect of adding hydrogen peroxide directly to enolase in the presence and absence of Fe^{3+}.

6.1.2. Role of the Conserved Cysteines for SP-22 Peroxidase Activity

To assess the role of the conserved cysteine residues for catalytic activity, the enolase inactivation and protection assays were repeated for the cysteine mutants (Fig. 6.3). C47S was established to be the catalytic residue, displaying no significant protection towards enolase, even in the presence of 2:1 C47S to enolase ratio. Less than 10% enolase activity remained following a 20 min incubation period with the FRS. There was no significant difference between the wild type, C66S and C168S mutants in their protection towards enolase, implying they are not required for SP-22 activity. High levels of enolase activity remained (80% and 75%) in the presence of maximal concentrations of C66S and C168S respectively. It is surprising that the C168S mutant efficiently protects enolase given its involvement in the disulphide bond chemistry of catalysis. This is unlikely to occur *in vivo* as thioredoxin reduces the enzyme via an intermediate stage in which it forms a disulphide bond with SP-22. Removal of C168 would prevent such an interaction. In the artificial system, however, DTT may directly reduce the C47 sulphenic acid group back to its cognate thiol without disulphide bond formation. In effect, this C168S mutant is acting as a 1-Cys peroxiredoxin under these conditions.
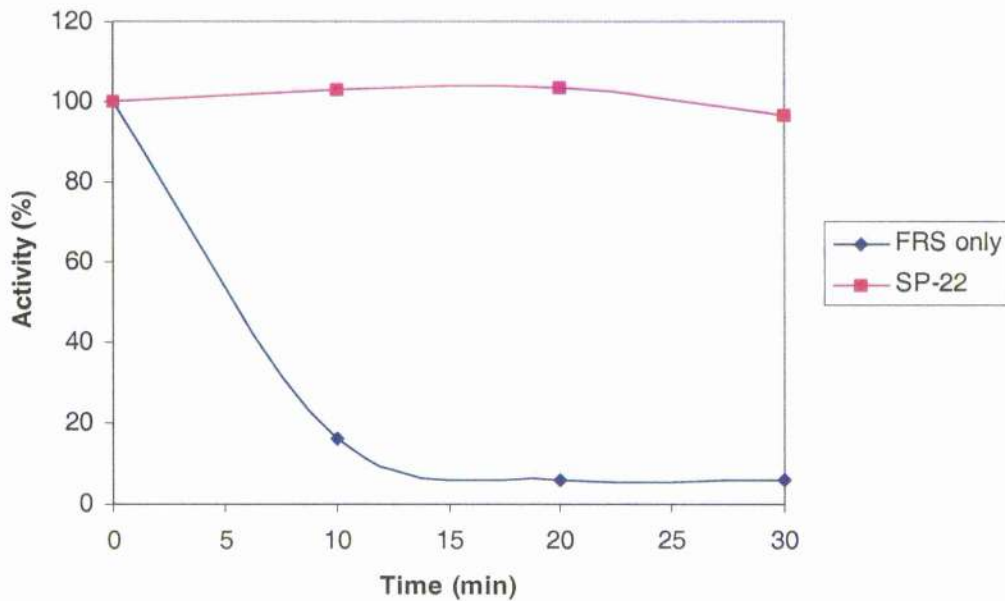
Figure 6.1. Enolase Inactivation by the FRS, and Protection by SP-22

A FRS (10μM FeCl$_3$, 30mM DTT, 50mM imidazole pH 7.0) was pre-incubated at 30°C in the absence or presence of 66μg purified SP-22 prior to addition of enolase (33μg). Experiments carried out in the absence of SP-22 contained 50mM imidazole pH 7.0, containing 150mM NaCl. At regular time intervals an aliquot was removed and added to 1mM EDTA to terminate the reaction. The sample was then assayed for remaining enolase activity by monitoring the A$_{240}$ increase corresponding to the conversion of 2-PGA to PEP. Results are expressed as the activity remaining, as a percentage of enolase activity at zero time. Values were calculated as an average of duplicate assays, differing by a maximum of ± 7%.
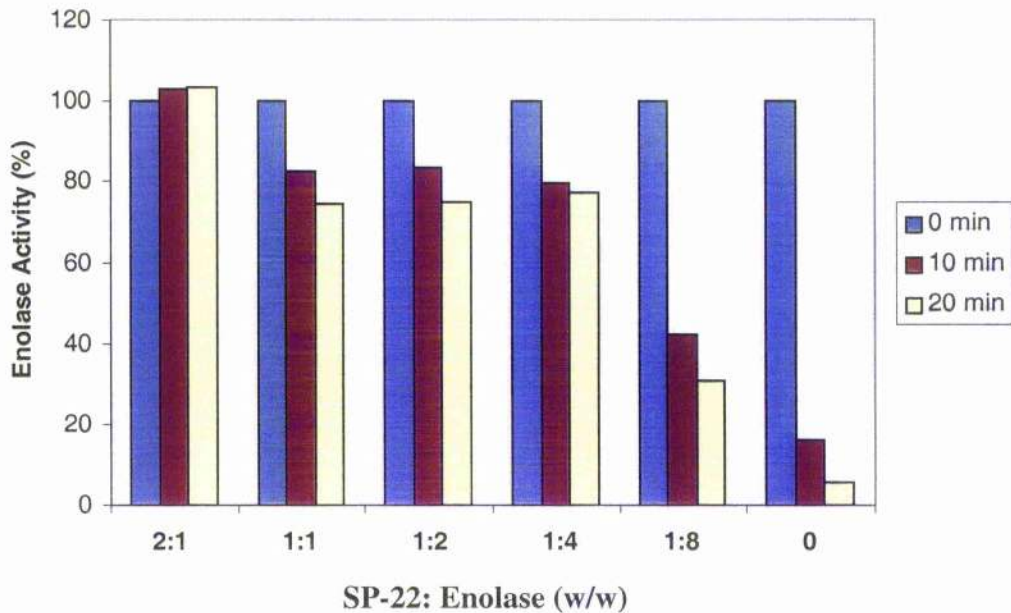
Figure 6.2. Effect of SP-22 Concentration on Enolase Protection

A FRS (10μM FeCl$_3$, 30mM DTT, 50mM imidazole pH 7.0) was pre-incubated for 5 min at 30°C in the presence or absence of decreasing concentrations of purified SP-22, prior to addition of enolase (33μg). At regular time intervals thereafter, an aliquot was removed and added to 1mM EDTA to terminate the reaction.   The sample was then assayed for remaining enolase activity by monitoring the A$_{240}$ increase corresponding to the conversion of 2-PGA to PEP. Results are expressed as the activity remaining as a percentage of enolase activity at zero time. Values were calculated as an average of duplicate assays differing by a maximum of ± 7%.
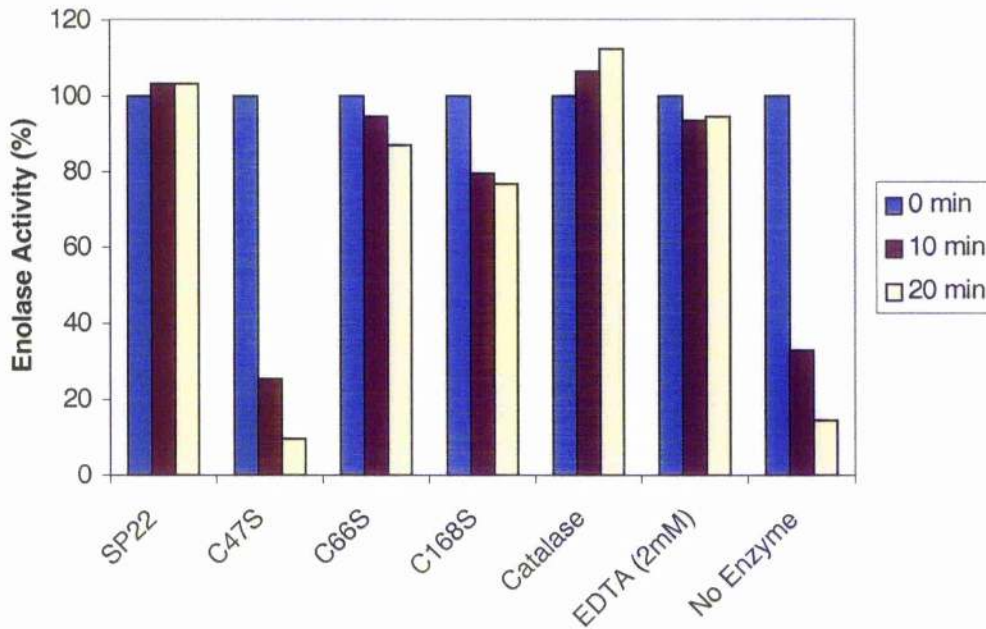
Figure 6.3. Protective Effects of the Cysteine Mutants Towards Enolase in Comparison to Wild Type SP-22

A FRS (10μM $FeCl_3$, 30mM DTT, 50mM imidazole pH 7.0) was pre-incubated at 30°C with either 66μg of purified SP-22, C47S, C66S, or C168S prior to addition of enolase (33μg). Control incubations containing 2mM EDTA and catalase (66μg) were also prepared. At regular time intervals an aliquot was removed and added to 1mM EDTA to terminate the reaction. The sample was then assayed for remaining enolase activity by monitoring the A_{240} increase corresponding to the conversion of 2-PGA to PEP. Results are expressed as the activity remaining, as a percentage of enolase activity at zero time. Values were calculated as an average of duplicate assays, differing by a maximum of ± 7%.

6.1.3. Peroxidase Activity of SP-22

To establish whether SP-22 has peroxidase activity comparable to that of catalase, the extent of hydrogen peroxide removal was assessed by monitoring the reduction in the A_{240} (Materials and Methods section 2.5.18). Bovine catalase or SP-22 were added to 50mM hydrogen peroxide in 50mM KPi pH 7.0, pre-heated to 30°C. Catalase (30µg) as predicted was extremely efficient removing 100% of 50mM hydrogen peroxide over 85s (Fig. 6.4). In contrast in the presence of ten-fold higher amounts of SP-22 (300µg), hydrogen peroxide removal was not evident. As SP-22 requires a source of thiol groups to be reduced following oxidation by hydrogen peroxide, the SP-22 experiment was carried out in the presence of 20mM DTT (Fig. 6.4).

6.1.4. Summary and Discussion

The protection of the free radical-sensitive enolase by recombinant SP-22 is reported, when subjected to a free-radical generating system. The extent of protection is concentration-dependent; however the requirement for the reducing agent DTT is undoubtedly a limiting factor in the regeneration of SP-22 for subsequent catalytic cycles, and must be taken into consideration. The highest concentration used (2: 1 (w/w) ratio of SP-22: enolase) exhibited complete protection, although substantial protection was also observed down to SP-22: enolase ratios of 1: 4. The *in vivo* SP-22/thioredoxin system using NADPH, thioredoxin reductase and thioredoxin as a physiological electron donor is likely to be even more efficient.

The conserved cysteine residue at position 47 was established to be the catalytic residue, as C47S exerted no protective effect towards enolase. The C66S and C168S mutants displayed significant protection, comparable with that of wild type SP-22, implying that they are not critical for catalytic function. The unexpected protection exhibited by C168S is a likely result of direct reduction of C47 by DTT rather than via thioredoxin as *in vivo*, which would typically require the disulphide bond formation between C47 and C168 as a key intermediate step in the catalytic cycle.
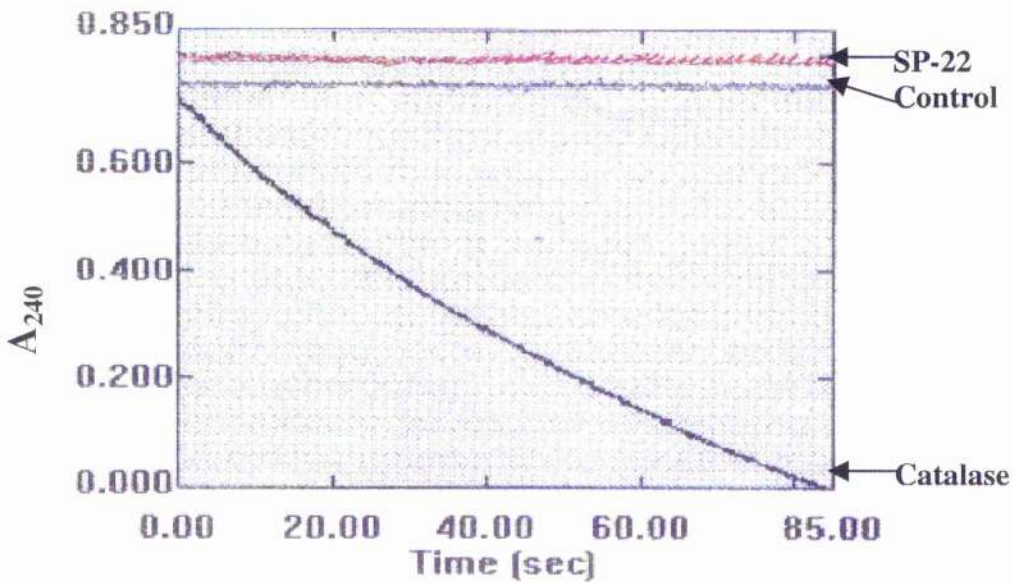
Figure 6.4. Comparison of Hydrogen Peroxide Removal by Catalase and SP-22

Assay mixtures contained 1ml 50mM hydrogen peroxide prepared in 0.1M KPi pH 7.0, preincubated at 30°C in a quartz cuvette. The incubation mix additionally contained 20mM DTT for SP-22 experiments. Hydrogen peroxide removal by catalase (30μg) and SP-22 (300μg) was assessed by tracing the reduction in A_{250} over 85s. Also shown is a no enzyme control.

Catalase was also demonstrated to protect enolase from damage exerted by the FRS, suggesting that the ROS that modifies the enzyme is either hydrogen peroxide or its degradation product the hydroxyl radical, generated via the Fenton reaction. To assess whether SP-22 possesses catalase-like peroxidase activity, the rate of hydrogen peroxide removal was assessed with increasing concentrations of SP-22. There was no obvious removal of hydrogen peroxide by SP-22 in comparison with catalase, implying that they have divergent mechanisms. These results are consistent with previous findings for other 2-Cys members, suggesting that their roles are to remove only micromolar levels of hydrogen peroxide and thus can regulate cell-signalling pathways that are controlled by fluctuating amounts of hydrogen peroxide. It remains to be established if the low levels of activity attributed to SP-22, reflect the limitations of the assay procedure in which conversion of the enzyme back to its reduced state is dependent on non-enzymatic reduction by DTT. The catalase system in conjunction with the glutathione peroxidase system, in contrast, removes hydrogen peroxide extremely rapidly even when present at elevated levels.

Chapter 6
Section 2

6.2.0. Introduction

SP-22 is one of two mitochondrial 2-Cys Prxs identified to date, and comprises 5% of total matrix protein of mitochondria isolated from bovine adrenal cortex, emphasising its importance in the removal of hydrogen peroxide from this compartment. Therefore its role may be pertinent in the protection of the many key enzymes responsible for the large number of metabolic processes occurring in the mitochondrion.

As previously discussed (Chapter 1 section 1.5), several diseases, particularly autoimmune diseases and neurodegenerative disorders contain characteristically high levels of oxidatively modified proteins. Excessive production of hydrogen peroxide has been observed in the ageing brain. Mitochondrial enzymes appear to be especially vulnerable to oxidative damage, not surprising given their close proximity to ROS generated by oxidative phosphorylation. Modification of mitochondrial enzymes can severely compromise the metabolism of an organism and ultimately lead to its death. The principal enzymes targeted by oxidation, demonstrated in yeast and bacteria, include the TCA cycle enzymes aconitase and the mitochondrial 2-oxoacid dehydrogenase complexes, particularly the pyruvate dehydrogenase complex (PDC), and the 2-oxoglutarate dehydrogenase complex (OGDC) (Cabiscol *et al*, 2000; Tamarit *et al*, 1998). Inactivation studies on the branched-chain 2-oxoacid dehydrogenase complex (BCOADC) are limited, however available literature suggests it is the least sensitive of the multienzyme complexes.

Studies carried out on isolated nerve terminals determined that aconitase is the most susceptible TCA cycle enzyme to damage by hydrogen peroxide, and is completely inactivated at concentrations $\leq 50\mu M$. OGDC is also inactivated, but only partially at slightly higher concentrations of $\leq 100\mu M$ (Tretter and Adam-Vizi, 2000). These findings imply that under conditions of oxidative stress aconitase is initially inactivated, followed by OGDC partial inactivation, therefore slowing down the TCA cycle and consequently NADH formation and cellular respiration. Therefore inactivation of these two enzymes may be the principal

factor responsible for mitochondrial impairment when exposed to acute levels of hydrogen peroxide. This has important implications in the treatment and prevention of several neuropathologies.

The effect of the aldehyde, 4-hydroxy-2-nonenal (HNE) generated by lipid peroxidation on the activity of the 2-oxoacid dehydrogenase complexes, and their individual subunits in cultured human cells has also been investigated (Moreau *et al*, submitted for publication). HNE is an extremely powerful oxidant due to its hydrophilic and hydrophobic properties, enabling its movement between different cellular compartments and its wide range of substrates. It has been demonstrated to inactivate PDC and OGDC by inflicting damage on the lipoyl moieties of their dihydrolipoamide acyltransferase (E2) and E3-binding protein (E3BP) components. The E2-E3BP complex was severely affected by HNE treatment in comparison with the other complex constituents. The dihydrolipoamide dehydrogenase (E3) component and other thiol-containing molecules were demonstrated to protect the E2/E3BP complex from damage by HNE. Thiol groups are predominantly modified by HNE, therefore would be targeted instead of the E2-E3BP complex (Korotchkina *et al*, 2001).

As for enolase, experiments were carried out to establish whether SP-22 might protect the 2-oxoacid dehydrogenase complexes from oxidative damage. The protection of E3 individually was also assessed as it is easy to assay and it contains reactive sulphydryl groups that may be the potential targets of oxidation. As inactivation was not achieved with the FRS previously used suggesting that the complexes were not susceptible to free radical-mediated inhibition, hydrogen peroxide was added directly to the purified complexes.

Results

6.2.1. PDC and OGDC Inactivation by Hydrogen Peroxide

Inactivation of PDC and OGDC was attempted with the FRS used above, however inactivation was not achieved, even after 40 min with increasing $FeCl_3$ concentrations (results not shown). This is not surprising given the findings in

previous studies that the levels of hydrogen peroxide required to inhibit the 2-oxoacid dehydrogenase complexes are in the millimolar range. The FRS would not be able to generate such high levels of hydrogen peroxide. Consequently hydrogen peroxide-induced inactivation was assessed by adding it directly to the purified complexes, at concentrations of 1, 5 and 10mM (Materials and Methods section 2.5.16). Increased inactivation of PDC and OGDC was observed with increasing hydrogen peroxide concentration, however even after incubation with 10mM hydrogen peroxide at 30°C for 40 min, activity was not completely abolished (Fig. 6.5 and 6.7). At 1mM hydrogen peroxide, approx. 20% and 40% activity of PDC and OGDC respectively, still remained. If inactivation of the complexes occurred via oxidative modification of the redox-active sulphydryl groups of E3 and for E2, they would need to be in their reduced form; therefore experiments were repeated in the presence of 0.1mM NADH to determine if susceptibility to inactivation was increased. Surprisingly there was no significant alteration in susceptibility of PDC or OGDC to inactivation by hydrogen peroxide. The inactivation of PDC in the presence of 0.1mM NADH is illustrated (Fig. 6.6).

6.2.3. Inactivation of Bovine E3 by Hydrogen Peroxide

As bovine E3 contains reactive sulphydryl groups it is a potential target of oxidation by ROS including hydrogen peroxide. Experiments monitoring the extent of hydrogen peroxide inactivation of E3 were carried out as for PDC and OGDC (Fig. 6.8). E3 displayed a higher degree of resistance to inactivation even at the highest concentration of hydrogen peroxide than the 2-oxoacid dehydrogenase complexes. ≥25% activity was remaining after 40 min incubation in 10mM hydrogen peroxide. The complexes are more susceptible because their activity is dependent on coordinated activity of each of their enzyme components.

Pre-incubating E3 in 0.1mM NADH as for the 2-oxoacid dehydrogenase complexes did not increase the rate of inhibition, suggesting that hydrogen peroxide does not directly modify active-site sulphydryl groups as the principal mechanism of inactivation (results not shown).
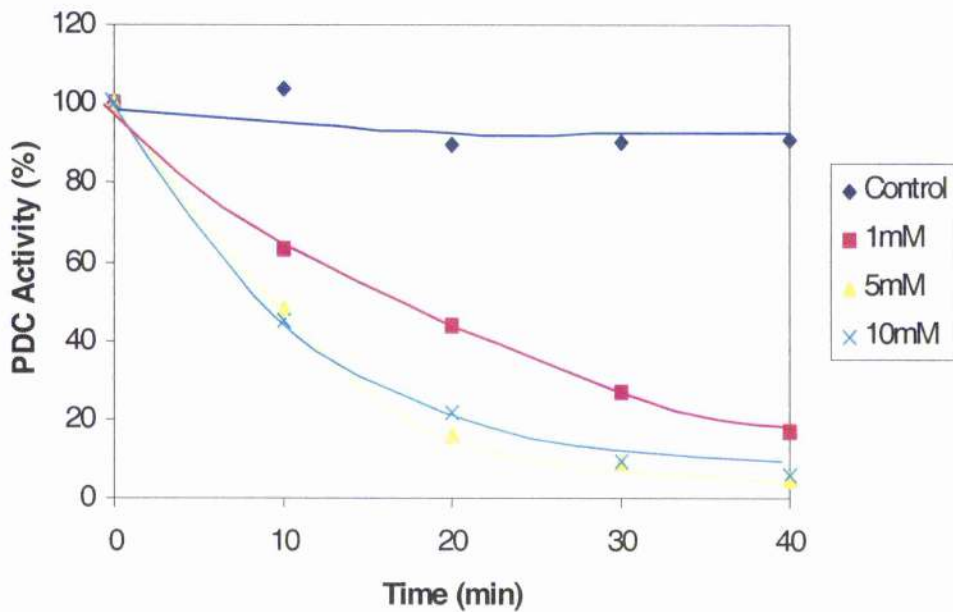
Figure 6.5. Inactivation of PDC with Increasing Concentrations of Hydrogen Peroxide

Purified bovine heart PDC (50μg) prepared in 50mM KPi buffer pH 7.0 was incubated at 30°C with increasing concentrations of hydrogen peroxide. At increasing time intervals 1-5μg of reaction mix was assayed in 670μl of 50mM KPi buffer pH 7.6, containing 3mM NAD$^+$, 2mM MgCl$_2$, 0.2mM ThDP, 14μl Solution B (0.13M cysteine-HCl and 6.8mM acetyl CoA) and 14μl 100mM pyruvate, recording the A$_{340}$ increase over 45s. Results were calculated as an average of duplicate readings differing by ±7%.

Figure 6.6. Inactivation of PDC (Pre-incubated with NADH) with Increasing Concentrations of Hydrogen Peroxide

Purified bovine heart PDC (50µg) prepared in 50mM KPi buffer pH 7.0 was pre-incubated at 30°C with 0.1mM NADH, prior to addition of increasing concentrations of hydrogen peroxide. At increasing time intervals 1-5µg of reaction mix was assayed in 670µl of 50mM KPi buffer pH 7.6, containing 3mM NAD^+, 2mM $MgCl_2$, 0.2mM ThDP, 14µl Solution B (0.13M cysteine-HCl and 6.8mM acetyl CoA), and 14µl 100mM pyruvate, recording the A_{340} increase over 45s. Results were calculated as an average of duplicate readings differing by ±7%.
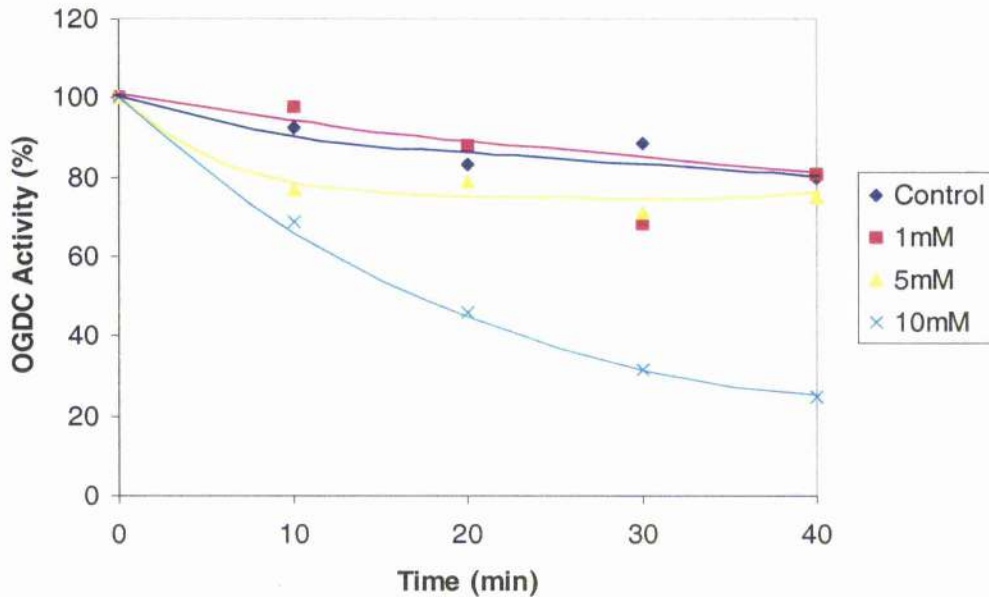
Figure 6.7.   Inactivation of OGDC with Increasing Hydrogen Peroxide Concentrations

Purified bovine heart OGDC (50µg) prepared in 50mM KPi buffer pH 7.0 was incubated at 30°C with increasing concentrations of hydrogen peroxide.   At increasing time intervals 1-5µg of reaction mix was assayed in 670µl of 50mM KPi buffer, pH 7.6, containing 3mM NAD^+, 2mM $MgCl_2$, 0.2mM ThDP, 14µl Solution B (0.13M cysteine-HCl and 6.8mM acetyl CoA) and 14µl 100mM ketoglutarate, recording the A_{340} increase over 45s. Results were calculated as an average of duplicate readings differing by ±7%.
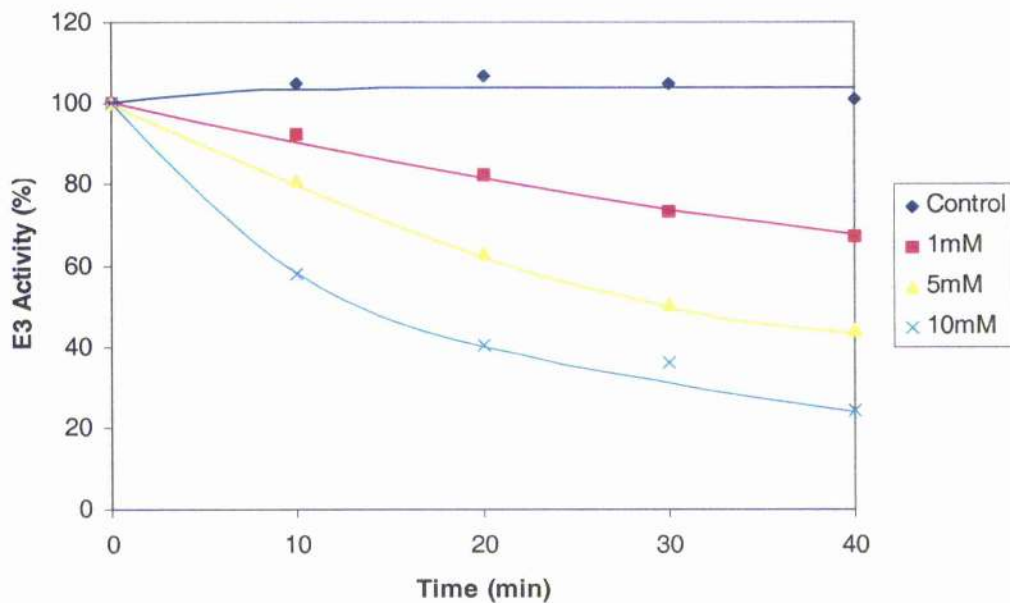
Figure 6.8. Inactivation of Bovine E3 with Increasing Concentrations of Hydrogen Peroxide

Bovine E3 prepared in 0.1M KPi buffer pH 7.0 was incubated with increasing concentrations of hydrogen peroxide (1, 5, and 10mM) at 30°C. At various time intervals remaining activity was assessed monitoring the A_{340} increase over 45s on addition of E3 (5-50µg) to 670µl of 50mM KPi buffer pH 7.6, containing 3mM NAD^+, 2mM $MgCl_2$, and 0.2mM ThDP. The reaction was initiated upon addition of 14µl 2.0mM dihydrolipoamide. Results were calculated as an average of duplicate readings differing by ±7%.

6.2.4. Summary and Discussion

As mentioned earlier, it has been reported that although the multienzyme complexes are the principal targets of oxidation, higher levels of hydrogen peroxide than normal are required for their inactivation in comparison with other enzymes involved in the processes involved in aerobic respiration. Indeed it is proposed that in several neurodegenerative diseases, inactivation of OGDC by oxidative modification is responsible for the decrease in brain metabolism in these patients (Gibson *et al*, 2000). The requirement for higher hydrogen peroxide concentrations to inactivate E3, PDC and OGDC accounts for the observation that these enzymes were resistant to damage by the metal-catalysed FRS, which successfully inactivated enolase in the previous section. Consequently three concentrations of hydrogen peroxide (1, 5 and 10mM) were used to inactivate PDC, OGDC and their common E3 component. There was a corresponding decrease in activity with an increase in hydrogen peroxide concentration, although not to a particularly great extent. It was surprising that for all three susceptible subjects, 10mM hydrogen peroxide did not completely abolish their activities after incubation for 40 min. Consequently the protection of these enzymes by SP-22 as in the enolase experiments could not be assessed.

To render the possible susceptible chemical groupings of the enzyme components accessible to oxidation in an attempt to increase their vulnerability, the experiments were repeated in the presence of 0.1mM NADH. Incubation in the presence of NADH reduces the disulphides of E3 to their cognate sulphydryl groups, and reduces the disulphide bond on the diothiolane ring of the lipoate cofactor of E2. Both these groupings have the potential to be oxidised by free radicals and ROS. Surprisingly however, inactivation on addition of hydrogen peroxide was not significantly different to the experiments carried out in the absence of NADH suggesting that the redox-active cysteines of E3 are not accessible, and may be protected within the overall structure. Indeed the thiol groups of PDC E3 are not accessible to modification by NEM unless the complex is completely denatured, shown previously in chapter 1 (Fig.1.11).

With respect to the resistance of E2 to oxidative modification, it has been demonstrated that it is possible to remove >50% of the lipoate groups of E2 without resulting in loss of enzymatic activity (Guest *et al*, 1985). It is possible therefore that the lipoate groups are being oxidised, but not to such an extent where inactivation is achieved.

A further possibility that would account for the resistance to inactivation would be that hydrogen peroxide only reversibly modifies the groupings of PDC and OGDC. As the assay mix contains millimolar levels of cysteine-SH it is possible that upon addition to the mix the modified groups are repaired. Consequently the extent of inactivation observed in these studies may only represent the irreversible oxidative modification of the complexes. Indeed, it has been reported in intact rat mitochondria that micromolar levels of hydrogen peroxide reversibly inhibits OGDC (Nulton-Persson and Szweda, 2001). Moreover, this report implies that hydrogen peroxide may have a role in regulation of the complexes by modulating the redox status of the mitochondria rather than by direct inactivation of OGDC.

Chapter 7

Section 1

7.1.0. Introduction

Previous studies, unrelated to SP-22 investigations, involving the dissociation of the pyruvate dehydrogenase complex (PDC) into its cognate enzyme components, highlighted the possibility of an interaction between the dihydrolipoamide dehydrogenase component (E3) and SP-22. PDC was purified under associative conditions from bovine heart (Materials and Methods section 2.5.12). Following high-speed centrifugation of the purified complex, the resuspended multienzyme complex was analysed by SDS-PAGE. An additional protein with a M_r 22,000 was found to co-purify with PDC, despite the ultracentrifugation step that favours the isolation of high molecular mass species. PDC was subsequently separated into its constituent enzymes by gel exclusion chromatography in the presence of 2M salt. The additional protein was found to specifically co-elute with E3 during purification by size exclusion chromatography and, following N-terminal sequencing, was confirmed as SP-22 (R.G. McCartney (1998) Thesis, University of Glasgow).

E3, like thioredoxin reductase, is a member of the pyridine dinucleotide disulphide reductases and therefore immediately can be indirectly linked to SP-22, which is reported to exhibit thioredoxin-dependent peroxidase activity. Furthermore given the function of SP-22 in the removal of hydrogen peroxide, and the susceptibility of PDC to oxidative damage (Chapter 6 section 2), it may be postulated that SP-22 serves to protect this complex. Perhaps more specifically, SP-22 may protect the reactive sulphydryl groups of the E3, E2 and E3BP components of PDC accounting for their possible association. Interestingly, AhpC a bacterial alkyl hydroperoxide from *Salmonella typhimurium* with homology to SP-22 interacts with a second component AhpF, which is a member of the pyridine dinucleotide disulphide reductase family related to E3.

To provide evidence for a specific interaction between E3 and SP-22, studies were carried out employing isothermal titration calorimetry (ITC) and surface plasmon resonance (SPR).

A typical reaction between two components, A and B is as follows:

$$A + B \underset{k_d}{\overset{k_a}{\Longleftrightarrow}} AB$$
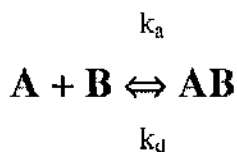
The rate of association (k_a) used to indicate the rate of complex formation, and the rate of dissociation (k_d) used to indicate the rate of complex decay, can be used to calculate the association equilibrium constant (K_A) of two interacting components, and the dissociation equilibrium constant (K_D). The K_A gives a measure of the strength of binding e.g. the higher the K_A, the higher the binding affinity. The K_D is the reciprocal of K_A and is generally the parameter used to define an interaction. The smaller the K_D, the greater the binding affinity.

ITC enables the measurement of the thermodynamics of a protein-protein interaction (Pierce *et al*, 1999). This information can also provide information on the also the strength of binding, the stoichiometry of binding, and the enthalpy of binding ($\triangle H_b$) between two interacting species.

The ITC instrument comprises two cells: one reference cell and one sample cell which will contain the macromolecule of interest. Both cells are identical and consist of an efficient thermal conducting material encased in an adiabatic jacket. Slight temperature changes occurring between the two cells and the cells and jacket are detected, activating the jacket to alter the temperatures so that they are identical. The reference cell contains the appropriate buffer minus the macromolecule. A constant power ($<1mW$) is exerted on the reference cell which consequently instructs a feedback circuit to activate the sample cell heater, and subsequently represents the baseline for experiment. The other ligand of interest is contained in a syringe and titrated into the macromolecular sample within the sample cell. The time-dependent input of power required to keep the reference and sample cells at identical temperatures is recorded. The power input is dependent on whether the protein-protein interaction is endothermic or exothermic. Exothermic reactions give rise to an increase in temperature in the

sample cell resulting in a drop in power input, and vice versa for endothermic reactions. The heat exchange is proportional to the fraction of bound ligand. A disadvantage of this method is that high concentrations of titrant are required. Another technique, requiring lower protein concentrations that can provide detailed information on the binding kinetics of an interaction is surface plasmon resonance.

SPR is a relatively new technology that characterises macromolecular interactions, providing information on the affinity and rate of binding within the nanomolar to micromolar range (McDonnell, 2001). SPR is an optical technique that uses the evanescent wave phenomenon to assess the refractive index change that occurs when an analyte and its ligand interact. The ligand is immobilized on the surface of a sensor chip and the analyte is present in solution. When an analyte binds to a ligand there is a change in the refractive index due to the increase in mass on the chip surface. Binding is measured in response units (RU) with 1RU being equivalent to $0.1°$ change in the angle of reflected light from the chip surface, also equivalent to 1ng of bound protein per mm^2. Typically the macromolecule with the lower molecular weight should be immobilised to the chip surface, however for publication it is usually necessary to carry out experiments in both orientations. The principal advantage of SPR is that the analyses can be carried out rapidly and accurately in intricate detail, over a range of macromolecular concentrations and environmental conditions.

The company Biacore (Uppsala, Sweden) was the first to offer an instrument to investigate interactions by SPR and it has continued to dominate the SPR market despite several other companies offering cheaper alternatives (Mullett et al, 2000). The Biacore sensor chip is a 100nm gold-coated slide held within a plastic support, coated with a carboxy-methylated dextran that allows immobilisation of the desired ligand via a number of chemical groupings such as amines, sulphydryls, hydrazines and maleimides. The hydrophilic properties of this matrix also minimises the occurrence of non-specific binding, which can affect the accuracy of the analysis.

Results

7.1.1. Stoichiometry of SP-22/E3 Binding by Isothermal Titration Calorimetry

For ITC high concentrations of injectant are required, therefore to detect an interaction between SP-22 and E3, human recombinant E3 was used instead of bovine E3, owing to our ability to produce the human enzyme in large amounts. Both E3 and SP-22 were extensively dialysed for ITC to minimise buffer mismatches that may create a signal during the injection process (Materials and Methods section 2.5.23). The dialysate was placed into the reference cell and SP-22 ($10\mu M$) was placed in the sample cell. Prior to injection of the ligand (E3) into the sample (SP-22), E3 was injected into buffer only to determine its heat of dilution. The data illustrated have been corrected taking into account the heat of dilution of E3. The injection of E3 into SP-22 resulted in an endothermic heat pulse (not shown) and generated a profile that was consistent with a single-site binding model (Fig. 7.1). Although the stoichiometry of binding was not accurately determined, the data fitted well to a 1:1 interaction. The association constant was calculated using ORIGIN software (OriginLab Corporation) and was in the micromolar range ($18.3\mu M$) representing a relatively high affinity interaction. Given that E3 is of human origin and SP-22 is bovine, it is possible that tighter binding may occur with enzymes of the same source. Even so, an interaction between SP-22 and E3 is clearly indicated.
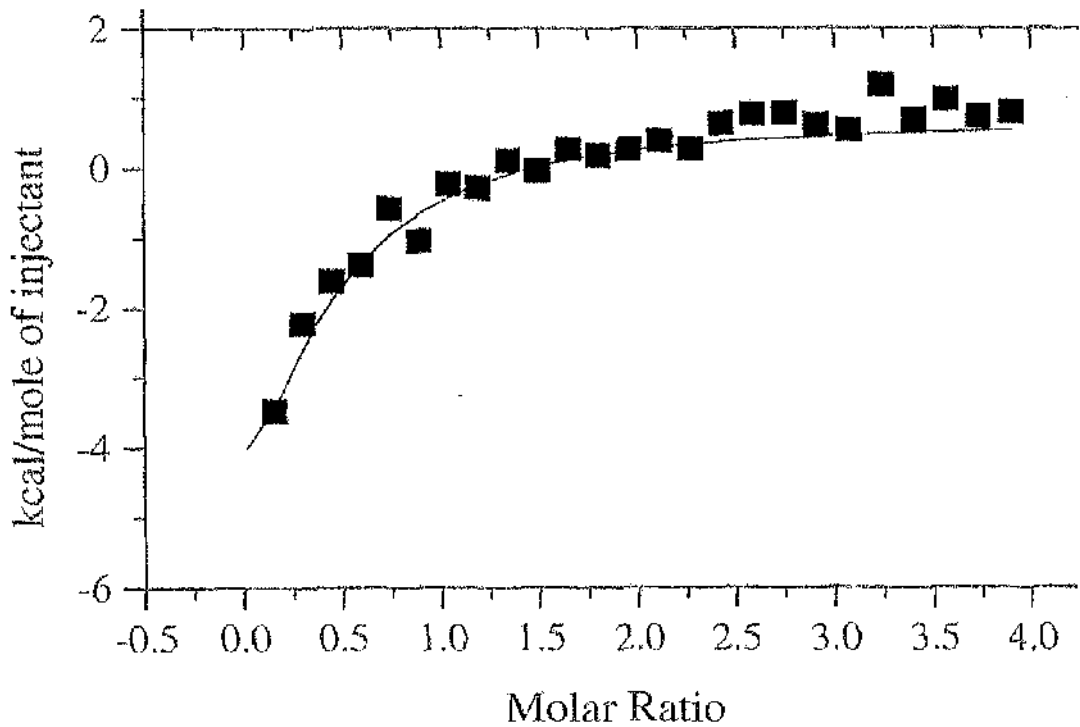
Figure 7.1. Titration of Human Recombinant E3 into Bovine SP-22

Purified human E3 (200μM) was titrated in 10μl injections into purified SP-22 (10μM). Both proteins had previously been extensively dialysed together in the same container into 0.1M KPi buffer pH 7.0, containing 0.15M NaCl. The experiment was carried out at controlled temperature (25°C) and data were generated using a single-site binding model. The heat of binding is shown against the molar ratio of injectant (E3): cell sample (SP-22).

7.1.2. Binding Studies Between SP-22 and Bovine E3

To further elucidate the interaction between E3 and SP-22, SPR was adopted. This technique requires small protein concentrations in the micromolar range; therefore it was possible to use bovine E3 in these experiments instead of human recombinant E3.

A CM-5 sensor chip was activated and bovine E3 (50μg/ml) prepared in 0.1M sodium acetate buffer pH 4.5, was immobilised onto the chip surface via amine coupling (Materials and Methods section 2.5.24). The amount of protein bound to the chip is measured in response units (RU). Bovine E3 (1143.8 RU) was successfully immobilized onto the chip. Five concentrations of SP-22 (10, 50, 250, 500, and 1000nM) were prepared in HBS buffer pH 7.4 for the binding studies (Materials and Methods section 2.5.24). Experiments were carried out at 25°C with a flow rate of 20μl/min, and 60μl injections of each concentration were passed over the chip surface, followed by 10μl injections of 1M NaCl to regenerate the chip surface for the next run. The binding curves for each run were evaluated using the BIAevaluation 3.0 software, and the curves were fitted according to the Langmuir 1:1 model of binding. The success of a fit was reflected by Chi^2 values less than 1. The best curves generated were for the highest SP-22 concentrations (1000 and 500nM), displaying rapid *on* rates (k_a), and slower *off* rates (k_d), with Chi^2 values less than 0.5 (Fig. 7.2.). The results for two concentrations of SP-22 are tabulated below (Table 4).

[SP-22] (nM)	k_a ($M^{-1}s^{-1}$)	k_d (s^{-1})	$K_A (k_a/k_d)$ (M^{-1})	$K_D (k_d/k_a)$ (M)
1000	3.64×10^4	4.39×10^{-3}	8.34×10^6	1.2×10^{-7}
500	8.33×10^3	7.25×10^{-3}	1.15×10^6	8.71×10^{-7}

Table 4. Kinetic Analysis of the Interaction Between SP-22 and Bovine E3, at differing SP-22 Concentrations
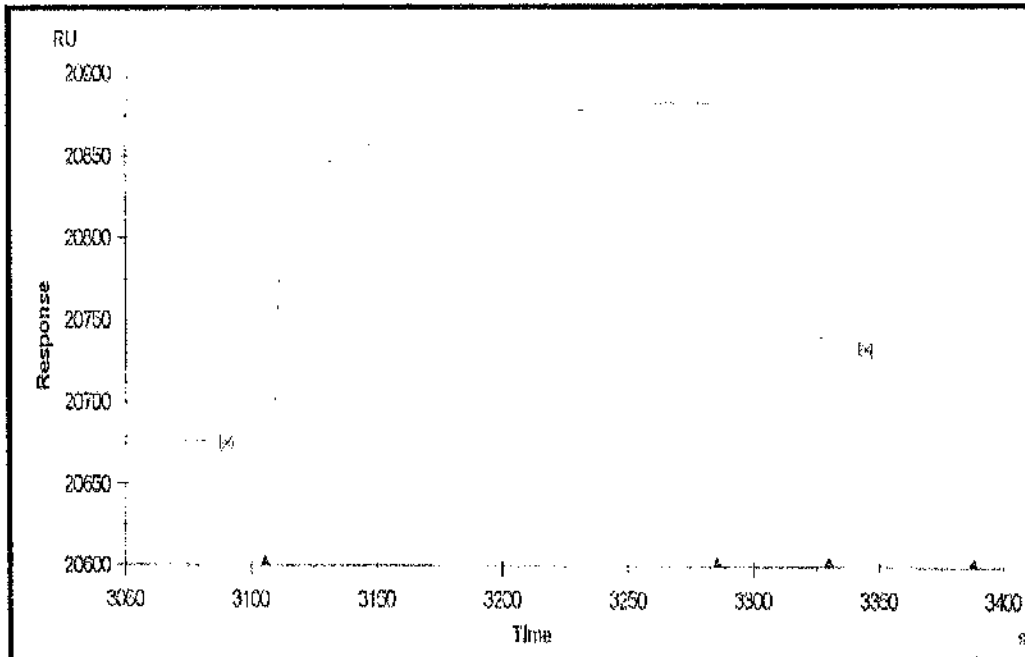
Figure 7. 2. SPR Binding Profile of SP-22 with Bovine E3

A sample (60μl) of purified SP-22 (1μM), prepared in equilibrium buffer (HBS, pH 7.4), was passed over bovine E3 bound to a CM-5 sensor chip via amine coupling. The experiment was carried out at 25°C at a flow rate of 20μl/min in a BIAcore 2000 machine (Uppsala, Sweden). Chip regeneration was achieved on injection of 1M NaCl over the chip surface. The small triangles indicate the pre- and post-injection stages of SP-22 onto the chip, the end of the run and the subsequent injection point of 1M NaCl. Binding can be detected by monitoring the number of response units (RU) generated over time in seconds (s).

It can be seen from these preliminary studies that SP-22 and bovine E3 do interact relatively tightly, with a binding affinity in the micromolar range. At the highest concentration of SP-22 (1000nM), the K_D is $0.12\mu M$, and $0.87\mu M$ for 500nM. Concentrations at less than 500nM did not generate binding curves to permit the kinetic analysis. Further kinetic analysis and future experiments are required to consolidate these findings.

7.1.3. Summary and Discussion

The initial observation implying that a physical interaction may occur between SP-22 and E3 of PDC isolated from bovine heart was made following the co-elution of these proteins using gel exclusion chromatography. Given the present knowledge that SP-22 is a large oligomer with an approximate molecular weight ranging from between $500\text{-}600,000M_r$ and with the tendency to form toroidal stacks of two and three rings, it is possible that this co-elution was a result of SP-22 oligomers co-sedimenting along with the PDC on ultracentrifugation due to size, rather than an actual physical association.

The highly sensitive technique of surface plasmon resonance was utilised to clarify whether an interaction occurs between SP-22 and bovine E3. A clear interaction was observed with a dissociation constant (K_D) of between $0.1\text{-}0.9\mu M$, regarded as a relatively tight association. It would be of interest to repeat the binding studies with other components of PDC, and also by coupling SP-22 to the sensor chip with E3 as the analyte to ensure that the results are consistent. Furthermore the influence of mass transport on the interaction between SP-22 and E3 requires assessment, repeating the experiment at a range of flow rates. Owing to time constraints this was not achieved for this thesis.

To ascertain the stoichiometry of binding between SP-22 and E3, isothermal titration calorimetry was employed. Owing to the high concentrations of E3 required for this technique, human recombinant E3 was used instead of the commercially available bovine E3. The stoichiometry of binding was not accurately established, but fitted well to a 1:1 model of binding, and together with

the SPR studies, indicates a clear interaction between SP-22 and E3. The binding affinity established by ITC was lower yet similar to that that determined by SPR, although human recombinant E3 was used in this ITC study. Further experiments were hampered by the tendency of SP-22 to precipitate at concentrations higher than 10mg/ml, which is necessary when repeating the experiment in reverse i.e. with SP-22 in the syringe.

Chapter 7

Section 2

7.2.0. Introduction

In the previous section, evidence has been provided for the presence of a clear physical interaction between SP-22 and the E3 component of PDC. This implies that a functional relationship may also exist between these two enzymes. This possibility is further supported by the sequence homology that exists between the two components of the alkyl hydroperoxide reductase system from *Salmonella typhimurium*, AhpC and AhpF, and SP-22 and E3, respectively. In the alkyl hydroperoxide reductase system AhpC breaks down organic hydroperoxides to their corresponding alcohols and water using reducing equivalents supplied by the NADH-dependent AhpF (Fig 1.6a, Chapter 1). Furthermore the AhpC component of *Mycobacterium tuberculosis* has been demonstrated to interact with the E3 and E2 components of OGDC via an additional adaptor protein called AhpD, to scavenge both peroxides and peroxynitrite (Bryk *et al*, 2000; Bryk *et al*, 2002).

To elucidate the functional significance of the interaction between SP-22 and E3, the possibility of PDC, OGDC, E2 and/or E3 providing the reducing equivalents for the peroxidase activity of SP-22 was assessed using reducing and non-reducing SDS-PAGE analysis.

7.2.1. Determination of the Specificity of SP-22 Reduction

The Prx family were originally named thiol-specific antioxidant proteins owing to their requirement for reducing equivalents provided by thiol-containing molecules (Netto *et al*, 1996). To ascertain whether the reduction of SP-22 is thiol-specific, SDS-PAGE analysis of SP-22 was carried out in the absence (**Lane 1**) and presence of 10mM DTT (**Lane 2**), 10mM DHL (**Lane 4**), or 10mM ascorbic acid (**Lane 3**) (Fig. 7.3). DTT and DHL are both thiol-containing compounds shown to successfully reduce oxidised (dimeric) SP-22 to its monomeric form. Ascorbic acid, also called vitamin C is a commonly used reducing agent; however it lacks a thiol group. Indeed the reduction of SP-22 was demonstrated to be thiol-specific, indicated by the maintenance of SP-22 in its disulphide-bonded (dimeric) form
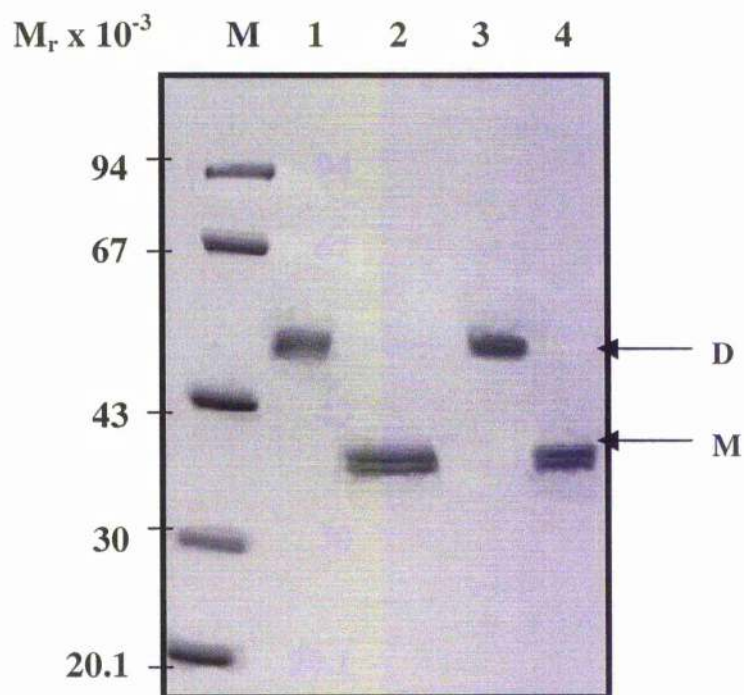
Figure 7.3. Determination of the Thiol-Specific Reduction of SP-22

Purified SP-22 (5μg) was pre-incubated for 5 min at room temperature in the absence of reducing agent (**Lane 1**), or in the presence of either 10mM DTT (**Lane 2**), 10mM ascorbic acid (**Lane 3**) or 10mM dihydrolipoamide (**Lane 4**). The incubation mix was analysed on a 12% polyacrylamide gel following denaturation in Laemmli sample buffer at 70°C for 5 min. Protein bands were stained using Coomassie Brilliant Blue. The monomeric (M) and dimeric (D) forms of SP-22 are indicated by the arrows.

when in the presence of ascorbate. Furthermore, in subsequent experiments, the ability of NADH and thioredoxin to reduce SP-22 was also assessed. As expected thioredoxin reduced SP-22 successfully whereas NADH did not (**Lanes 3 and 6**, Fig. 7.4).

7.2.2. Assessment of the Reduction of SP-22 by E3

Using the fact that SP-22 contains disulphide-bonded subunits that migrate as dimers or monomers in the oxidised or reduced states of the enzyme, on a polyacrylamide gel, SDS-PAGE analysis was utilised to determine whether other compounds and enzymes could promote reduction of SP-22.

As the activity of SP-22 revolves around its reduction following oxidation by its substrate and E3 contains reactive sulphydryl groups, the potential for SP-22 reduction by E3 in place of thioredoxin was assessed. E3 (5μg) and SP-22 (5μg) in the presence and absence of 1mM NADH were incubated together for 5 min at 37°C, then denatured in Laemmli sample buffer for 15 min at 37°C and analysed on a 10-12% gradient NOVEX gel (Fig. 7.4). All proteins involved in these experiments were prepared in 50mM KPi buffer pH 7.0 containing 10mM NaCl. Low salt was employed to prevent disruption of potential electrostatic protein-protein interactions.

Successful reduction of SP-22 was indicated by its conversion from its dimeric to monomeric form. Dimeric (**Lane 1**) and monomeric (**Lane 2**) marker incubations of SP-22 were prepared. It was apparent that E3 did not reduce SP-22 (**Lane 4**), even when pre-incubated with 1.0mM NADH which would render E3 entirely in its reduced state (**Lane 5**). A control incubation containing NADH alone also did not reduce SP-22 (**Lane 3**). As expected, reduced thioredoxin the recognised physiological substrate for SP-22 converted it completely to its monomeric (reduced) state (**Lane 6**).

Interestingly when SP-22 was incubated with thioredoxin, E3 and NADH it was present in its oxidised state (**Lane 8**). This was a surprising observation given

that thioredoxin reduces SP-22 in the presence of E3, in the absence of NADH (**Lane 7**). Furthermore incubating SP-22 with E3, thioredoxin and 1mM NAD^+ rendered SP-22 entirely in its monomeric form (**Lane 9**). On consulting the literature, it was noted that E3 possesses NADH-dependent oxidase (diaphorase) activity (Gazaryan *et al*, 2002). Such activity results in the generation primarily of hydrogen peroxide, but also to a lesser extent the superoxide anion from the oxidation of NADH. Following the reduction of SP-22 by thioredoxin, any hydrogen peroxide generated from E3-linked diaphorase activity would re-oxidise SP-22 back to its dimeric state. This phenomenon was also observed when SP-22 was incubated in the presence of thioredoxin, with 25μg of PDC and OGDC (**Lanes 5-8**, Fig. 7.5). As SP-22 incubated in the presence of NAD^+ is monomeric this implies electrons cannot be transferred from reduced SP-22 to NAD^+ either directly or via thioredoxin and E3.

It is known that *in vitro* E3 can transfer the electrons supplied by exogenous NADH to E2, therefore reducing its covalently linked lipoamide groups. Furthermore it was demonstrated that exogenous DHL can reduce SP-22 (Fig. 7.3). Thus, it is possible that E2 may facilitate electron transfer from its bound DHL group to SP-22 (Diagram 1, Fig. 7.6). This would be difficult to investigate however, in the light of knowledge that E3 has diaphorase activity. Any successful reduction of SP-22 by E2 via the transfer of electrons from NADH to E3 would be masked by the re-oxidation of SP-22 by hydrogen peroxide, generated by the diaphorase activity of E3 (Diagram 2, Fig 7.6).
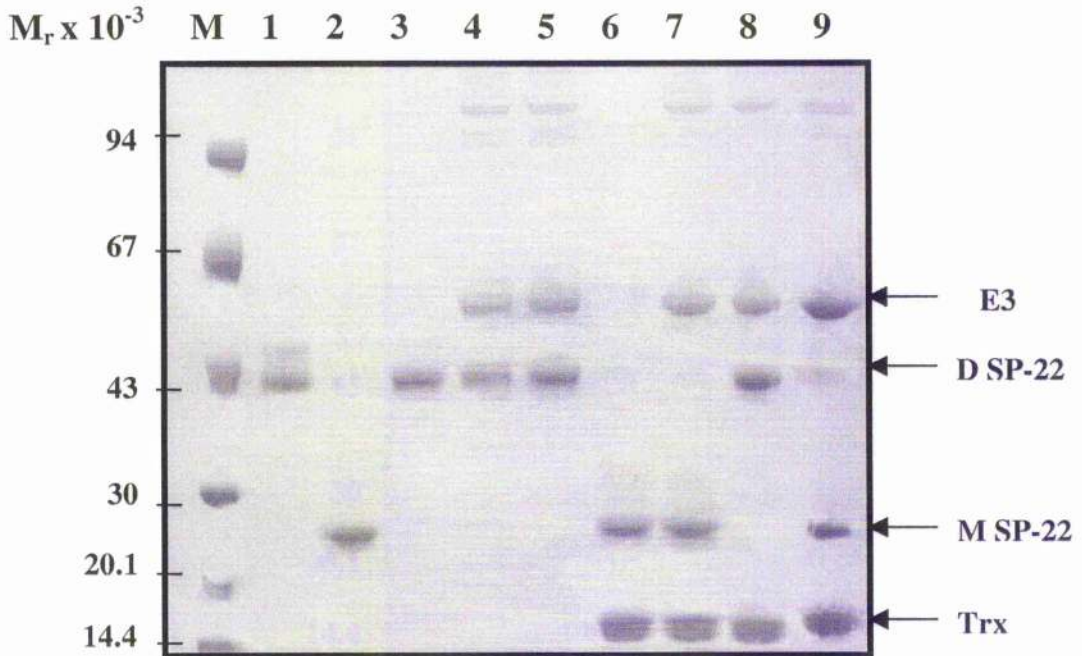
Figure 7.4. Analysis of SP-22 and E3 Interaction by SDS-PAGE

Purified SP-22 (5µg) was pre-incubated with combinations of bovine E3 (5µg) and thioredoxin (5µg) for 5 min at 37°C in the absence or presence of 1.0mM NADH or NAD⁺, then made up to a total volume of 20µl with Laemmli sample buffer and denatured for a further 15min at 37°C. The entire incubation mix was analysed on a 10-12% gradient NOVEX gel, staining with Coomassie Brilliant Blue. Oxidised (-DTT) and reduced (+ 150mM DTT) SP-22 controls were also prepared. **Lane 1** (SP-22), **2** (SP-22 + 150mM DTT), **3** (SP-22 + NADH), **4** (SP-22 + E3), **5** (SP-22 + E3 + 1mM NADH), **6** (SP-22 + Trx), **7** (SP-22 + E3 + Trx), **8** (SP-22 + E3 + Trx + 1mM NADH), **9** (SP-22 + E3 + Trx + 1mM NAD⁺). Arrows indicate thioredoxin (Trx), E3 and the dimeric (D) and monomeric (M) forms of SP-22.
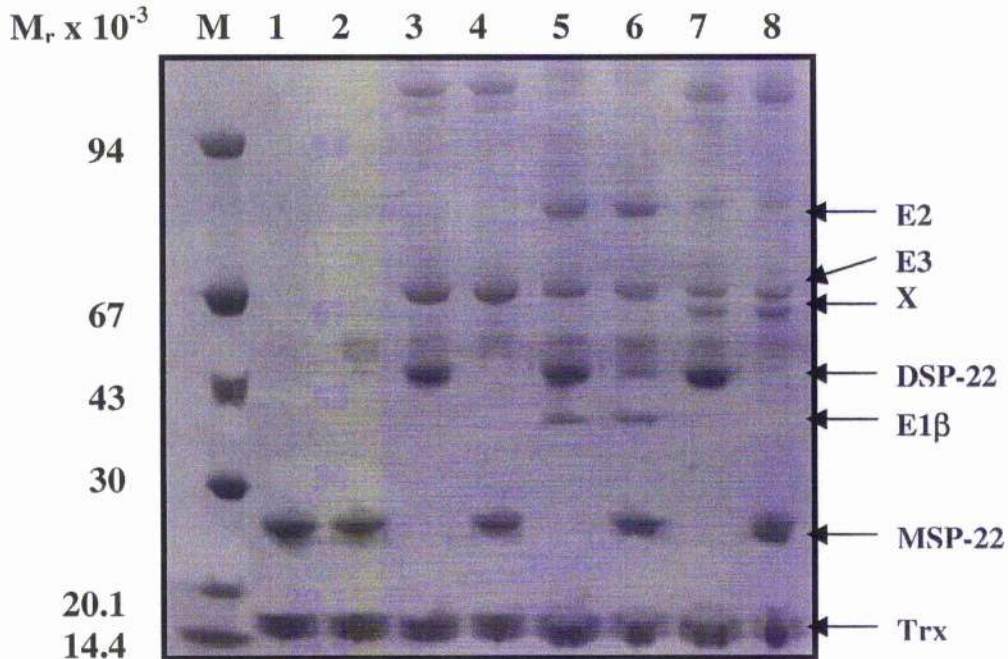
Figure 7.5. Comparison of E3, PDC and OGDC Reduction of SP-22 in the Presence of NAD⁺ and NADH

Purified SP-22 (5μg) was pre-incubated for 5min at 37°C with combinations of bovine E3 (5μg), thioredoxin (5μg) and PDC (25μg) or OGDC (25μg), in the presence of 1.0mM NAD⁺ or NADH, then made up to a total volume of 20μl with Laemmli sample buffer, and denatured for a further 15 min at 37°C. The entire incubation mix was analysed on a 10-12% gradient NOVEX gel, staining with Coomassie Brilliant Blue. **Lane 1** (SP-22 + Trx + NADH), **2** (SP-22 + Trx + NAD⁺), **3** (SP-22 + Trx + E3 + NADH), **4** (SP-22 + Trx + E3 + NAD⁺), **5** (SP-22 + Trx + OGDC + NADH), **6** (SP-22 + Trx + OGDC + NAD⁺), **7** (SP-22 + Trx + PDC + NADH), and **8** (SP-22 + Trx + PDC + NAD⁺). Arrows indicate thioredoxin (Trx), E3, the dimeric (D) and monomeric (M) forms of SP-22, and the other PDC/OGDC components.

1. Proposed Electron Routes of Electron Transport
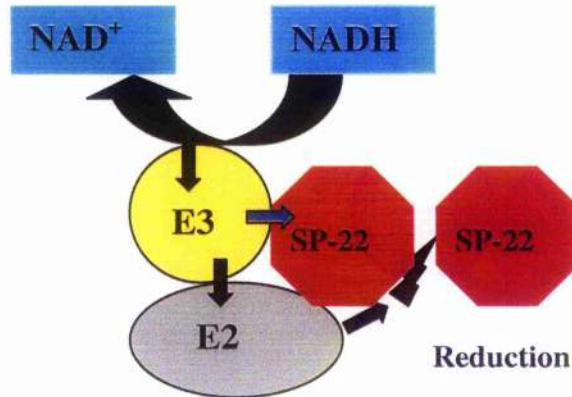
2. Diaphorase Activity of E3
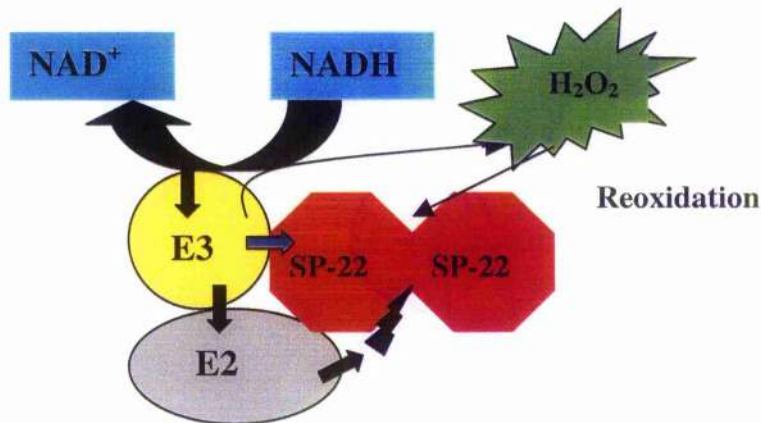
Figure 7.6. The Diaphorase Effect of E3 on SP-22

Diagram 1 illustrates the proposed reduction of SP-22 into its monomeric form by dihydrolipoamide thiols or directly by E3 (blue arrows). Diagram 2 shows the re-oxidation of SP-22 back to its disulphide-bonded form by hydrogen peroxide, generated as a consequence of the diaphorase activity of E3. The small black arrows depict the proposed flow of electrons. Although not shown it is also possible that thioredoxin and/or an additional adaptor protein like the AhpD component in *Mycobacterium tuberculosis* may be required to complete the electron transport pathway.

7.2.3. Summary and Discussion

SP-22 has been assigned to a family of 2-Cys thioredoxin-dependent hydroperoxide reductases but this does not exclude the possibility that there may be alternative physiological substrates. Recently a direct link has been established between the E2 (OGDC) and E3 components of *Mycobacterium tuberculosis*, participating in a system involved in the NADH-dependent removal of peroxide and peroxynitrite substrates by the AhpC Prx (Bryk *et al*, 2002). In this system electrons are transferred from NADH to E3, to E2, to an adaptor protein called AhpD, then finally to AhpC.

The reduction mechanism of SP-22 was shown to rely on thiol groups as a source of reducing equivalents. This was reflected by the ability of the thiol compounds DTT, DHL and thioredoxin to convert SP-22 to its monomeric state, together with the inability of non-thiol reductants such as ascorbate and NADH to reduce SP-22. These results are consistent with those for other 2-Cys Prx family members. The demonstration that SP-22 could be reduced by DHL was of particular interest, raising the possibility that E2 of PDC and/or OGDC may be able to reduce SP-22 comparable with the *Mycobacterium tuberculosis* system.

Initially, as a direct physical interaction was observed between E3 and SP-22, it was postulated that E3 (+NADH) might supply reducing equivalents directly to SP-22, therefore substituting the requirement for thioredoxin. However reduction of SP-22 by E3 in the presence of NADH was not observed. This experiment was repeated in the presence of thioredoxin, E3 and NADH. Interestingly SP-22 was observed to be in its dimeric form, indicating that SP-22 is being re-oxidised in some way on addition of NADH. It is reported that E3 can catalyse the generation of hydrogen peroxide and to a lesser extent, the superoxide anion, via NADH oxidation by dissolved oxygen in solution (Gazaryan *et al*, 2002).

At present, it is unclear if E3 can mediate electron transfer directly to SP-22 or via thioredoxin owing to its intrinsic diaphorase activity. However, SP-22 remains in its reduced form when incubated with thioredoxin, E3 and NAD^+ suggesting that

electron transfer cannot occur from SP-22 to NAD^+, although it is still possible that thioredoxin can transfer electrons to E3.

Also investigated was the possibility that E3 may be able to transfer reducing equivalents to SP-22 via E2. Initially this proposal seemed promising given that exogenous dihydrolipoamide successfully reduced SP-22. However incubation of SP-22 with E2 in the presence and absence of NADH and E3, did not reduce SP-22. As both E3 and NADH are present in the incubation it is likely that diaphorase activity is occurring once more. Therefore any successful transfer of electrons from E2 to SP-22 would be masked by the re-oxidation of SP-22 by hydrogen peroxide. One possible future experiment would be to pre-incubate E3, E2 and NADH with catalase prior to the addition of SP-22. The catalase would scavenge any available hydrogen peroxide allowing us to observe whether electrons can be transferred to SP-22, thereby reducing it.

An additional factor that may be important for successful SP-22 reduction is the presence of an adaptor protein like AhpD of the *Mycobacterium tuberculosis* system, which mediates the NADH-dependent transfer of reducing equivalents from E3 and E2, to AhpC. A final possibility is the association of SP-22 with E3 may be simply to maintain it in close proximity to protect the 2-oxoacid dehydrogenase complexes from oxidative damage, including the hydrogen peroxide generated by the intrinsic diaphorase activity of E3. Thus it remains to be proven whether there is a direct functional linkage between these major metabolic assemblies and the mitochondrial antioxidant system as represented by SP-22.

General Discussion

General Discussion

SP-22 was initially identified as a substrate protein for a mitochondrial ATP-dependent protease in bovine adrenal cortex; however following sequence analysis it was assigned to a novel peroxidase family, the peroxiredoxins (Prxs) (Rhee *et al*, 1999). The divergent functions of the Prxs, including roles in cell proliferation and apoptosis, revolve around their ability to scavenge reactive oxygen species (ROS) and the intracellular messenger hydrogen peroxide. Hydrogen peroxide is also extremely destructive to key intracellular biomolecules, both directly and also indirectly, via the hydroxyl radical generated by the Fenton reaction.

Elevated levels of ROS are produced in mitochondria as by-products of oxidative phosphorylation. Electron leakage is proposed to occur mainly from complexes I and III of the electron transport chain, generating the superoxide anion which can further spontaneously dismutate to form hydrogen peroxide (Finkel and Holbrook, 2000; Liu *et al*, 2002). Several mitochondrial enzymatic systems have evolved to protect mitochondrial DNA, proteins and lipids from damage by ROS, in addition to reactive sulphur species and reactive nitrogen species which are equally destructive (Nordberg and Arner, 2001). Oxidative modification of several mitochondrial enzymes including the 2-oxoacid dehydrogenase complexes has been implicated in the pathogenesis of several neurodegenerative disorders and ageing, underlining the necessity for an effective barrage of antioxidant systems in this compartment (Gibson *et al*, 2000).

There are two subgroups (1-Cys and 2-Cys) of the Prxs depending on the number of conserved cysteine residues present within their primary sequences. Both subgroups contain a basic dimeric unit and the site of catalysis is the N-terminal cysteine. The active site cysteine-sulphydryl of the 1-Cys subgroup is oxidised by hydrogen peroxide to a sulphenic acid coupled to the release of water and molecular oxygen (Kang *et al*, 1998a). The oxidised form of the enzyme is inactive and must be regenerated by a thiol-specific reductant for subsequent catalytic cycles. *In vitro* small thiol compounds including DTT and

mercaptoethanol are capable of reducing 1-Cys members; however, *in vivo* the physiological electron donor has been reported, in the work of one paper, to be cyclophilin A (Lee *et al*, 2001).

All the mammalian Prxs are of the 2-Cys category which are also termed thioredoxin-dependent peroxide reductases, on account of their reliance on thioredoxin as a source of reducing equivalents for peroxidase activity. A recent report however, also suggests that cyclophilins may be able to reduce the 2-Cys members back to their reduced states (Lee *et al*, 2001). 2-Cys Prxs can further be distinguished from 1-Cys members by the presence of two intermolecular disulphide bonds formed between the N-terminal conserved cysteine of one subunit and the C-terminal cysteine of the opposing monomer. SP-22 is a member of this subgroup, containing three conserved cysteines (C47, C66 and C168); this third cysteine is not atypical of this subgroup.

In general, the 2-Cys Prxs studied to date, excluding the mitochondrial member PRDX5, all exist as homodimeric enzymes that further adopt a larger oligomeric form. This larger assembly is toroidal in conformation, formed by the interaction of five dimers joined end-to-end (Hirotsu *et al*, 1999; Schröder *et al*, 2000).

Research into the precise physiological role of SP-22 is limited, with studies focusing on its ability to protect several free-radical sensitive enzymes (Watabe *et al*, 1997; Watabe *et al*, 1999). In addition to SP-22 only one other mitochondrial Prx (PRDX5) has been identified. PRDX5 is a 2-Cys member; however, it represents a novel subgroup of Prxs as it does not contain intermolecular disulphides and is, in fact, exclusively monomeric (Declercq *et al*, 2001). The structure of SP-22 has not been investigated to date; therefore the primary aim of this thesis was to elucidate the structure and function of SP-22 in more detail.

Cloning, Overexpression and Purification of SP-22

To ascertain whether the structure of SP-22 was similar to that of the other 2-Cys Prxs or instead the mitochondrial PRDX5, it was necessary to obtain sufficient

quantities of protein for biophysical analysis. Published studies on SP-22 have been carried out with the native enzyme isolated from tissue sources such as adrenal cortex, which is often time-consuming and cumbersome. The first successful overexpression of recombinant SP-22 as a His-tagged protein in bacterial cells is reported here using the pET vector system. The conditions for optimal protein solubility were determined by manipulating the induction temperature of the overexpression. It was observed that solubility increased with a corresponding reduction in temperature, with 22°C being sufficient to generate the required levels of soluble protein. The incorporation of the six-histidine residue-tag onto the N-terminus of SP-22 enabled its subsequent purification by metal chelate chromatography. Approximately 20-30mg of pure SP-22 was produced per 500ml culture using a BioCAD® SPRINT™ Workstation.

Biophysical and TEM Studies of Wild Type and Mutant SP-22s

It was determined by SDS-PAGE analysis of purified SP-22 in reducing and non-reducing conditions that SP-22 forms a dimeric unit containing two intermolecular disulphide bonds. As the purified enzyme appears completely trapped in its oxidised state, it runs as a dimer when analysed by non-reducing SDS-PAGE. Three cysteine mutants were generated by site-directed mutagenesis, overexpressed and purified as for wild type SP-22. Following SDS-PAGE analysis of the mutants in reducing and non-reducing conditions, it was established that C47 formed an intermolecular disulphide bond with C168 of the opposing subunit. C66 was shown not to participate in disulphide bond formation, with this mutant remaining in its dimeric form in the absence of reducing agent as for wild type SP-22. Therefore it was concluded that SP-22 adopts the same basic dimeric subunit organisation identified in other 2-Cys Prxs.

As mentioned previously the 2-Cys Prxs can form a larger oligomeric assembly, arranged as a decameric toroid comprising five dimers. It was established using gel exclusion chromatography and sedimentation equilibrium ultracentrifugation (SEU) that SP-22 too forms a large oligomer. The apparent molecular weight of the SP-22 oligomer was established by SEU to range between 615-635kDa

corresponding possibly to a double toroid containing 10 or 12 subunits per ring. SEU is an extremely accurate means of molecular weight determination, yet the results generated were unexpected and did not correspond to a single decameric toroid. However, it became apparent following transmission electron microscopy (TEM) that SP-22 does not exist as a single species, and can form stacks of two and three rings. Therefore it is likely that the size obtained by SEU represents the average molecular weight of all the oligomeric species present in solution, which may be at dynamic equilibrium. Experiments repeated in the presence of DTT and for C47S established that the integrity of the SP-22 oligomer is not maintained by disulphide bonds. In addition, aggregate formation was observed for C47S, later confirmed by TEM.

Circular Dichroism (CD) in the far UV spectra was used to establish the secondary structural composition of wild type SP-22. The α-helix contribution was the greatest constituting nearly 50% of the overall structure. The alignment of SP-22 with the 2-Cys Prx members TPx-B and HBP23 indicated extremely high (>90%) sequence and structural homology. Secondary structure determination for C47S was also carried out, and it was established that mutation of C47 does not have an observable effect on the secondary structure composition; the CD profiles of wild type SP-22 and C47S were comparable. As CD offers only an estimation of secondary structural composition it will be necessary to use a high-resolution technique such as X-ray crystallography to determine this more accurately.

The stability of the SP-22 oligomer was also assessed by monitoring CD spectral changes in the near UV region on gradual denaturation in increasing urea concentration. Overall the oligomer was extremely stable, even following overnight incubations at maximal denaturant concentration. At the highest concentration of urea (9.5M) the oligomer remained partially folded, retaining approx. 25% of native ellipticity. The contribution of the disulphide bonds to global stability was further assessed by studying the unfolding profiles of the mutants. Experiments for wild type and mutant SP-22s were also carried out in

the presence of 20mM DTT to prevent the formation of non-specific disulphide interactions that may form during the unfolding process. Slight destabilisation in the range of 4-6M urea was observed for wild type SP-22 in the presence of DTT; however complete denaturation was not achieved, confirming that the cysteines have a minor role in stabilising those elements of structure that unfold between 4-6M urea and are not necessary for overall subunit integrity. CD analysis of the cysteine mutants in the presence and absence of reducing agent further supported this finding.

It is possible to trace the discrete events in a folding pathway using fluorescence spectroscopy by monitoring the changes in tryptophan fluorescence with gradual denaturation. Typically tryptophan residues are located internally or are present at protein-protein interfaces; therefore dissociation of adjacent subunits and subsequent unfolding theoretically would result in a concomitant increase or decrease in tryptophan fluorescence. An unfolding profile can be plotted by calculating the fluorescence changes (as a percentage of the total change between native and denatured forms of the protein) against the concentration of denaturant. This can then be compared with the unfolding profile generated in CD experiments. Unfortunately however, the fluorescence changes between native and denatured SP-22 were minor, and an unexpected decrease in absorbance was observed for the latter form. This was attributed to internal fluorescence quenching which commonly occurs when a protein is denatured, generating unfavourable positioning of amino acids side chains. Furthermore disulphides and external quenching agents such as DTT can also cause a molecule to lose energy, thus resulting in a related decrease in fluorescence. The observed small changes in fluorescence subsequently prevented the construction of an unfolding titration profile.

The toroidal structure of SP-22, characteristic of the 2-Cys Prxs, was clearly observed by negative staining TEM. From 188 individual SP-22 toroids the average external diameter was established to be approx 15nm. Stacks comprising two and three SP-22 toroids arranged in a lateral arrangement were also observed.

This phenomenon has also been reported for the human erythrocyte protein TPx-B; however stacking was more prevalent for recombinant SP-22 (Harris *et al*, 2001).

To investigate the possibility that the His-tags mediated stacking via tethering by contaminating zinc ions from the purification procedure, gel exclusion chromatography was carried out in the presence of the chelating agent EDTA, DTT or with thrombin-cleaved SP-22 (Linder *et al*, 1992). The molecular weight remained higher ($\geq$450,000) than that predicted for a decamer (approx 250,000Da) implying that the His-tags do not mediate stacking. Stacking has also been observed in SP-22 purified from adrenal cortex, supporting the proposal that His-tags are not responsible for stacking (Wood *et al*, 2003). It should also be noted that the accurate molecular weight determination of SP-22 by gel exclusion chromatography is also complicated by the presence of a central cavity that gives rise to a larger-than-predicted effective diameter.

As a caveat to the above conclusion however, TEM studies on SP-22 conducted in the presence of DTT produced mainly single rings. It has already been established by SEU, gel filtration and CD that the cysteine residues are not structural. It is known that DTT can bind zinc ions with high affinity; therefore, it is possible that although the His-tags are not responsible for stacking, they can increase its prevalence. The factors governing stacking and the physiological relevance of this phenomenon requires further investigation.

A ubiquitous feature of the rings requiring further probing is the presence of radial spikes projecting outwards from the central cavity of the rings, believed to be too regularly positioned to be artefacts of the staining procedure. Furthermore, electron-dense material was also frequently observed within the central cavity. Following silver staining and immunoblotting of purified SP-22 with a His-tag monoclonal antibody, it was determined that the cavity material was likely to be part of SP-22 structure and not adventitiously bound *E. coli* proteins. The possibility that this electron-dense material could be attributed to partially folded

SP-22 subunits was considered unlikely as additional oligomeric forms of SP-22 were not observed in gel exclusion chromatography and sedimentation equilibrium experiments. This feature requires further investigation, as does the elucidation of the exact number of subunits per ring. The SP-22 monomers of the toroid are packed extremely tightly together, preventing complete penetration of the stain round the edges of each monomer. It is probable that SP-22 will be decameric, consistent with other 2-Cys members. To confirm this, cryo-negative staining which offers greater resolution is presently being carried out.

SP-22 Functional Studies

The second aim of this thesis was to elucidate the precise function of SP-22, which has remained elusive to date except in its protection of several free-radical sensitive enzymes (Watabe *et al*, 1997; Watabe *et al*, 1999). The structure of SP-22 and indeed the 2-Cys Prxs in general appears rather complex for a simple antioxidant function.

Initially it was necessary to determine whether heterologously-expressed SP-22 was in fact active. This was achieved by measuring the protective effect of SP-22 on enolase inactivation in the presence of a free-radical generating system. SP-22 was demonstrated to be active in this assay and exhibited significant protection towards enolase at a range of concentrations. To confirm the contributions of the cysteine residues in the peroxidation mechanism, the protective effect of the cysteine mutants towards enolase was also studied. The N-terminal C47S mutant displayed no protection towards enolase confirming its role as the catalytic residue. The extent of protection by the C66 mutant was comparable with that of wild type SP-22, indicating its lack of involvement in the catalytic mechanism. Unexpectedly the C-terminal mutant (C168S) exhibited significant protection towards enolase inactivation. In effect this mutant appeared to function in a manner not dissimilar to the 1-Cys Prxs, bypassing the requirement for the intermediate step in which disulphide bond formation occurs during the catalytic cycle. Consequently DTT must be able to directly reduce C47 from its sulphenic

acid back to its sulphydryl form. This illustrates the non-equivalence of the N- and C-terminal cysteines towards the peroxidase activity of SP-22.

Catalase was also demonstrated to protect enolase from inactivation, thus implying that hydrogen peroxide is involved in the inactivation of enolase consistent with the role of SP-22 as a peroxidase. The removal of hydrogen peroxide by catalase prevents direct damage and also indirect damage via the generation of the hydroxyl radical by the Fenton reaction, which is considered to be the most potent ROS. A comparison of the removal of hydrogen peroxide by catalase and SP-22 in the presence and absence of DTT by tracing the fall in A_{240} over time demonstrated that SP-22 does not exhibit detectable peroxidase activity in this assay. This is consistent with previous suggestions that the Prxs can only remove micromolar amounts of hydrogen peroxide involved in cell signalling networks, and not millimolar levels like catalase and glutathione peroxidase. It is likely, however, that the reduction of SP-22 from its oxidised (inactive) state to its reduced (active) state in this situation is also limited by the use of DTT as a non-physiological substrate.

SP-22 Protection of the 2-Oxoacid Dehydrogenase Complexes

Given the previous finding in our laboratory that SP-22 co-elutes with the E3 component of bovine heart PDC following gel exclusion chromatography, the function of SP-22 with respect to protection of the 2-oxoacid dehydrogenase complexes against oxidative damage was investigated. All the components of the 2-oxoacid dehydrogenase complexes contain chemical groupings that are susceptible to oxidative modification. E1 contains several reactive cysteines, E2 and E3BP contain lipoate groups and E3 contains reactive sulphydryl groups involved in catalysis.

The free-radical generating system used in the above inactivation studies on enolase did not appear to inactivate the 2-oxoacid complexes and bovine E3 to any significant extent; therefore inactivation by the direct addition of hydrogen peroxide was assessed, in the presence and absence of 0.1mM NADH, to render

the subunit thiols in their reduced forms. PDC, OGDC and E3 activity was not abolished, with 10-30% activity still remaining following incubation for 40 min at the highest hydrogen peroxide concentration (10mM). The addition of 0.1mM NADH had no significant effect on the sensitivity of the enzymes to inhibition. This implies that hydrogen peroxide is not especially damaging to the complexes.

Inactivation studies have been carried out on OGDC using intact rat mitochondria exposed to micromolar levels of hydrogen peroxide (Nulton-Persson and Szweda, 2001). In this report OGDC was found not to be particularly sensitive to inactivation by 50μM hydrogen peroxide, following incubation for 7.5 min, with only an observed 39% reduction in activity. Furthermore the activity of OGDC was recovered to control levels following the removal of hydrogen peroxide by catalase, suggesting that the inactivation of this enzyme is a reversible process. This was only observed in intact mitochondria however, and not in disrupted mitochondria. Consequently these authors propose that hydrogen peroxide may have a role in the regulation of OGDC via modulating the redox status of the mitochondria, as hydrogen peroxide reversibly inhibits the rate of respiration and ATP synthesis. This would certainly account for SP-22's association with the complexes.

Additional inactivation studies have been carried out to investigate the susceptibility of mitochondrial enzymes to hydrogen peroxide, particularly in brain nerve terminals; however to date no studies have been carried out on the purified enzymes. Despite this the unequivocal finding is that higher-than-expected levels of hydrogen peroxide are required for inactivation of the 2-oxoacid dehydrogenase complexes. It was demonstrated that 500μM hydrogen peroxide did not completely abolish OGDC activity in guinea pig nerve terminals, with 20% of control activity remaining after a 10 min incubation period (Tretter and Adam-Vizi, 2000).

The resistance to inactivation in the case of the purified enzymes may be because the susceptible groups of the PDC and OGDC components are inaccessible to

hydrogen peroxide and are protected and buried within the overall structure. This is supported by the observation that the thiol compound NEM cannot modify the reactive thiols of E3 unless it is completely denatured (Fig. 1.11). Furthermore it has been shown that E2 can remain active even when 50% or more of its lipoyl groups have been removed (Guest *et al*, 1985). It has also been proposed by Nulton-Persson and Szweda (2001) that OGDC is not particularly sensitive to damage by hydrogen peroxide. Moreover it was demonstrated that OGDC inactivation in intact mitochondria was reversible, as mentioned previously.

In the work described here, it is possible that the damaged groups of PDC and OGDC are being repaired on addition to the assay mixture, due to the presence of cysteine-SH at millimolar levels. Subsequently our results may reflect only irreversible damage to the complexes and would explain why high levels of hydrogen peroxide (5-10mM) were required for inactivation. In the study of Tretter and Adam-Vizi (2000) cysteine-SH or equivalent thiol compound is not included in the assay mixture, thus their results may represent reversible damage inflicted on OGDC, accounting for the low levels of hydrogen peroxide (500μM) required for inactivation.

The Relationship Between SP-22 and E3

A physical interaction between SP-22 and the E3 component has been confirmed using Isothermal Titration Calorimetry (ITC) and Surface Plasmon Resonance (SPR). ITC indicated an interaction between human recombinant E3 and SP-22 with a binding affinity of approx. 18μM, fitting well to a 1:1 model of binding. Preliminary SPR studies further elucidated a tighter binding affinity in the micromolar range (0.1-0.9μM) between bovine E3 and SP-22. This physical interaction implies a functional significance; therefore using the conversion of SP-22 from its dimeric (oxidised) to monomeric (reduced) form observed by SDS-PAGE, the possibility that PDC, OGDC, E2 and E3 may be able to reduce SP-22 in the place of thioredoxin was assessed.

In *Mycobacterium tuberculosis* the Prx AhpC is involved in peroxide and peroxynitrite removal; however its partner AhpF is absent, suggesting alternative enzyme components are involved. It was established that AhpC is reduced by an adaptor protein called AhpD, in a NADH-dependent system involving E3 and succinyltransferase (E2) (Bryk *et al*, 2002). The electron flow is the reverse of that in OGDC during catalysis, and proceeds from NADH to E3, to E2, to AhpD and finally to AhpC which is reduced for subsequent catalytic cycles. It was demonstrated that exogenous lipoate can substitute for the E2 component to a limited extent, although *in vivo* there is probably no free lipoate available.

Initially it was established that small thiol compounds including DTT, dihydrolipoamide (DHL) and thioredoxin could all reduce SP-22, whereas the non-thiol-containing reductants ascorbate and NADH, could not. The finding that exogenous DHL could reduce SP-22 (comparable to AhpC in *Mycobacterium tuberculosis*) highlighted the possibility that the lipoamide prosthetic groups of E2 may also be able to reduce SP-22. SDS-PAGE analysis, however, demonstrated that SP-22 remained in its oxidised state in the presence of E2. This is not surprising given E2's requirement for reducing equivalents supplied by E3. It is also possible that the lipoate group of E2 is not accessible to the active site of SP-22, or that E2 is not capable of transferring electrons to SP-22.

It was then investigated whether E3 had the potential to reduce SP-22 given its established physical interaction. However, even in the presence of NADH, which renders the reactive sulphydryls of E3 in their reduced states, SP-22 remains oxidised. It was subsequently proposed that the flow of electrons between E3 and SP-22 could occur via thioredoxin. Given the homology between E3 and thioredoxin reductase this appears a feasible mechanism. Interestingly in the presence of SP-22, E3, thioredoxin and NADH, SP-22 is found in its oxidised state. This was highly unexpected given that reduced thioredoxin, the *in vivo* physiological electron donor, is present. Furthermore in the presence of E3, thioredoxin and NAD^+, SP-22 is successfully reduced. This implies that when NADH is present SP-22 oxidation is promoted by an unknown mechanism.

It has been reported that E3 has intrinsic diaphorase activity, generating hydrogen peroxide and lower levels of the superoxide anion by oxidation of NADH (Gazaryan *et al*, 2002). This could indeed account for the results obtained. This diaphorase activity was also observed when SP-22 was incubated with PDC and OGDC in the presence of thioredoxin and NADH. It can also be postulated that the close association of SP-22 with the mitochondrial complexes is essential to quench the hydrogen peroxide generated by the diaphorase activity of the E3 component, thereby protecting them and other mitochondrial enzymes from oxidative modification. In addition, as previously mentioned a role for hydrogen peroxide in the regulation of the 2-oxoacid complexes has been postulated (Nulton-Persson and Szweda, 2001). Initially, however, further experimentation is required to confirm that the diaphorase activity of E3 is responsible for the unexpected oxidation of SP-22 under these conditions, as NADH-mediated reduction of SP-22 via the putative E3/E2-thioredoxin pathway would be masked in this assay by the generation of hydrogen peroxide.

Future experiments pre-incubating with catalase prior to addition of SP-22 and thus removing hydrogen peroxide generated by E3-mediated diaphorase activity, may aid the determination of whether SP-22 can be reduced by specific components of the 2-oxoacid dehydrogenase complexes.

Although a specific functional relationship between SP-22 and the 2-oxoacid dehydrogenase complex remains to be elucidated, the confirmed physical interaction between E3 and SP-22 together with the ability of DHL to reduce SP-22 highlights a possible direct connection. Alternatively, the connection between SP-22 and the 2-oxoacid dehydrogenase complexes may occur via thioredoxin, which has been previously reported to activate both OGDC and PDC and can oxidise E2 in place of E3 (Bunik *et al*, 1997; Bunik *et al*, 1999). Further work is required to probe this relationship in more detail, together with further interaction studies to assess whether SP-22 has a physical and functional interaction with any of the other constituent enzymes of PDC/OGDC.

There are many interesting structural and functional features of SP-22 that have been established as a result of this work, requiring future work and understanding. It has become apparent that SP-22, following its initial identification is not simply a substrate for an ATP-dependent protease, and has divergent functions dependent on its role as a peroxidase that may include the protection of the 2-oxoacid dehydrogenase complexes from oxidative damage.

References

References

Adrian, M., Dubochet, J., Fuller, S. D., and Harris, J. R. (1998) Cryo-negative staining. *Micron.* **29**, 145-160.

Alphey, M. S., Bond, C. S., Tetaud, E., Fairlamb, A. H., and Hunter, W. N. (2000) The structure of reduced tryparedoxin peroxidase reveals a decamer and insight into reactivity of 2Cys-peroxiredoxins. *J.Mol.Biol.* **300**, 903-916.

Amici, A., Levine, R. L., Tsai, L., and Stadtman, E. R. (1989) Conversion of amino acid residues in proteins and amino acid homopolymers to carbonyl derivatives by metal-catalyzed oxidation reactions. *J.Biol.Chem.* **264**, 3341-3346.

Antunes, F., Han, D., and Cadenas, E. (2002) Relative contributions of heart mitochondria glutathione peroxidase and catalase to H(2)O(2) detoxification in *in vivo* conditions. *Free Radic.Biol.Med.* **33**, 1260-1267.

Araki, M., Nanri, H., Ejima, K., Murasato, Y., Fujiwara, T., Nakashima, Y., and Ikeda, M. (1999) Antioxidant function of the mitochondrial protein SP-22 in the cardiovascular system. *J.Biol.Chem.* **274**, 2271-2278.

Arner, E. S. and Holmgren, A. (2000) Physiological functions of thioredoxin and thioredoxin reductase. *Eur.J.Biochem.* **267**, 6102-6109.

Arthur, J. R. (2000) The glutathione peroxidases. *Cell Mol.Life Sci.* **57**, 1825-1835.

Aust, A. E. and Eveleigh, J. F. (1999) Mechanisms of DNA oxidation. *Proc.Soc.Exp.Biol.Med.* **222**, 246-252.

Avila-Sakar, A. J. and Chiu, W. (1996) Visualization of beta-sheets and side-chain clusters in two-dimensional periodic arrays of streptavidin on phospholipid monolayers by electron crystallography. *Biophys.J.* **70**, 57-68.

Berlett, B. S. and Stadtman, E. R. (1997) Protein oxidation in aging, disease, and oxidative stress. *J.Biol.Chem.* **272**, 20313-20316.

Bradford, M. M., (1976) A rapid and sensitive method for the quantitation of microgram quantities of protein utilizing the principle of protein-dye binding. *Anal. Biochem.* **72**, 248-254.

Brenner, S. and Horne, R. W. (1959) A negative staining method for high resolution electron microscopy of viruses. *Biochim. Biophys. Acta* **34**, 60–71.

Brown, J. P. and Perham, R. N. (1976) Selective inactivation of the transacylase components of the 2-oxo acid dehydrogenase multienzyme complexes of *Escherichia coli. Biochem.J.* **155**, 419-427.

Bryk, R., Griffin, P., and Nathan, C. (2000) Peroxynitrite reductase activity of bacterial peroxiredoxins. *Nature* **407**, 211-215.

Bryk, R., Lima, C. D., Erdjument-Bromage, H., Tempst, P., and Nathan, C. (2002) Metabolic enzymes of mycobacteria linked to antioxidant defense by a thioredoxin-like protein. *Science* **295**, 1073-1077.

Bunik, V., Follmann, H., and Bisswanger, H. (1997) Activation of mitochondrial 2-oxoacid dehydrogenases by thioredoxin. *Biol.Chem.* **378**, 1125-1130.

Bunik, V., Raddatz, G., Lemaire, S., Meyer, Y., Jacquot, J. P., and Bisswanger, H. (1999) Interaction of thioredoxins with target proteins: role of particular structural elements and electrostatic properties of thioredoxins in their interplay with 2-oxoacid dehydrogenase complexes. *Protein Sci.* **8**, 65-74.

Cabiscol, E., Piulats, E., Echave, P., Herrero, E., and Ros, J. (2000) Oxidative stress promotes specific protein damage in *Saccharomyces cerevisiae. J.Biol.Chem.* **275**, 27393-27398.

Cadenas, E. and Davies, K. J. (2000) Mitochondrial free radical generation, oxidative stress, and aging. *Free Radic.Biol.Med.* **29**, 222-230.

Calabrese, V., Scapagnini, G., Ravagna, A., Fariello, R. G., Giuffrida Stella, A. M., and Abraham, N. G. (2002) Regional distribution of heme oxygenase, HSP70, and glutathione in brain: relevance for endogenous oxidant/antioxidant balance and stress tolerance. *J.Neurosci.Res.* **68**, 65-75.

Carothers, D. J., Pons, G., and Patel, M. S. (1989) Dihydrolipoamide dehydrogenase: functional similarities and divergent evolution of the pyridine nucleotide-disulfide oxidoreductases. *Arch.Biochem.Biophys.* **268**, 409-425.

Castegna, A., Aksenov, M., Thongboonkerd, V., Klein, J. B., Pierce, W. M., Booze, R., Markesbery, W. R., and Butterfield, D. A. (2002) Proteomic identification of oxidatively modified proteins in Alzheimer's disease brain. Part II: dihydropyrimidinase-related protein 2, alpha-enolase and heat shock cognate 71. *J.Neurochem.* **82**, 1524-1532.

Chae, H. Z., Kim, H. J., Kang, S. W., and Rhee, S. G. (1999) Characterization of three isoforms of mammalian peroxiredoxin that reduce peroxides in the presence of thioredoxin. *Diabetes Res.Clin.Pract.* **45**, 101-112.

Chae, H. Z., Robison, K., Poole, L. B., Church, G., Storz, G., and Rhee, S. G. (1994a) Cloning and sequencing of thiol-specific antioxidant from mammalian brain: alkyl hydroperoxide reductase and thiol-specific antioxidant define a large family of antioxidant enzymes. *Proc.Natl.Acad.Sci.U.S.A* **91**, 7017-7021.

Chae, H. Z., Uhm, T. B., and Rhee, S. G. (1994b) Dimerization of thiol-specific antioxidant and the essential role of cysteine 47. *Proc.Natl.Acad.Sci.U.S.A* **91**, 7022-7026.

Choi, H. J., Kang, S. W., Yang, C. H., Rhee, S. G., and Ryu, S. E. (1998) Crystal structure of a novel human peroxidase enzyme at 2.0 A resolution. *Nat.Struct.Biol.* **5**, 400-406.

Claiborne, A., Yeh, J. I., Mallett, T. C., Luba, J., Crane, E. J., III, Charrier, V., and Parsonage, D. (1999) Protein-sulfenic acids: diverse roles for an unlikely player in enzyme catalysis and redox regulation. *Biochemistry* **38**, 15407-15416.

Curtin, J. F., Donovan, M., and Cotter, T. G. (2002) Regulation and measurement of oxidative stress in apoptosis. *J.Immunol.Methods* **265**, 49-72.

Das, K. C., Lewis-Molock, Y., and White, C. W. (1997) Elevation of manganese superoxide dismutase gene expression by thioredoxin. *Am.J.Respir.Cell Mol.Biol.* **17**, 713-726.

Declercq, J. P., Evrard, C., Clippe, A., Stricht, D. V., Bernard, A., and Knoops, B. (2001) Crystal structure of human peroxiredoxin 5, a novel type of mammalian peroxiredoxin at 1.5 A resolution. *J.Mol.Biol.* **311**, 751-759.

De Marcucci, O. G., Hodgson, J. A., Lindsay, J. G. (1986) The Mr-50 000 polypeptide of mammalian pyruvate dehydrogenase complex participates in the acetylation reactions. *Eur.J.Biochem.* **158**, 587-594.

Dickinson, D. A. and Forman, H. J. (2002) Cellular glutathione and thiols metabolism. *Biochem.Pharmacol.* **64**, 1019-1026.

Ejima, K., Nanri, H., Araki, M., Koji, T., Shibata, E., Kashimura, M., and Ikeda, M. (2000) Expression of mitochondrial thioredoxin-dependent antioxidant protein, SP-22, in normal human and inflammatory mouse placentae. *Placenta* **21**, 847-852.

Esteve, J. M., Mompo, J., Garcia, d. l. A., Sastre, J., Asensi, M., Boix, J., Vina, J. R., Vina, J., and Pallardo, F. V. (1999) Oxidative damage to mitochondrial DNA and glutathione oxidation in apoptosis: studies *in vivo* and *in vitro*. *FASEB J.* **13**, 1055-1064.

Fang, Y. Z., Yang, S., and Wu, G. (2002) Free radicals, antioxidants, and nutrition. *Nutrition* **18**, 872-879.

Finkel, T. (2000) Redox-dependent signal transduction. *FEBS Lett.* **476**, 52-54.

Finkel, T. and Holbrook, N. J. (2000) Oxidants, oxidative stress and the biology of ageing. *Nature* **408**, 239-247.

Floyd, R. A. (1999) Antioxidants, oxidative stress, and degenerative neurological disorders. *Proc.Soc.Exp.Biol.Med.* **222**, 236-245.

Frank,J., Radermacher,M., Penczek,P., Zhu,J., Li,Y., Ladjadj,M., and Leith,A. (1996). SPIDER and WEB: processing and visualization of images in 3D electron microscopy and related fields. *J. Struct. Biol.*, **116**, 190-199.

Fridovich, I. (1997) Superoxide anion radical (O_2^-), superoxide dismutases, and related matters. *J.Biol.Chem.* **272**, 18515-18517.

Gazaryan, I. G., Krasnikov, B. F., Ashby, G. A., Thorneley, R. N., Kristal, B. S., and Brown, A. M. (2002) Zinc is a potent inhibitor of thiol oxidoreductase activity and stimulates reactive oxygen species production by lipoamide dehydrogenase. *J.Biol.Chem.* **277**, 10064-10072.

Gewaltig, M. T. and Kojda, G. (2002) Vasoprotection by nitric oxide: mechanisms and therapeutic potential. *Cardiovasc.Res.* **55**, 250-260.

Ghafourifar, P. and Richter, C. (1997) Nitric oxide synthase activity in mitochondria. *FEBS Lett.* **418**, 291-296.

Gibson, G. E., Park, L. C., Sheu, K. F., Blass, J. P., and Calingasan, N. Y. (2000) The alpha-ketoglutarate dehydrogenase complex in neurodegeneration. *Neurochem.Int.* **36**, 97-112.

Giles, G. I. and Jacob, C. (2002) Reactive sulfur species: an emerging concept in oxidative stress. *Biol.Chem.* **383**, 375-388.

Giles, G. I., Tasker, K. M., Collins, C., Giles, N. M., O'rourke, E., and Jacob, C. (2002) Reactive sulphur species: an in vitro investigation of the oxidation properties of disulphide S-oxides. *Biochem.J.* **364**, 579-585.

Gilgun-Sherki, Y., Melamed, E., and Offen, D. (2001) Oxidative stress induced-neurodegenerative diseases: the need for antioxidants that penetrate the blood brain barrier. *Neuropharmacology* **40**, 959-975.

Gorog, D. A., Ahmed, N., and Davies, G. J. (2002) Elevated plasma lipid peroxide levels in angina pectoris and myocardial infarction. *Cardiovasc.Pathol.* **11**, 153-157.

Guest, J. R., Lewis, H. M., Graham, L. D., Packman, L. C., and Perham, R. N. (1985) Genetic reconstruction and functional analysis of the repeating lipoyl domains in the pyruvate dehydrogenase multienzyme complex of Escherichia coli. *J.Mol.Biol.* **185**, 743-754.

Harris, J. R. (1991) Negative staining-carbon film technique: new cellular and molecular applications. *J.Electron Microsc.Tech.* **18**, 269-276.

Harris, J. R., Pluckthun, A., and Zahn, R. (1994) Transmission electron microscopy of GroEL, GroES, and the symmetrical GroEL/ES complex. *J.Struct.Biol.* **112**, 216-230.

Harris, J. R., Schroder, E., Isupov, M. N., Scheffler, D., Kristensen, P., Littlechild, J. A., Vagin, A. A., and Meissner, U. (2001) Comparison of the decameric

structure of peroxiredoxin-II by transmission electron microscopy and X-ray crystallography. *Biochim.Biophys.Acta* **1547**, 221-234.

Hawkins, C. F., Borges, A., and Perham, R. N. (1990) Cloning and sequence analysis of the genes encoding the alpha and beta subunits of the E1 component of the pyruvate dehydrogenase multienzyme complex of Bacillus stearothermophilus. *Eur.J.Biochem.* **191**, 337-346.

Henle, E. S. and Linn, S. (1997) Formation, prevention, and repair of DNA damage by iron/hydrogen peroxide. *J.Biol.Chem.* **272**, 19095-19098.

Hiroi, T., Watabe, S., Takimoto, K., Yago, N., Yamamoto, Y., and Takahashi, S. Y. (1996) The cDNA sequence encoding bovine SP-22, a new defence system against reactive oxygen species in mitochondria. *DNA Seq.* **6**, 239-242.

Hirotsu, S., Abe, Y., Okada, K., Nagahara, N., Hori, H., Nishino, T., and Hakoshima, T. (1999) Crystal structure of a multifunctional 2-Cys peroxiredoxin heme-binding protein 23kDa/proliferation-associated gene product. *Proc.Natl.Acad.Sci.U.S.A* **96**, 12333-12338.

Hodgson, J. A., De Marcucci, O. G., and Lindsay, J. G. (1986) Lipoic acid is the site of substrate-dependent acetylation of component X in ox heart pyruvate dehydrogenase multienzyme complex. *Eur.J.Biochem.* **158**, 595-600.

Howard, M. J., Chauhan, H. J., Domingo, G. J., Fuller, C., and Perham, R. N. (2000) Protein-protein interaction revealed by NMR T(2) relaxation experiments: the lipoyl domain and E1 component of the pyruvate dehydrogenase multienzyme complex of *Bacillus stearothermophilus*. *J.Mol.Biol.* **295**, 1023-1037.

Ikegami, T., Suzuki, Y., Shimizu, T., Isono, K., Koseki, H., and Shirasawa, T. (2002) Model mice for tissue-specific deletion of the manganese superoxide dismutase (MnSOD) gene. *Biochem.Biophys.Res.Commun.* **296**, 729-736.

Jaschke, A., Mi, H., and Tropschug, M. (1998) Human T cell cyclophilin18 binds to thiol-specific antioxidant protein Aop1 and stimulates its activity. *J.Mol.Biol.* **277**, 763-769.

Kamata, H. and Hirata, H. (1999) Redox regulation of cellular signalling. *Cell Signal.* **11**, 1-14.

Kang, S. W., Baines, I. C., and Rhee, S. G. (1998a) Characterization of a mammalian peroxiredoxin that contains one conserved cysteine. *J.Biol.Chem.* **273**, 6303-6311.

Kang, S. W., Chae, H. Z., Seo, M. S., Kim, K., Baines, I. C., and Rhee, S. G. (1998b) Mammalian peroxiredoxin isoforms can reduce hydrogen peroxide generated in response to growth factors and tumor necrosis factor-alpha. *J.Biol.Chem.* **273**, 6297-6302.

Kelly, S. M. and Price, N. C. (2000) The use of circular dichroism in the investigation of protein structure and function. *Curr.Protein Pept.Sci.* **1**, 349-384.

Kim, K., Rhee, S. G., and Stadtman, E. R. (1985) Nonenzymatic cleavage of proteins by reactive oxygen species generated by dithiothreitol and iron. *J.Biol.Chem.* **260**, 15394-15397.

Kim, K., Kim, I. H., Lee, K. Y., Rhee, S. G., and Stadtman, E. R. (1988) The isolation and purification of a specific "protector" protein which inhibits enzyme inactivation by a thiol/Fe(III)/O2 mixed-function oxidation system. *J.Biol.Chem.* **263**, 4704-4711.

Kim, A. T., Sarafian, T. A., and Shau, H. (1997) Characterization of antioxidant properties of natural killer-enhancing factor-B and induction of its expression by hydrogen peroxide. *Toxicol.Appl.Pharmacol.* **147**, 135-142.

Kochi, H. and Kilkuchi, G. (1976) Mechanism of reversible glycine cleavage reaction in *Arthrobacter globiformis*. Function of lipoic acid in the cleavage and synthesis of blycine. *Arch.Biochem.Biophys.***173**, 171-181.

Korotchkina, L. G., Yang, H., Tirosh, O., Packer, L., and Patel, M. S. (2001) Protection by thiols of the mitochondrial complexes from 4-hydroxy-2- nonenal. *Free Radic.Biol.Med.* **30**, 992-999.

Laemmli, U. K. (1970) Cleavage of structural proteins during the assambly of the head bacteriophage T4. *Nature.* **227**, 680-685.

Laue, T. M. and Stafford, W. F., III (1999) Modern applications of analytical ultracentrifugation. *Annu.Rev.Biophys.Biomol.Struct.* **28**, 75-100.

Lee, S. P., Hwang, Y. S., Kim, Y. J., Kwon, K. S., Kim, H. J., Kim, K., and Chae, H. Z. (2001) Cyclophilin a binds to peroxiredoxins and activates its peroxidase activity. *J.Biol.Chem.* **276**, 29826-29832.

Levine, R. L. (1983) Oxidative modification of glutamine synthetase. I. Inactivation is due to loss of one histidine residue. *J.Biol.Chem.* **258**, 11823-11827.

Linder, P., Guth, B., Wülfing, C, Krebber, C., Steipe, B., Müller, F., Plückthun. (1992) Purification of native proteins from the cytoplasm and periplasm of *Escherichia coli* using IMAC and histidine tails: A comparison of proteins and protocols. *Methods* **4**, 41-56.

Liu, S., Baker, J. C., Andrews, P. C., and Roche, T. E. (1995) Recombinant expression and evaluation of the lipoyl domains of the dihydrolipoyl acetyltransferase component of the human pyruvate dehydrogenase complex. *Arch.Biochem.Biophys.* **316**, 926-940.

Liu, Y., Fiskum, G., and Schubert, D. (2002) Generation of reactive oxygen species by the mitochondrial electron transport chain. *J.Neurochem.* **80**, 780-787.

Marnett, L. J. (1999) Lipid peroxidation-DNA damage by malondialdehyde. *Mutat.Res.* **424**, 83-95.

Marnett, L. J. (2000) Oxyradicals and DNA damage. *Carcinogenesis* **21**, 361-370.

McCartney, R. G., Sanderson, S. J., and Lindsay, J. G. (1997) Refolding and reconstitution studies on the transacetylase-protein X (E2/X) subcomplex of the mammalian pyruvate dehydrogenase complex: evidence for specific binding of the dihydrolipoamide dehydrogenase component to sites on reassembled E2. *Biochemistry* **36**, 6819-6826.

McCartney, R. G. (1998) Folding and assembly studies on the components of Mammalian PDC and OGDC. Doctoral Thesis. University of Glasgow.

McCartney, R. G., Rice, J. E., Sanderson, S. J., Bunik, V., Lindsay, H., and Lindsay, J. G. (1998) Subunit interactions in the mammalian alpha-ketoglutarate dehydrogenase complex. Evidence for direct association of the alpha-ketoglutarate dehydrogenase and dihydrolipoamide dehydrogenase components. *J.Biol.Chem.* **273**, 24158-24164.

McDonnel, J. M. (2001) Surface plasmon resonance: towards an understanding of the mechanisms of biological molecular recognition. *Curr.Opin. Chem. Biol.* **5**, 572-577.

Mitsumoto, A., Takanezawa, Y., Okawa, K., Iwamatsu, A., and Nakagawa, Y. (2001) Variants of peroxiredoxins expression in response to hydroperoxide stress. *Free Radic.Biol.Med.* **30**, 625-635.

Moreau, R., Heath S.D., Doneanu, C.E., Lindsay, J.G., and Hagen, T.M. (2002) Increased 4-hydroxynonenal adduction to α-ketoglutarage dehydrogenase in the aging rat heart: Evidence for a compensatory mechanism by the enzyme. (Submitted for publication).

Mullett, W. M., Lai, E. P. C., Yeung, J. M. (2000) Surface plasmon resonance-based immunoassays. *Methods* **22**, 77-91.

Netto, L. E. S., Chae, H. Z., Kang, S. W., Rhee, S. G., and Stadtman, E. R. (1996) Removal of hydrogen peroxide by thiol-specific antioxidant enzyme (TSA) is involved with its antioxidant properties. TSA possesses thiol peroxidase activity. *J.Biol.Chem.* **271**, 15315-15321.

Nikitovic, D. and Holmgren, A. (1996) S-nitrosoglutathione is cleaved by the thioredoxin system with liberation of glutathione and redox regulating nitric oxide. *J.Biol.Chem.* **271**, 19180-19185.

Noor, R., Mittal, S., and Iqbal, J. (2002) Superoxide dismutase--applications and relevance to human diseases. *Med.Sci.Monit.* **8**, RA210-RA215.

Nordberg, J. and Arner, E. S. (2001) Reactive oxygen species, antioxidants, and the mammalian thioredoxin system. *Free Radic.Biol.Med.* **31**, 1287-1312.

Nulton-Persson, A. C. and Szweda, L. I. (2001) Modulation of mitochondrial function by hydrogen peroxide. *J.Biol.Chem.* **276**, 23357-23361.

Patel, M. S. and Roche, T. E. (1990) Molecular biology and biochemistry of pyruvate dehydrogenase complexes. *FASEB J.* **4**, 3224-3233.

Patel, M. S. and Harris, R. A. (1995) Mammalian alpha-keto acid dehydrogenase complexes: gene regulation and genetic defects. *FASEB J.* **9**, 1164-1172.

Pedrajas, J. R., Miranda-Vizuete, A., Javanmardy, N., Gustafsson, J. A., and Spyrou, G. (2000) Mitochondria of Saccharomyces cerevisiae contain one-conserved cysteine type peroxiredoxin with thioredoxin peroxidase activity. *J.Biol.Chem.* **275**, 16296-16301.

Perham, R. N. (1991) Domains, motifs, and linkers in 2-oxo acid dehydrogenase multienzyme complexes: a paradigm in the design of a multifunctional protein. *Biochemistry* **30**, 8501-8512.

Peshenko, I. V. and Shichi, H. (2001) Oxidation of active center cysteine of bovine 1-Cys peroxiredoxin to the cysteine sulfenic acid form by peroxide and peroxynitrite. *Free Radic.Biol.Med.* **31**, 292-303.

Pierce, M. M., Raman, C. S., and Nall, B. T. (1999) Isothermal titration calorimetry of protein-protein interactions. *Methods* **19**, 213-221.

Poole, L. B. and Ellis, H. R. (1996) Flavin-dependent alkyl hydroperoxide reductase from *Salmonella typhimurium*. 1. Purification and enzymatic activities of overexpressed AhpF and AhpC proteins. *Biochemistry* **35**, 56-64.

Poole, L. B., Reynolds, C. M., Wood, Z. A., Karplus, P. A., Ellis, H. R., and Li, C. M. (2000) AhpF and other NADH:peroxiredoxin oxidoreductases, homologues of low Mr thioredoxin reductase. *Eur.J.Biochem.* **267**, 6126-6133.

Powis, G. and Montfort, W. R. (2001) Properties and biological activities of thioredoxins. *Annu.Rev.Biophys.Biomol.Struct.* **30**, 421-455.

Price, N. C. (2000) Conformational issues in the characterization of proteins. *Biotechnol.Appl.Biochem.* **31**, 29-40.

Radi, R., Beckman, J. S., Bush, K. M., and Freeman, B. A. (1991a) Peroxynitrite oxidation of sulfhydryls. The cytotoxic potential of superoxide and nitric oxide. *J.Biol.Chem.* **266**, 4244-4250.

Radi, R., Turrens, J. F., Chang, L. Y., Bush, K. M., Crapo, J. D., and Freeman, B. A. (1991b) Detection of catalase in rat heart mitochondria. *J.Biol.Chem.* **266**, 22028-22034.

Rhee, S. G., Kang, S. W., Netto, L. E., Seo, M. S., and Stadtman, E. R. (1999) A family of novel peroxidases, peroxiredoxins. *Biofactors* **10**, 207-209.

Sanderson, S. J., Khan, S. S., McCartney, R. G., Miller, C., and Lindsay, J. G. (1996) Reconstitution of mammalian pyruvate dehydrogenase and 2-oxoglutarate dehydrogenase complexes: analysis of protein X involvement and interaction of homologous and heterologous dihydrolipoamide dehydrogenases. *Biochem.J.* **319**, 109-116.

Sayre, L. M., Perry, G., Atwood, C. S., and Smith, M. A. (2000) The role of metals in neurodegenerative diseases. *Cell Mol.Biol.* **46**, 731-741.

Schroder, E., Isupov, M. N., Naran, A., and Littlechild, J. A. (1999) Crystallization and preliminary X-ray analysis of human thioredoxin peroxidase-B from red blood cells. *Acta Crystallogr.D.Biol.Crystallogr.* **55**, 536-538.

Schroder, E., Littlechild, J. A., Lebedev, A. A., Errington, N., Vagin, A. A., and Isupov, M. N. (2000) Crystal structure of decameric 2-Cys peroxiredoxin from human erythrocytes at 1.7 A resolution. *Structure.Fold.Des* **8**, 605-615.

Seo, M. S., Kang, S. W., Kim, K., Baines, I. C., Lee, T. H., and Rhee, S. G. (2000) Identification of a new type of mammalian peroxiredoxin that forms an intramolecular disulfide as a reaction intermediate. *J.Biol.Chem.* **275**, 20346-20354.

Shau, H. and Kim, A. (1994) Identification of natural killer enhancing factor as a major antioxidant in human red blood cells. *Biochem.Biophys.Res.Commun.* **199**, 83-88.

Shau, H., Kim, A. T., Hedrick, C. C., Lusis, A. J., Tompkins, C., Finney, R., Leung, D. W., and Paglia, D. E. (1997) Endogenous natural killer enhancing factor-B increases cellular resistance to oxidative stresses. *Free Radic.Biol.Med.* **22**, 497-507.

Sreerama, N., Woody, R.W. (1993) A self-consistent method for the analysis of protein secondary structure from circular dichroism. *Anal.Biochem.* **209**, 32-44.

Sreerama, N., Venyaminov, S. Y., and Woody, R. W. (1999) Estimation of the number of alpha-helical and beta-strand segments in proteins using circular dichroism spectroscopy. *Protein Sci.* **8**, 370-380.

Stadtman, E. R. and Berlett, B. S. (1991) Fenton chemistry. Amino acid oxidation. *J.Biol.Chem.* **266**, 17201-17211.

Stanley, C. J. and Perham, R. N. (1980) Purification of 2-oxo acid dehydrogenase multienzyme complexes from ox heart by a new method. *Biochem. Journal* **191**, 147-154

Tamarit, J., Cabiscol, E., and Ros, J. (1998) Identification of the major oxidatively damaged proteins in *Escherichia coli* cells exposed to oxidative stress. *J.Biol.Chem.* **273**, 3027-3032.

Tretter, L. and Adam-Vizi, V. (2000) Inhibition of Krebs cycle enzymes by hydrogen peroxide: A key role of [alpha]-ketoglutarate dehydrogenase in limiting NADH production under oxidative stress. *J.Neurosci.* **20**, 8972-8979.

Wallis, N. G., Allen, M. D., Broadhurst, R. W., Lessard, I. A., and Perham, R. N. (1996) Recognition of a surface loop of the lipoyl domain underlies substrate channelling in the pyruvate dehydrogenase multienzyme complex. *J.Mol.Biol.* **263**, 463-474.

Wang, M. X., Wei, A., Yuan, J., Clippe, A., Bernard, A., Knoops, B., and Murrell, G. A. (2001) Antioxidant enzyme peroxiredoxin 5 is upregulated in degenerative human tendon. *Biochem.Biophys.Res.Commun.* **284**, 667-673.

Wang, M. X., Wei, A., Yuan, J., Trickett, A., Knoops, B., and Murrell, G. A. (2002) Expression and regulation of peroxiredoxin 5 in human osteoarthritis. *FEBS Lett.* **531**, 359-362.

Watabe, S., Hara, T., Kohno, H., Hiroi, T., Yago, N., and Nakazawa, T. (1993) In vitro degradation of mitochondrial proteins by ATP-dependent protease in bovine adrenal cortex. *J.Biochem.(Tokyo)* **113**, 672-676.

Watabe, S., Kohno, H., Kouyama, H., Hiroi, T., Yago, N., and Nakazawa, T. (1994) Purification and characterization of a substrate protein for mitochondrial ATP-dependent protease in bovine adrenal cortex. *J.Biochem.(Tokyo)* **115**, 648-654.

Watabe, S., Hasegawa, H., Takimoto, K., Yamamoto, Y., and Takahashi, S. Y. (1995) Possible function of SP-22, a substrate of mitochondrial ATP-dependent protease, as a radical scavenger. *Biochem.Biophys.Res.Commun.* **213**, 1010-1016.

Watabe, S., Hiroi, T., Yamamoto, Y., Fujioka, Y., Hasegawa, H., Yago, N., and Takahashi, S. Y. (1997) SP-22 is a thioredoxin-dependent peroxide reductase in mitochondria. *Eur.J.Biochem.* **249**, 52-60.

Watabe, S., Makino, Y., Ogawa, K., Hiroi, T., Yamamoto, Y., and Takahashi, S. Y. (1999) Mitochondrial thioredoxin reductase in bovine adrenal cortex its purification, properties, nucleotide/amino acid sequences, and identification of selenocysteine. *Eur.J.Biochem.* **264**, 74-84.

Wei, Y. H. and Lee, H. C. (2002) Oxidative stress, mitochondrial DNA mutation, and impairment of antioxidant enzymes in aging. *Exp.Biol.Med.(Maywood.)* **227**, 671-682.

Wen, S. T. and Van Etten, R. A. (1997) The PAG gene product, a stress-induced protein with antioxidant properties, is an Abl SH3-binding protein and a physiological inhibitor of c-Abl tyrosine kinase activity. *Genes Dev.* **11**, 2456-2467.

Wood, Z. A., Poole, L. B., Hantgan, R. R., and Karplus, P. A. (2002) Dimers to doughnuts: redox-sensitive oligomerization of 2-cysteine peroxiredoxins. *Biochemistry* **41**, 5493-5504.

Wood, Z. A., Schroder, E., Robin, H. J., and Poole, L. B. (2003) Structure, mechanism and regulation of peroxiredoxins. *Trends Biochem.Sci.* **28**, 32-40.

Wray,W., Boulikas,T., Wray,V.P.,Hancock,R. (1981) Silver staining of proteins in polyacrylamide gels. *Anal. Biochem* **118**, 197-203.

Zelko, I. N., Mariani, T. J., and Folz, R. J. (2002) Superoxide dismutase multigene family: a comparison of the CuZn-SOD (SOD1), Mn-SOD (SOD2), and EC-SOD (SOD3) gene structures, evolution, and expression. *Free Radic.Biol.Med.* **33**, 337-349.